Scholars' Mine

Masters Theses   Student Theses and Dissertations

Fall 2020

Inclusion control in steel castings

Koushik Karthikeyan Balasubramanian

Recommended Citation

INCLUSION CONTROL IN STEEL CASTINGS

by

KOUSHIK KARTHIKEYAN BALASUBRAMANIAN

A THESIS

Presented to the Graduate Faculty of the

MISSOURI UNIVERSITY OF SCIENCE AND TECHNOLOGY

In Partial Fulfillment of the Requirements for the Degree

MASTER OF SCIENCE

in

MATERIALS SCIENCE AND ENGINEERING

2020

Approved by:

Dr.Laura Bartlett, Advisor
Dr.Ronald O'Malley
Dr.Simon Lekakh

PUBLICATION THESIS OPTION

This thesis consists of the following three articles, prepared for journal publication in the style used by the Missouri University of Science and Technology:

Paper I, found on pages 39–68, has been published in the International Journal of Metalcasting (IJMC).

Paper II, found on pages 69–107, are intended for submission to International Journal of Metalcasting (IJMC).

Paper III, found on pages 108–135, are intended for submission to International Journal of Metalcasting (IJMC).

ABSTRACT

Non-metallic inclusions are mainly comprised of oxides, sulfides, and nitrides, and are formed in liquid steel during the melting and refining process, as a result of reoxidation, worn-out refractories, or entrained slag. The notch toughness of high strength steels is particularly susceptible to the type, number, size, and distribution of non-metallic inclusions. High manganese and aluminum austenitic steels, or Fe-Mn-Al steels, have gained much interest in the military and automotive sector because of their excellent combinations of high strength and toughness. However, these steels are subject to both oxide bifilms and aluminum nitride, AlN, inclusions which form during melting and casting. During the casting process, the gating system plays an important role in determining the casting quality and the overall level of inclusions and bifilm defects. Two solutions to control inclusions during mold filling include molten metal filtration and design of novel "naturally pressurized" gating systems that control metal flow into the casting cavity and reduce air entrainment. However, the use of filters and these naturally pressurized gating systems add an additional cost and generally reduce casting yield. In the current study, the effects of filtration and gating design on reduction of bifilms and inclusions in Fe-Mn-Al steel were determined using two novel mold designs. A parallel gating study involving an aluminum deoxidized, cast composition of SAE 8630 was also performed. The results of this study showed that ceramic foam filters were more effective at removing solid oxide bifilms and aluminum nitride inclusions from Fe-Mn-Al steel castings than the naturally pressurized gating systems. Future studies should be directed at developing naturally pressurized gating systems with filters.

ACKNOWLEDGMENTS

First, I would like to thank God and my parents, Mr. M.S. Balasubramanian and Mrs. Uma Balu, for all their love, support, and sacrifices without which I would not have been able to make it this far in life. I would like to extend my heartfelt thanks and gratitude to my advisor, Dr. Laura Bartlett, for believing in me and providing me with an opportunity to work under her wing. Apart from being an advisor, she was also a great mentor, guide, and motivation. I would like to thank her for all her time and knowledge, and for helping me better myself at every stage of my journey, in graduate school. I would like to acknowledge the support provided by Dr. Ronald O'Malley, Dr. Simon Lekakh, and Dr. Mingzhi Xu for helping me understand and solve the challenges, faced in my research. I am grateful to Mr. Doug Imrie and Mr. Zach Henderson from SouthernCast Products for all their inputs and being the industrial sponsors. I am thankful to Mr. Miguel Gastelum and Mr. Dan Coyle from MagmaSoft for all the technical guidance. I would like to extend my gratitude to Mr. Nathan Inskip, Mr. Brian Bullock, Ms. Denise Eddings and Ms. Teneke Hill for their patience and time, experimental support and for ensuring that all the processes happened in a smooth and organized manner. I would like to thank the American Foundry Society for sponsoring this project. I would like to thank all my fellow graduate and undergraduate students for their support during experiments. I extend my special thanks to Michael Piston, Rairu Vaz Penna, and Soumava Chakraborty. Finally, I would like to thank my roommates, friends, and family without whom I would not be standing here. I would take this opportunity to specially mention Sivaramakrishnan Jayaram and Poorna Hariramakrishnan for being a constant source of emotional and moral support.

TABLE OF CONTENTS

PAPER

LIST OF ILLUSTRATIONS

PAPER III

LIST OF TABLES

1. INTRODUCTION

1.1. PROJECT PURPOSE AND OVERVIEW

The control of inclusions in the steelmaking and casting process has become increasingly important because of the demand for high-quality castings and increased mechanical property requirements. Non-metallic inclusions are mainly oxides, nitrides or sulfides and are generally undesirable for surface quality, machinability, and mechanical properties, especially fatigue and toughness.[1-2] Most of the applications of steel castings for industries such as rail, mining, construction, power generation, and military applications require high strength with high toughness and good ductility (typically greater than 10% elongation). For high strength steels of similar strength and microstructure, ductility and especially fracture and notch toughness are a strong function of steel cleanliness. The fracture toughness of high strength steels with good ductility is controlled by the size of the plastic zone ahead of the propagating crack as well as the number, type, morphology and distribution of inclusions within the plastic zone that can fracture or de-bond from the matrix.[3] Recent research has shown as much as a 65% reduction in the dynamic fracture toughness of quenched and tempered Cr-Mo-Ni cast steels when the inclusion density was doubled from 115 to 247 #/mm^2.[4]

Inclusions can form endogenously as a result of the deoxidation practice as well as during subsequent refining operations. Exogenous inclusions are generally formed external to the refining process and are more detrimental to mechanical properties because they are typically much larger than endogenous inclusions. Exogenous inclusions can result from slag entrainment, worn refractories, mold erosion, and reoxidation of the melt during

pouring and mold filling operations. Recent work has shown that up to 80% of the inclusions found in steel castings may be the result of reoxidation products that are often created during pouring and mold filling.[5] Other filling related reoxidation defects such as solid oxide bifilms and entrained gas defects are particularly detrimental to toughness and ductility and can cost the foundry in weld repair and casting rejects. Inclusions can be discrete or clustered, however, oxide bifilms are solid oxide films that become folded into the melt during pouring and mold filling. During mold filling, bifilms can result from air entrainment and abrupt changes in molten metal flow rate and direction that result in hydraulic jumps and eddy current formation when the liquid is in the turbulent regime.[6] For surface reactive metals such as aluminum alloys, ductile irons, and aluminum added steels, these conditions result in entrained surface oxide films that are primarily composed of alumina, spinel, or complex magnesium oxides.[7,8] These oxides films typically have a thickness of less than a micron, however, they are extensive in area, and can be up to tens of millimeters in length, essentially producing a crack-like flaw and a significant reduction in mechanical properties.[7] Bifilms can also absorb dissolved gases and act as nucleation sites for both gas and shrinkage microporosity.[8]

Unfortunately, prediction of the actual metal damage due to reoxidation inclusions and bifilm defects created by the filling process is largely based on theory. Most foundries in the United States are still using the rule-of-thumb gating practices for steel castings that were developed by the American Foundry Society in the 1960's; and these rules do not consider the effect of turbulent fill on metal damage.[9,10] Work by Campbell has shown that surface turbulence plays a critical role in the entrainment of oxide bifilms in aluminum alloys and that for smooth flow, the velocity of any metal should not exceed a critical

velocity of 0.5 m/s.[9] In reality however, practical industrial gating design is often a compromise between metal quality and yield. Recent advances in gating systems with counter gravity filling in aluminum alloys have shown a reduction in the overall level of defects, however the beneficial use of these systems at reducing the level of inclusions and bifilm defects has not been proven out. In addition, these gating systems often add additional mass to the system and can reduce the already poor yield of steel castings when compared with aluminum alloys. Molten metal filtration using various types of ceramic filters in the gating system is another solution remove inclusions. However, the efficiency of inclusion filtration varies with the type of filter and has been shown to be a function of physical and chemical characteristics of the inclusion [11]. In addition, many foundries are hesitant to add filters as they create additional expense. Modern use of computational fluid mechanics and heat transfer simulation packages that model filling and solidification have greatly enhanced the ability to spot potential areas of excessive metal velocity and air entrainment. Commercially available simulation packages can model the change in metal flow due to the incorporation of filters, however, they cannot predict the filtration efficiency of the filter. Additionally, these simulation tools do not incorporate the actual formation of oxide defects during different filling conditions and they cannot predict the effect of filling related defects on porosity or mechanical properties. In addition, the computational models do not take into account the thermodynamics or morphology of inclusion and bifilm formation that will be different based on the chemistry and deoxidation practice of the steel. Because of this, serious consequences can occur when attempting to interpret simulation results. This highlights the need for studies that link filling and

solidification modeling to actual measured defect levels as a function of gating practice and the associated effect on mechanical properties.

High manganese and aluminum steels, or Fe-Mn-Al steels, are particularly sensitive to reoxidation and solid oxide film formation during melt transfer operations and mold filling. These steels typically contain between 3-12 wt.% of aluminum, which is balanced by additions of 15 to 30 wt.% Mn and 0.7 to 1.2% wt.% C to produce a mainly austenitic steel with high combinations of strength and toughness.[12] Depending on the composition, the addition of Al produces up to an 18% reduction in density below that of quenched and tempered martensitic steels without a sacrifice in mechanical properties.[13] However, the elevated levels of aluminum also promote the formation of alumina bifilms during melting and pouring of these steels. Figure 1.1 (a) shows an optical micrograph of an oxide bifilm defect in a Fe-Mn-Al steel casting caused by turbulent filling of the mold cavity. These bifilm defects cause a reduction in Charpy V notch, CVN, impact toughness and an oxide bifilm defect are shown covering the fracture surface in Figure 1.1 (b). Oxide bifilms in FeMnAl steels can also absorb nitrogen resulting in nucleation of gas porosity as well as precipitation of AlN plates during subsequent heat treatment.

Solid AlN inclusions are also stable in FeMnAl steels during steelmaking and their hard and angular morphology negatively affects ductility and toughness. As shown in Figure 1.1 (c), the CVN breaking energy at -40°C in a nominal Fe-30wt.%Mn-9wt.%Al-1wt.%Si-0.9wt.%C-0.5 wt.% Mo composition steel was reduced by almost 50% when the AlN particle density increased to 50 inclusions/mm^2.[14]
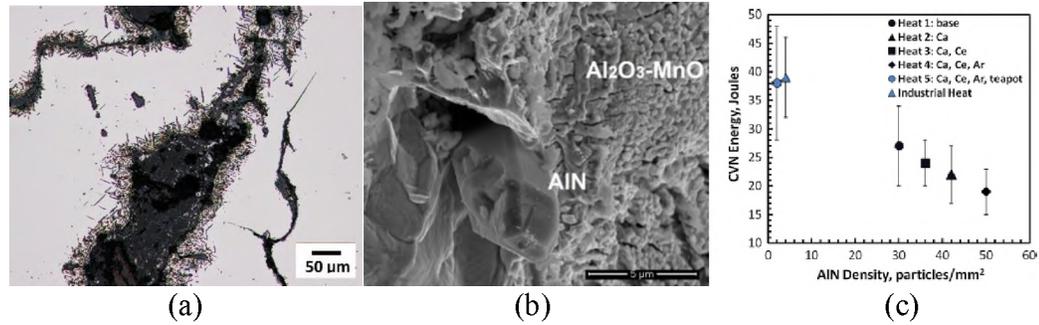
Figure 1.1. Defects in FeMnAl castings. (a) Optical micrograph of an oxide bifilm defect in a Fe-Mn-Al steel casting caused by turbulent filling of the mold cavity. (b) The secondary electron micrograph of a fractured Charpy V notch, CVN, test specimen shows that low energy fracture was initiated by a large complex aluminum oxide bifilm defect. (c) CVN, breaking energy at -40°C in a nominal Fe-30%Mn-9%Al-1%Si-0.9%C-0.5%Mo composition steel is a strong function of AlN particle density [14]

The above review highlights three very important conclusion: bifilm and inclusion defects caused by pouring and mold filling can greatly decrease the quality and toughness of steel castings, computational models cannot currently predict their occurrence, and the filling conditions that produce these defects are not well understood or controlled. This discussion shows the need for a comprehensive study to quantitatively evaluate the role of different filling conditions on steel casting quality and mechanical properties. The goal will be to determine a best practices gating system for FeMnAl steel castings in comparison to gating systems commonly used for high strength low alloy steel castings. In the current study, a combination of computational fluid dynamics and solidification modeling software was utilized to design a series of identical laboratory and industrially produced steel test castings with different gating systems to produce different filling conditions; (1) a horizontal gated pressurized system, (2) a horizontal gated non-pressurized system, and (3) two different naturally pressurized systems that employed a terminal vortex spin trap at the end of the runner. The efficiency of inclusion removal by filtration utilizing a ceramic

foam filter was also evaluated. The ability of these gating systems to reduce inclusions and bifilm defects in a lightweight FeMnAl steel was quantitatively compared to that of a cast composition of SAE 8630 steel utilizing a combination of computational fluid dynamics, optical metallography, automated non-metallic inclusion analysis, and evaluation of CVN impact toughness. The outcome of this project is intended to significantly increase the technical understanding of how filling affects metal quality and mechanical properties in steel castings that are prone to reoxidation defects.

1.2. NON-METALLIC INCLUSIONS IN STEEL

Efforts to control non-metallic inclusions in steel have gained prominence over the last 50 years because of the increased demand for cleaner steels with higher mechanical property performance. A greater understanding of the effect of the type, size and morphology of inclusions, casting performance combined with research on their origins within the manufacturing process have led to increased casting quality and a reduction in costs associated with defect re-work and casting rejections.

1.2.1. Classification of Inclusions. The sources of inclusion formation can be briefly described as exogenous or endogenous in nature. The inclusions that are generated primarily in the steelmaking process (deoxidation practices) are called endogenous inclusions, while inclusions which originate from the external sources like worn-out refractories, reoxidation and entrapped slag are called exogenous inclusions. Most inclusions can be classified as oxides, sulfides, or nitride-based inclusions. [1]

Endogenous inclusions are formed in liquid steel because of deoxidation practice and subsequent refining additions as well as during cooling and solidification. The deoxidation practice generally dictates type, number, size, and distribution of endogenous

inclusions in steel castings. Deoxidation is the practice of adding small amounts of reactive elements to liquid steel that have a high thermodynamic affinity to react with dissolved oxygen within the melt. This aids in the removal of excess oxygen from steel by forming stable solid or liquid oxide inclusions, thus preventing the formation of blow holes that are formed when the oxygen in steel combines with the excess carbon to form carbon monoxide. [15] The most common deoxidizers used in steel foundries are aluminum, manganese, silicon, and calcium or a combination of these elements. Sometimes complex deoxidation practices are also performed in the presence of other metals like titanium and zirconium that are used to control nitrogen. This process of addition of deoxidizers to steel is called killing the steel, since there is no gas evolution during solidification.

Solid alumina in low alloy aluminum killed steels and liquid manganese silicate inclusions in manganese and silicon killed steels are the primary deoxidation products.[2] Various alumina morphologies have been reported in steel like dendritic, faceted, aggregates, planar and spherical. The morphology of these inclusions and their growth is controlled by a variety of factors like holding time, liquid flow conditions and the degree of supersaturation with respect to dissolved aluminum and oxygen.[16] The spherical alumina inclusions shown in Figure 1.2 (a) are singular and have a sizes that typically range from 1μm to 5 μm. Faceted inclusions in Figure 1.2(b) occur as a result of slow growth rate in Al-killed steels and are obtained at low degrees of supersaturation. As shown by Steinmetz et al., the effect of deoxidant and oxygen concentration on oxide inclusion morphology is shown schematically as seen in Figure 1.3. At low deoxidation levels, spherical inclusions are formed. As the deoxidizer activity continuously increases, oxides become more stable, leading to dendritic growth of inclusions by accelerated growth rates.

As the activity of O decreases and the activity of deoxidizer increases, the dendritic growth become more compact changing to faceted shapes.[19] The formation of clustered alumina results from the collision and coalescence of individual inclusions because of high convective currents in the melt and a high difference in surface energy with the molten steel as seen in Figure 1.2(c).[15,17] Clustered inclusions and sharp and angular inclusions are generally more detrimental to toughness than spherical inclusions that are isolated.

(a)   (b)   (c)
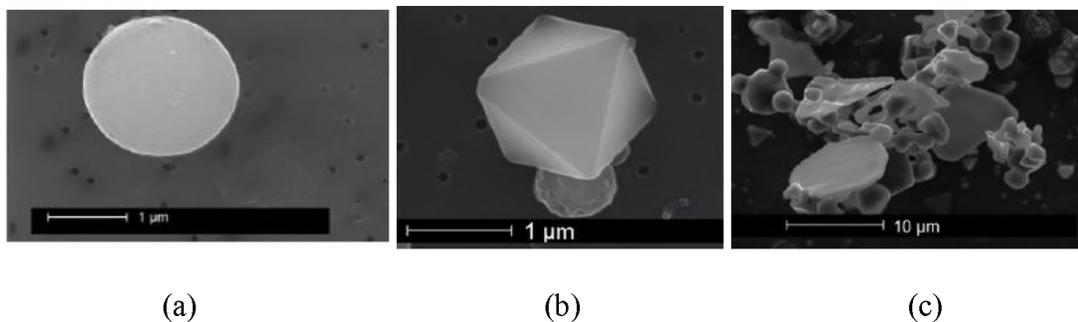
Figure 1.2. Morphologies of alumina inclusions. (a) The alumina inclusions are formed in various morphologies like (a) spherical (b) faceted and (c) clusters. The faceted inclusions are products of slow growth rates while clusters are formed because of high convective currents in the melt [18]

Precipitated inclusions are formed during the cooling and solidification stages of steelmaking and occur when the concentration of nitrogen/sulfur/oxygen in steels reduces and their solubility increases. [2] Sulfide inclusions precipitate during the final stages of solidification as the remaining liquid is enriched in sulfur. These sulfides are mainly manganese sulfide inclusions. The morphology and distribution of manganese sulfide inclusions have a significant effect on final properties of steel. [20, 21] Type I manganese sulfide inclusions are globular in shape and distributed randomly. These inclusions are formed when the activity of oxygen is high in the melt and are prevalent in Mn and Si

killed steels. Type II MnS inclusions occur as dendritic or fan like structures on grain boundaries and are eutectic in shape and distribution. These inclusions are found in steels in which strong deoxidizers like Ti and Al are used. Type II MnS are the most detrimental to toughness and elongation. The Type II inclusions occur in colonies and their volume fraction increases with the sulfur content of steel and cooling rate.
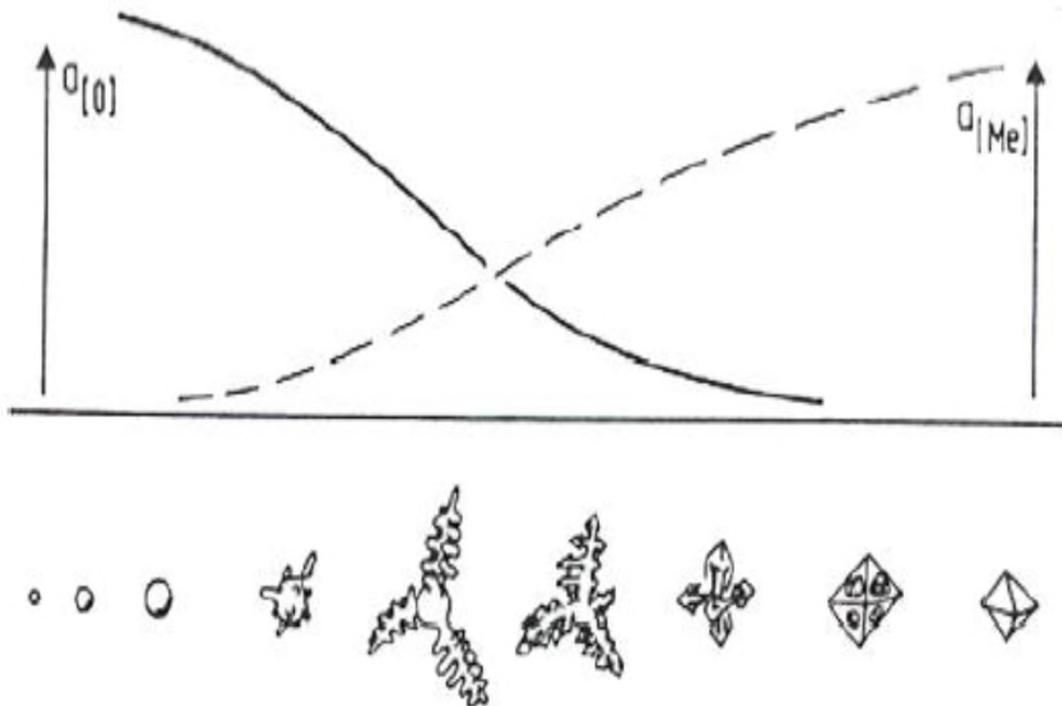
Figure 1.3. The growth of the different morphologies of oxide inclusions shown as a function of the deoxidizer activity (dashed line) and O activity (solid line) [19]

Type III MnS have an irregular shape and are isolated. Both type II and type III sulfides are more deleterious to the properties of steel than type I. The different types of manganese sulfide inclusions are shown in Figure 1.4. [22]

Depending on the steel composition and deoxidation conditions, different nitride inclusions are also stable in liquid steel. For example, it is well known that TiN is stable during steelmaking and casting.

<div align="center">(a)   (b)   (c)</div>
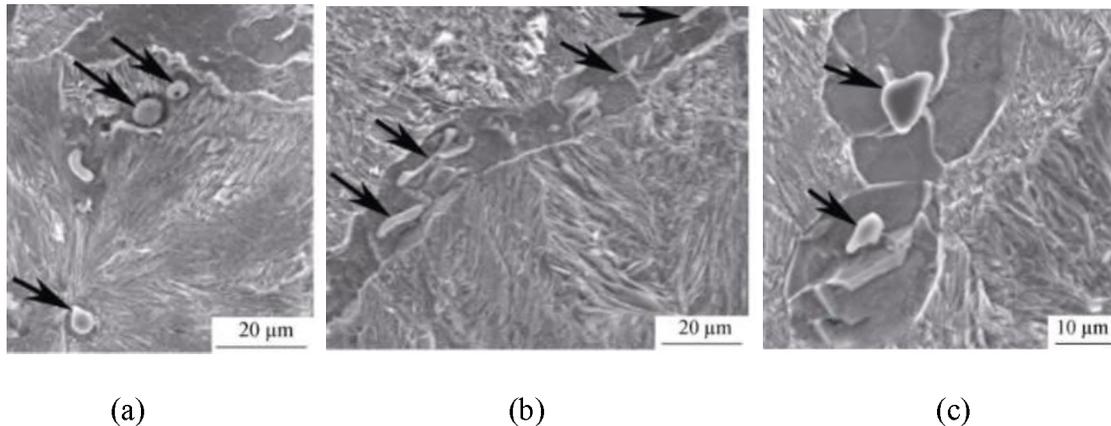
Figure 1.4. The manganese sulfides appear in various morphologies as shown in (a) globular type I sulfide (b) eutectic type II sulfide (c) type III angular faceted sulfide [20]

For that reason, Ti is commonly added before pouring to getter nitrogen and prevent embrittlement from AlN precipitation on austenite grain boundaries in the solid state. However, in FeMnAl steels, these inclusions are stable in the liquid. AlN inclusions have a hexagonal crystal structure and are observed to possess an angular morphology. [23, 24] The work done by Gigacher et al. [25] on high Mn-Al alloyed steel, show that AlN inclusions along with MnS are formed as primary inclusions in the melt. The influence of oxygen in AlN formation is high, since both oxygen and nitrogen compete with aluminum for formation of either alumina or AlN, respectively. Manganese is known to increase the solubility of nitrogen in steel and this increases the amount of AlN formation in FeMnAl steels as shown for a Fe-20Mn-1.3Al steel in work done by Park et al. [26]

The presence of these hard and angular AlN and Al_2O_3 inclusions are detrimental to the mechanical properties of high strength steels, especially ductility and notch toughness. Schulte et al. showed almost a 50% reduction in CVN toughness in a Fe-30wt.%Mn-9wt.%Al-1wt.%Si-0.9wt.%C-0.5 wt.% Mo when the number density of AlN inclusions increased to more than $50/mm^2$.[14] Hard alumina and AlN inclusions can also cause excessive tool wear during machining. MnS inclusions are more ductile, however, in high amounts, these inclusions can also result in poor ductility and toughness in both steel castings and hot rolled steels [28].

Exogenous inclusions result from outside of the deoxidation practices and subsequent precipitation reactions that happen as the steel solidifies and cools. These inclusions are the result of slag entrainment, entrainment of worn refractories, or as a consequence of reoxidation. Reoxidation inclusions are exogenous inclusions that are products of unintentional reaction of the liquid metal with the air. The work by Beckerman [30] on the composition of reoxidation inclusions shows that the composition of the inclusions varies as a function of deoxidation practice and oxygen concentration. Air entrainment during melt transfer and mold filling leads to reoxidation inclusions which is one of the most common sources of endogenous inclusions in steel castings. Reoxidation inclusions affect a number of various quality aspects of steel castings such as surface quality, machinability, and mechanical properties. High molten metal velocity, splashing, as well as improper gating system designs containing sharp corners, abrupt changes in direction, and downhill filling conditions all lead to the formation of reoxidation inclusions in steel.[31]. Once these inclusions are formed, they travel to the casting cavity and end up in the final part. [32]. The work by Griffin and Bates in 1991[5]. showed that reoxidation

inclusions lead to 83% of inclusions in low alloy steel castings and 48% of inclusions in stainless steel castings as shown in Figure 1.5.[5] Air entrainment and air entrapment are two distinct concepts that are often misunderstood in the metal casting industry. While air entrainment is the formation of bubbles which form due to irregularities in the flow of the molten metal, air entrapment refers to formation of pockets of air in the molten metal due to poor mold design or improper venting.
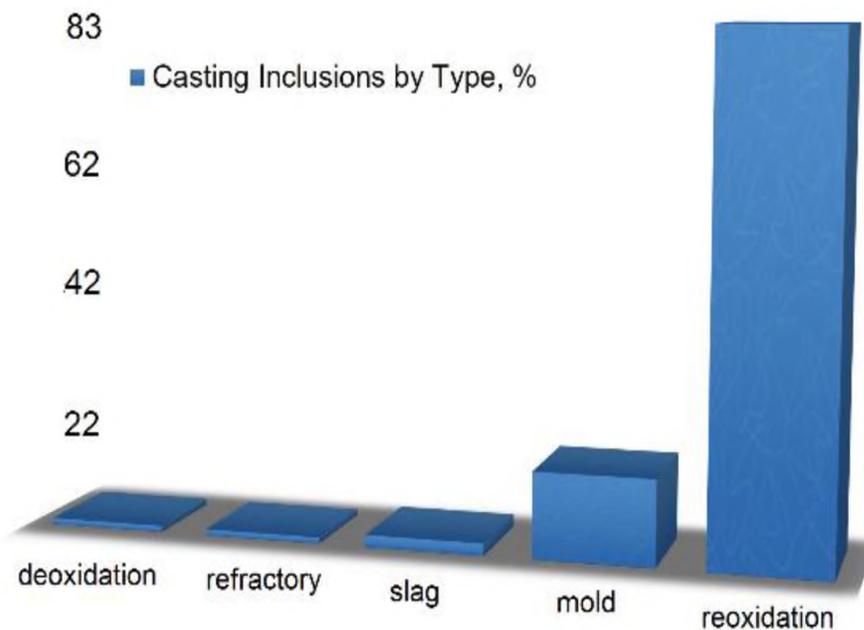
Figure 1.5. The work by Griffin and Bates showed that 83 % of all inclusions in low alloy steel castings are caused as the result of reoxidation [5]

. The work done by AJ. Melendez et al. [33] showed the inclusion volume fraction as a function of relative volume of entrained air, as observed in Figure 1.6, during mold filling. For air at room temperature it is seen that 3.5 cubic feet of air is entrained per cubic foot of steel during mold filling conditions. This leads to the presence of one cubic inch of inclusions per cubic foot of steel for a low alloy steel [34]. The exogenous inclusions can

also act as sites for heterogeneous nucleation for precipitation of new inclusions that form

from the breakdown of the slag and dross that are formed during steelmaking operations.

[16,24] Moreover, the glazed slag layer from previous pours can contaminate ladles and result

in exogenous inclusion formation. The erosion of the refractory lining and walls are

another major source of exogenous inclusions.[24]
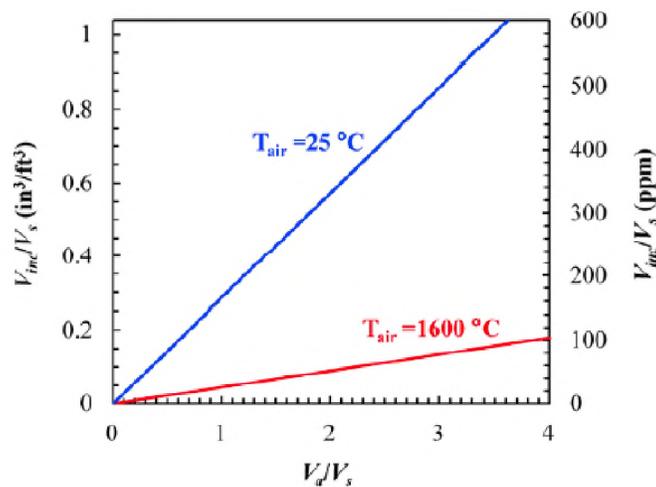
Figure 1.6. For a low carbon alloy steel, the variation in total inclusion volume (V_{inc}) is shown as a function of relative entrained air volume (V_a) at room temperature and when air is at 1600°C [34]. V_s indicates the total steel volume in the mold

1.2.2. Effect of Inclusions on Casting Quality. The presence of inclusions has a

negative impact on the mechanical properties of steel castings like fracture toughness,

tensile strength, and fatigue. The mechanical properties of a particular type of steel are

affected by various properties of the inclusions like their quantity, type, size, orientation,

and distribution.[24] Though the inclusions can be classified as micro and macro inclusions

according to their size, the shape of the inclusions also plays an important role. As shown

in Figure 1.10(a), ductile fracture in steels occurs by the process of nucleation, growth, and

coalescence of microvoids around inclusions and other second phase precipitants, leading

to final fracture. If the steel matrix is ductile enough to accommodate the plastic strain, this will result in crack tip blunting during fracture as shown in Figure 1.7 (a). In the case of brittle fracture, the presence of inclusions in the matrix, act as sites for cleavage crack initiation as seen in Figure 1.7(b). [35] For steels with high strength and sufficient ductility, such as quenched and tempered martensitic steels and FeMnAl steels, ductile fracture is the predominant fracture mode.

Ductile fracture happens by the following steps:

- Nucleation of voids around hard particles in the matrix by cleavage or debonding

- Growth of voids caused by these failures

- Coalescing of voids and their joining with the main crack

This leads to a formation of a fractured surface with a fibrous appearance characterized by dimples or cup and cone fracture.[36] For steels of similar microstructures and chemistries, the fracture toughness is influenced by various factors that such as the type, size, morphology, and distribution of inclusions as well as the solidification structure and the segregation of impurities. Deoxidation practice and oxygen content plays a major role because it affects the shape, morphology and distribution of inclusions.[16] The presence of strong deoxidizers like aluminum promotes type II eutectic sulfides which have a dendritic structure and are distributed as chain like formations along grain boundaries. These sulfides act as extreme stress raisers and are associated with low ductility in steel.[21] The work done by Chao Gu et al.(37), shows the stress distribution in the steel matrix around simulated Mg-Al-O, Al-Ca-O-S, TiN and MnS inclusions as shown in Figure 1.8. It is observed that the residual stress changes with the shape of the inclusion. Sharp edged

inclusions acted as severe stress raisers leading to stress concentrations as high as 2GPa at the inclusion-steel interface.

(a)   (b)
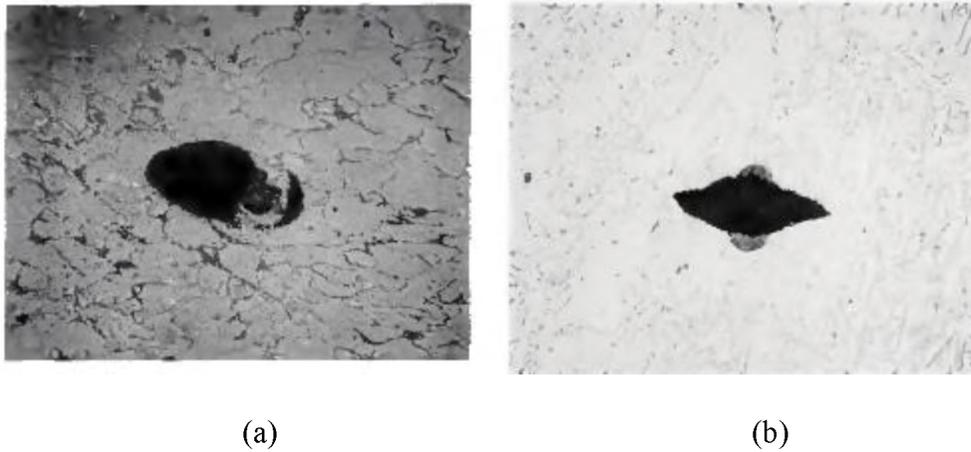
Figure 1.7. Inclusions leading to fracture. (a) An inclusion acting as a nucleation site for microvoid nucleation leading to ductile fracture (b) an inclusion acting as an initiator of a cleavage crack leading to brittle fracture [35]

(a)   (b)
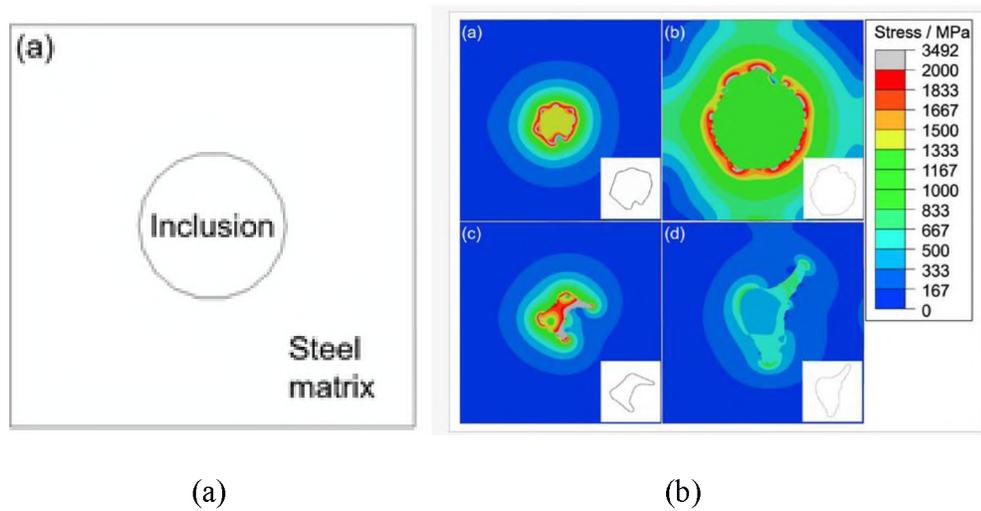
Figure 1.8. The stress concentration between different inclusions and steel matrix was simulated for different inclusion types and morphologies. (a) MgAlO (b) Al-Ca-O-S (c) TiN (d) MnS [37]

The nucleation of voids is therefore easier when the inclusion is hard and rigid and angular or when the inclusion has low cohesion with the surrounding matrix. It is observed that for hard and brittle inclusions, the void formation can be by inclusion fracture in the plastic zone ahead of the crack tip or by decohesion at the interface of inclusion/matrix.[38]. Bartlett et al. showed that the presence of TiN inclusions in 4130 steels lead to brittle fracture causing large void formation from fractured TiN that drastically reduced toughness. Heats that were deoxidized with Ca or Al, displayed globular inclusions with ductile fracture and higher dynamic fracture toughness. Reducing the inclusion content is shown to increase resistance to void nucleation and improve mechanical properties of steel. [4] The work by Knott et al., shows that decreasing the volume fraction of sulfide inclusions increases the crack opening displacement of steel.[39]. The presence of small inclusions are not as significant in crack initiation as very large inclusions are >5μm, although they do encourage in crack propagation and low energy fracture when they are closely spaced as seen in Figure 1.9.[38]
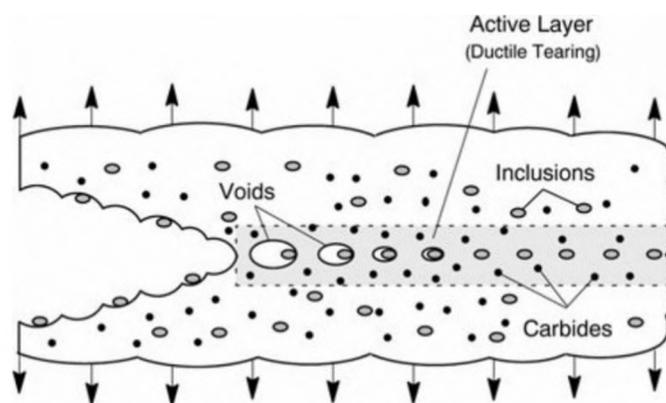
Figure 1.9. The nucleation of micro voids created by the presence of inclusions aiding in crack propagation and subsequent fracture [38]

Various models have been proposed by researchers to understand the effects of volume fraction, spacing, inclusion density and resistance to void nucleation on fracture toughness in high strength steels. The work done by Speich and Spitz on the impact of sulfide inclusions on Charpy V notch test of 4340 alloys, showed that the measure of toughness increased with decreasing volume fraction of manganese sulfide inclusions [40]. The model proposed by Rice and Johnson is given in equation 3.

$$K_{IC} = (2YEL)^{0.5} \tag{1}$$

Here, K_{IC} is the critical stress intensity factor, Y is the yield strength, E is the elastic modulus and L is the distance between inclusions. The fracture toughness, evaluated as critical stress intensity factor (K_{IC}) directly increases with the distance between the inclusions.[41]

Hahn et al. expanding on the above work and the following relationship is given in equation 4.

$$K_{IC} = [2YE \, (\Pi/6)^{(1/3)} \, D] \, F^{(-1/6)} \tag{2}$$

Here, D is the diameter of inclusions and F is the volume fraction of inclusions. It shows an increase in the spacing between inclusions with decreasing volume fraction. [4,42]

1.3. BIFILMS

1.3.1. Formation. Bifilms are formed when highly surface reactive molten metal is exposed to oxygen in the air and forms a solid oxide film on the surface which can become folded over itself and entrained within the melt. Since the internal layers of these

oxide films are not bonded together, they often contain a layer of entrapped gas. The formation of solid oxide bifilms is depicted in Figure 1.10. [43] Bifilms can be formed as a result of turbulent flow, eddy currents, and fragmentation of the molten metal meniscus during melt transfer, pouring, and mold filling operations. These films can also absorb gasses and serve as heterogeneous sites for gas and micro shrinkage porosity during solidification. [6] The presence of bifilms exerts a major influence on the reduction of resulting mechanical properties.
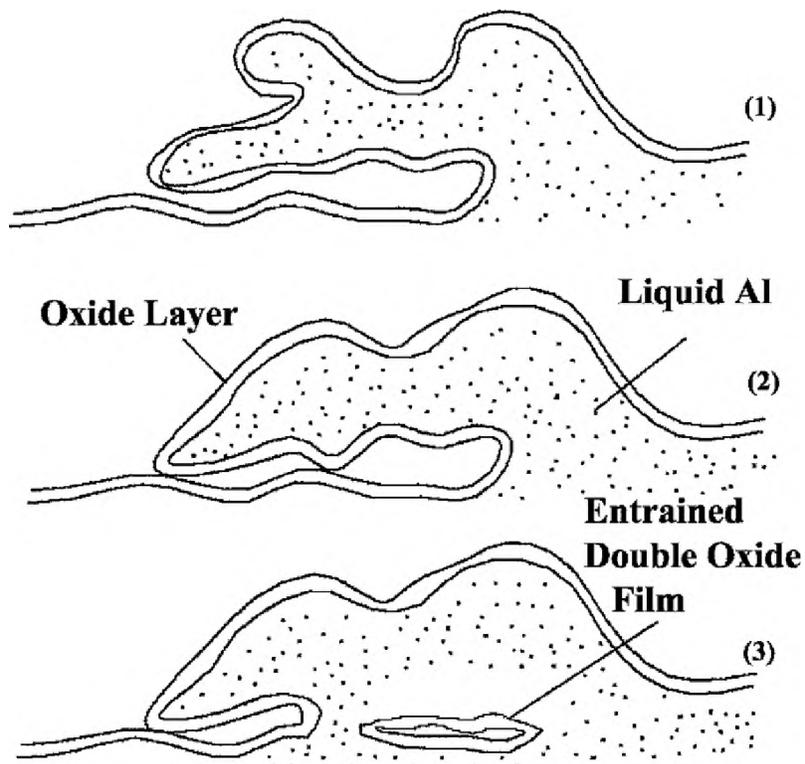
Figure 1.10. The formation of a bifilm defect generally takes place due to turbulent flow of metal. In the image (1) the turbulence in aluminum is observed while the image (2) shows the formation of bifilm with two unbonded internal side wetted by all direction in the outer direction [43]

Aluminum alloys are known to be especially sensitive to the formation of bifilm defects during furnace charging, melt transfer, and pouring operations. These oxide biflms are not able to readily float to the surface and be removed as well as discrete oxide particles.

The feature of an unbonded internal surface with a perfectly wetted outer surface is a key component of bifilms.[8,44] Surface turbulence is a major reason for bifilm formation and this is largely because of gravity pouring and creation of a plunging jet and poorly designed gating or rigging systems that encourage turbulent filling and splashing. Each time the surface of the liquid metal is broken, new surfaces are exposed to air leading to high entrainment of gases. [45] The effect of pouring distance was studied by Pavlak et al. on Al-7Si-Mg-Cu alloy. Pouring distance increases the velocity at the base of the downsprue and increased amount of gas porosity and oxide film formation. [46]

Bifilms are formed in different shapes and sizes like tangled, network layer, globular or strip clustered. They can appear as wrinkles on the casting surface or just beneath the surface and are sometimes several millimeters in thickness depending on their age. The young bifilms are characterized by their low thickness with only a few nanometers and are formed with relatively short oxidation times.[8] Formation of MgO bifilms have also been observed in ductile iron castings and can leads to cracking and failures. [7]

Hydrogen porosity nucleation in bifilms has been a major source of concern for researchers. It is seen that hydrogen porosity cannot nucleate heterogeneously or homogenously without the presence of bifilms. The work by Dispinar et al., shows that hydrogen gas entrapped in excess of solubility limit, comes out of solution and expands the bifilms into a pore as seen in Figure 1.11. [47]

Since the bifilms are formed in all size and shapes, these defects constitute some of the most detrimental defects in castings. The work done by Griffith and Sayed, on gassed and degassed Al-7Si-0.3Mg alloys shows that, the size of the oxide films was directly related to the amount of H found in the castings. When H content was $0.18cm^3/100g$ Al, they found films of area $4mm^2$ while for $0.08cm^3/100g$ Al the bifilm are area reduced to $1.8mm^2$.[48]
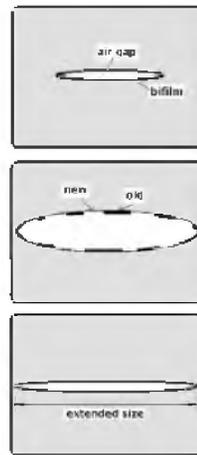
Figure 1.11. Hydrogen induced porosity formation. (a) The bifilm observed with an air gap in the matrix (b) the formation of an dense and an thin layer of bifilm that is formed because of pore expansion due to hydrogen diffusion or pressure change (c) The new enlarged area of the bifilm preventing its return to normal size [47]

1.3.2. Effect on Mechanical Properties. The presence of bifilms has a negative impact on the mechanical strength of the castings. For example, it was found that the bifilm index had an impact on the ultimate tensile strength and the elongation in A356 alloys as shown in the Figure 1.12.[47] The Weibull analysis performed on Al-7Si-0.3Mg castings showed that decreasing hydrogen content in bifilms caused a 400% increase in Weibull modulus and a 200% increase in elongation.[8] The work done by Liu and Samuel of A356

castings, established a linear relationship between the percentage elongation and log area percentage inclusions/oxide films.[49] The work done by Hsu et al., on ductile iron (ASTM 60-42-10) castings using different gating systems shows a clear impact of turbulence and bifilms on mechanical properties of castings. They used a top gating and a bottom gating system with a ceramic filter, and the Weibull modulus of 3.4 in the top gated system with a horizontal casting and 12 in the bottom gated system with a vertical casting as seen in Figure 1.13. This is attributed to the random distribution of bifilms in the top gated systems.[7]
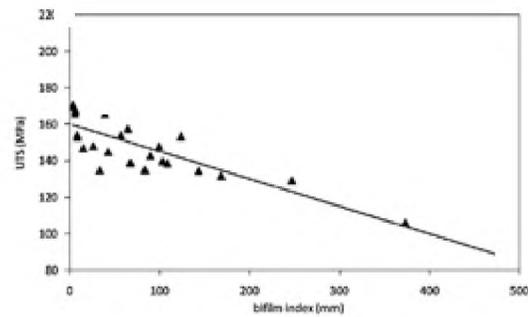
(a)
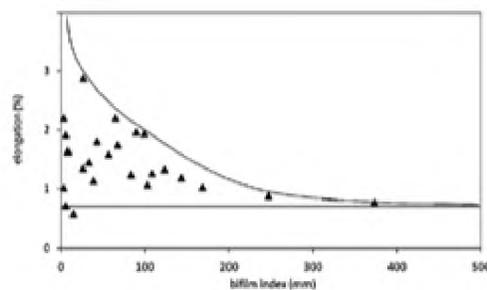
(b)

Figure 1.12. The RPT was performed on A356 alloys, showing that the bifilm index had a direct impact on the (a) ultimate tensile strength and (b) elongation in the test specimens [47]
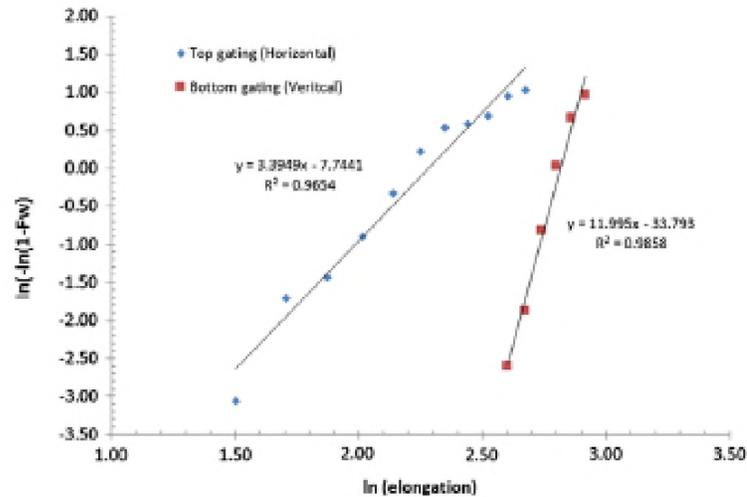
Figure 1.13. The Weibull modulus for the top gated system is 3.4 while for the bottom gated system it was observed to be 12. The difference in elongation, was attributed to the random distribution of bifilms in the top gated system [7]

In carbon steel castings, when right amount of deoxidizers (Al and Ca) are not used, it leads to the generation of thick solid oxide films. [50] This causes deep folds constituting of bifilms on the surface. When the surface oxide of the bifilm, is partially melted it gets scrambled in the melt and transforms into a sticky ball which floats out easily.[51] When the oxide film formed has a high melting temperature, it forms as a solid oxide film and gets entrained in the liquid melt. Some authors have suggested that bifilms in steel are also responsible for gas porosity and the resulting reduction in mechanical properties.[52] The presence of these bifilms can act as cracks, initiating failure. As previously noted, bifilm formation in FeMnAl steels can be problematic and is attributed to the high aluminum content of these alloys.

1.4. HIGH MANGANESE HIGH ALUMINUM STEELS

The high manganese high aluminum steel or FeMnAl steel is a derivative of austenitic manganese steel that was first developed by Sir Robert Hadfield in 1882.[53] FeMnAl steels generally contain 0.7-1.4% carbon, 6-25% manganese and 5-12% aluminum and possess properties like high toughness, high wear resistance, and oxidation resistance.[12]

The reduction density is mainly found to be a function of aluminum and manganese [13]. The presence of aluminum in these alloys offers a reduction density as observed in Figure 1.14, where a linear reduction is density is found as a combination of lattice parameter dilation and mass reduction as a function of aluminum. From the Figure 1.14, a reduction of 17% density is observed for a 12% aluminum addition.
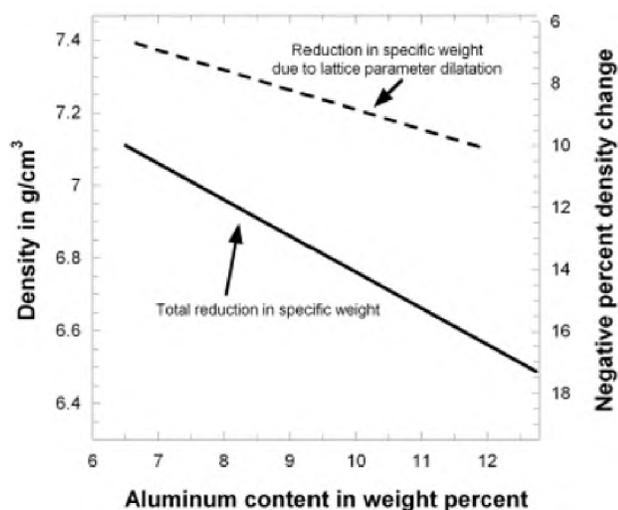
Figure 1.14. Increasing the aluminum from 6.5 to 12% in a Fe-30Mn-XAl-0.9C steel leads to a total reduction in density from 7.5 to 6.2 g/cm^{3}[13]

The work done by Kalashnikov et al. to achieve the best combination of strength, ductility and impact toughness in FeMnAl alloys shows that, a composition of 25-31%Mn,

6.2-9.7%Al, 0.7-1%C is optimum.[54] The addition of silicon is shown to prevent the precipitation of β-Mn[55] while the addition of molybdenum was shown to mitigate the impact of phosphorus on the fracture toughness in steel[56]. Thus, an alloy composition of Fe-28-30Mn-9Al-1C-0.9Si-0.5Mo has been commonly used by researchers for investigation. [57-59]

1.4.1. Composition and Heat Treatment. The strength of FeMnAl steel can be greatly increased by the precipitation of κ-carbides during aging. It was observed in FeMnAl alloys that at sufficiently high carbon and Al concentration, these alloys age hardened between 550-600°C providing a Brinell hardness between 345-475.[60,61]After age hardening alloys with 20-35%Mn, 10%Al, and 0.4%-1.4%C four phases have been identified (austenite, ferrite, κ-carbide, and β-Mn).[62]. Increased amounts of aluminum or carbon is linked to higher volume fraction of κ -carbide volume fraction while prolonged aging leads to β-Mn precipitation and loss of tensile ductility.[63]. Homogenous precipitation of κ-carbide happens under 650°C, while above 650°C, heterogeneous nucleation of κ-carbide appears on grain boundaries. Between temperatures of 500-650°C, the greatest strength in FeMnAl alloys have been reported and the aging temperature of 550°C has been commonly reported for alloys of composition Fe-30Mn-9Al-1C-0.9Si-0.5Mo.[13,61,64]Before aging, the FeMnAl specimens are solution treated at temperatures of 1000°C or greater.[57]. For a FeMnAl alloy of composition Fe-30Mn-9Al-0.9C, δ-ferrite is the primary phase followed by austenite formation well after the liquidus temperature of 1332°C. [65]In solution treated condition, an austenitic matrix with less than 10% ferrite was observed. For a fully austenitic microstructure steel, yield strengths up to 700Mpa and Charpy V notch toughness up to 200J have been observed. For an alloy composition of Fe-

32Mn-8.5Al-0.9C tensile strengths of up to 823Mpa with elongations of 64% have been reported in the solution treated condition [66]. Solution treated steels have a higher impact toughness but lower strength than the aged steels due to the precipitation of κ-carbides in aged specimens. κ-carbide precipitation increases the strength and hardness in aged steels but reduces impact toughness leading to brittle fracture in overaged steels. However, work done by Van Aken et al. for a steel composition of Fe-30.4Mn-8.83Al-1.07Si-0.9C-0.53Mo showed good combinations of both strength and toughness in underaged steels with ultimate tensile strengths of 953Mpa and a CVN toughness of 37 J at -40°C. [68]

1.4.2. Inclusions. The presence of high aluminum and manganese contents in FeMnAl steel affects leads to the formation of oxide and nitride inclusions as well as solid oxide bifilms. Inclusions like AlN, AlN-MnO, AlN-MnS and MnS have been frequently reported in high aluminum high manganese steels.[69] The presence of Al_2O_3 , MnO and $MnAl_2O_4$ have also been reported in a few studies.[69-70]The morphologies of different inclusions formed in a Fe-(10-20)Mn-(1-6.0)Al steel are shown in Figure 1.15.[70] The work done by Schulte et al. on nominal Fe-30Mn-9Al-1Si-0.9C-0.5Mo steel shows that the presence of AlN inclusions have direct impact on reducing the CVN energy. An increase in concentration of aluminum nitride inclusions from 12 inclusions/mm^2 to 210 inclusions/mm^2 resulted in a decrease in Charpy v notch toughness from 35J to 19J at -40°C [14). The use of a teapot style ladle for pouring the castings helped to reduce entrained inclusions and increase the notch toughness from 10J to 40J. Ductile fracture as a result of microvoid nucleation and coalescence around AlN inclusions was found to be the major failure mode.
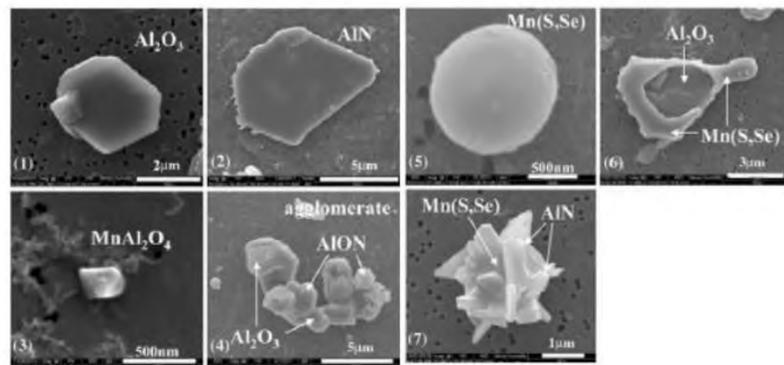
Figure 1.15. Secondary electron images of the different inclusions identified by Park et al. in a Fe-(10-20) Mn-(1-6) Al composition steel [70]

1.5. FILTRATION

Refining of inclusions in steel is a process which has challenged steelmakers for a long time and this process can be broadly classified as chemical and physical process. While ladle refining can be classified as a chemical refining process, filtration is classified as a physical refining process. Filters are widely used for both aluminum and steel castings and they can be broadly classified as three types, monolithic filters, tabular filters and foam ceramic filters (FCF) as shown in Figure 1.16[71-75]. The foam ceramic filters are considered one of the best in the casting industry because of their properties like high filtration efficiency, turbulence reduction, good refractoriness and their ability to resist erosion.[75]

1.5.1. Filtration Mechanism. The filtration mechanisms can be of two types, cake filtration and deep bed filtration namely. In cake bed filtration, inclusions accumulate on the surface of the filter where the inclusions are similar in size or larger than the diameter of the pores. The other kind of filtration is called the deep bed filtration which occurs where the particles having a diameter smaller than the pore. In this case the inclusions get attached to the walls of the pores. In the cake filtration method, there is a large rise is back pressure

or ΔP with inclusion capture while in deep bed filtration a more gradual rise in ΔP with inclusion capture is observed. This is mainly because the inclusions are distributed throughout the filter thickness in deep bed filtration. It should be noted in the deep bed filtration that the diameter of the particles are smaller than the smallest opening, the "window size" as shown in Figure 1.17. The filters are usually classified based on the size of the pores which are represented as "ppi" (pores per inch).
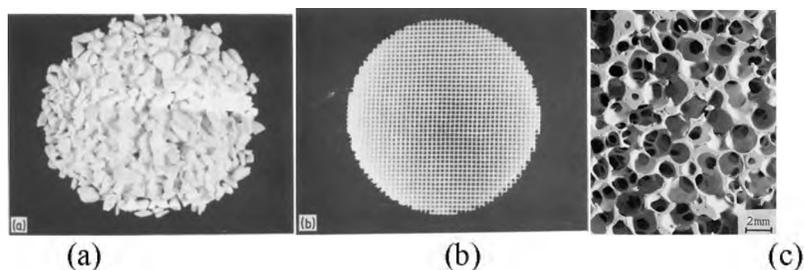
Figure 1.16. Photographs showing (a) tabular filters (b) monolithic filters [9] (c) ceramic foam filters [72]

(a)
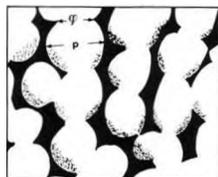
(b)

Figure 1.17. Cake filtration showing the filter medium. (a) The wavy lines and particles represent the incoming inclusions and impurities in the melt (b) the deep bed filtration process where "p" represents the cell size and Ø represents the "window size"[72]

The structure of the foam filter is designed in such a way that it has an unique, tortuous path which helps the inclusions to get trapped in the walls which not only allows for inclusion removal but also ensures smooth turbulent free filling into the casting cavity as seen in Figure 1.18 [74]
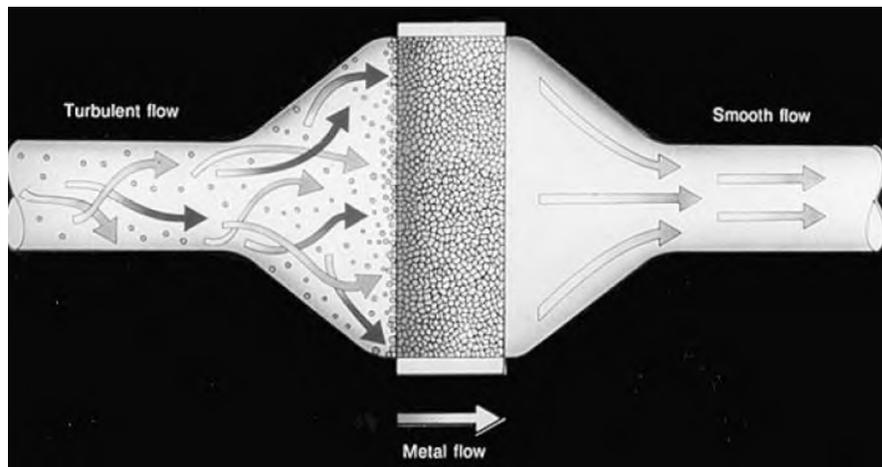
Figure 1.18. A filter enables in trapping particles from the incoming metal and helps to reduce turbulence when the metal passes to the other side of the filter [74]

The inclusion removal efficiency of a filter is determined by the following equation 1, [71]

$$\eta = \frac{C_i - C_0}{C_i}$$

(3)

η = inclusion filtration efficiency

C_i = concentration of inclusions in the melt at the inlet to the filter

C_o = concentration of inclusions in the melt at the outlet of the filter

1.5.2. Parameters Affecting Filtration. There are various parameters which determine the efficiency of inclusion removal in a filter. They are tortuosity, wetting behavior, permeability, pore count, velocity of the melt, length of the filter and alloy type. [91,92,93]. Tortuosity can be briefly described as the ratio between the original path that a fluid undertakes in its streamlined motion and the path during its convoluted flow in a porous media as shown in Figure 1.19. Work by GS Armatas [75], has shown that for porous media, if we consider only the pore geometry and no other parameters, the matrix which contains a high porosity/low ppi will have the least tortuosity and vice versa.
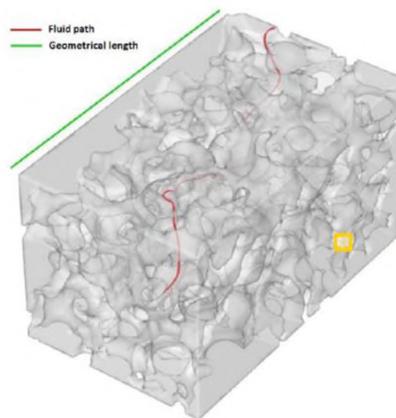
Figure 1.19. The comparison between the streamlined flow of a fluid (green line) and the flow path of the fluid inside a porous media (red line) [76]

The work done by Sarina Bao et al.[77] on Al_2O_3 and SiC, shows that wetting is dependent on temperature, since higher temperatures leads to a decrease in surface tension and improves wettability. The permeability of a filter can be used to characterize ceramic foam filters (FCF) since they aid in predicting pressure drop at a specific flow rate or vice versa. The experiments conducted by Kexu Zhang[73] on permeability of CFF of different ppi shows that there is no specific permeability for a type of filter and it is a factor which

is expressed as a function of fluid flow. Regarding the effect of velocity of metal flow on the filter, the equation derived by Apelian et al. as shown in the following equation (2). [71]

$$\eta = 1 - \exp\left(-\frac{K_0 L}{U_m}\right)$$

(4)

where, η = filtration efficiency

K_0 = kinetic parameter

L = length of the filter

U_m = superficial melt velocity

The equation (2) shows that filtration efficiency increases at the melt velocity decreases and the efficiency increases with increase in filter length.

1.6. GATING SYSTEM IN CASTINGS

A lot of research has been conducted over the years on understanding gating systems and it has been observed that the size of and design of the flow patterns have an impact on the final quality of the castings. The requirements that are essential for designing a good gating system are as follows

- The mold must fill quickly to minimize air entrainment and prevent premature freezing

- Reduction of turbulence in metal flow into the gates

- Prevention of reoxidation of metal in the casting

- Compatibility with the pouring system that is being used

- Removal of slag and dross defects entrained during filling

- Prevention of distortion and hot tearing during solidification

- Easy removal

- Maximization of casting yield

1.6.1. Components of a Gating System. In a gating or rigging system, the major elements are the pouring basin, down sprue, sprue well, runner, gates and the casting as shown in Figure 1.20.[78] Gating systems are the entrance path for molten metal into the casting cavity and hence play a significant role in maintaining casting quality during production.[79,80].

1.6.2. Pouring Cup. A pouring cup is the first point of contact from a ladle to the mold and designing a good pouring cup is essential to avoid bubbles or splashing. Traditionally, a conical cup is used which is simple and economical for small castings. But in conical cups, the high velocity of the metal and the vortex effect leads to air aspiration and oxide formation. [9] In an offset rectangular pouring basin as shown in Figure 1.21, the initial metal falls directly into the basin first, allowing entrained air to rise and the flow to stabilize, before rolling over a dam into the sprue. This also helps to separate the bubbles and slag, which float to the top, from entering the sprue and minimizes metal spillage and vortex formation. In this type of pouring basins, it is essential to keep the pouring basin full, to prevent air and dross from entering the system. [9,10]. Figure 1.21(c), shows a direct comparison in velocity between the three pouring basins where the offset pouring clearly has a better flow velocity.[81]

1.6.3. Downsprue. The down sprue connects the pouring cup to the runners and the gates. The sizing and shape of the sprue plays a major role in determining the final quality of the casting. An oversized sprue affects metal quality by taking in air

continuously, leading to surface turbulence and oxidation of the binder in the sand. A tapered down sprue is better than a cylindrical sprue as it helps to keep the sprue full to prevent aspiration of gases into the cavities. In commonly used sprue and runner systems, a circular sprue is attached to a rectangular runner.
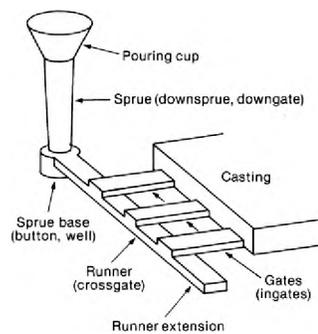
Figure 1.20. Elements of a gating system showing the pouring cup, sprue, sprue base, runner, runner extension, and multiple gates leading into the casting [78]

(a)   (b)
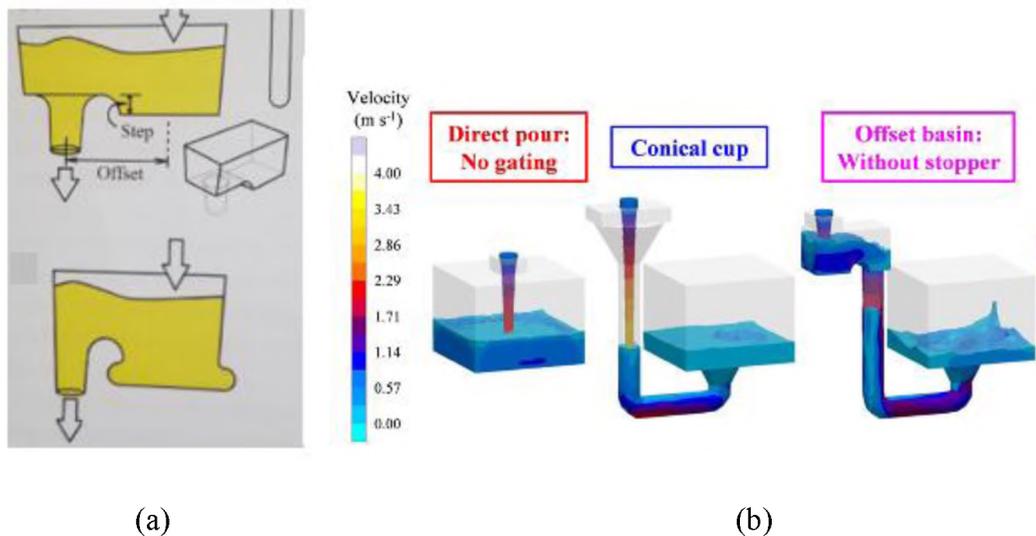
Figure 1.21. Use of offset basin and an undercut (a) An offset pouring basin helps to control the flow of the incoming liquid from the ladles and stabilizes it and an undercut that is provided to the basin to slow down the flow of metal and prevent it from splashing over the pouring basin (c) comparison of flow velocity between the three pouring systems[81]

In this system, the liquid metal continuously sways back and forth with the runner unable to fill the runner completely. The use a sprue well helps to minimize the damage as it reduces the velocity of the incoming metal and subsequently reducing the kinetic energy of the molten metal.[10] Research done by Jezierski et al., shows that a slimmer runner leads to a better laminar flow of the metal. A short tapered rectangular sprue offers various advantages like minimizing metal velocity, prevention of vortex formation, and aspiration of gases.[82] The taper should ideally mimic the shape of the pouring stream and can be estimated by the following formula.

$$A_{\text{bottom of sprue}} / A_{\text{top of sprue}} = \left(h_{\text{pouring cup}} / h_{\text{total}}\right)^{0.5} \tag{5}$$

where A is the area and h is the height of the sprue. Thus, a sprue should be ideally a single, smooth, nearly vertical tapering channel, without any interruptions as seen in Figure 1.22.[82].
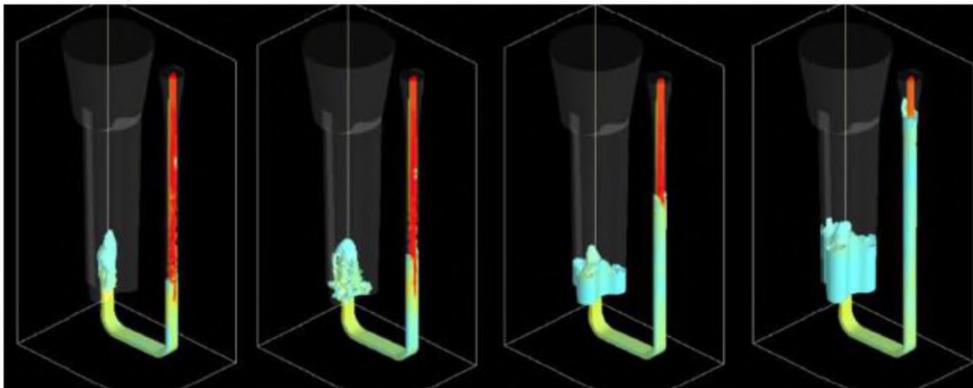
Figure 1.22. The transition of a sprue from a circular opening to a slim rectangular cross section ensures smooth filling and flow velocity. (red = high velocity) (blue = low velocity) [82]

1.6.4. Runners. The runner connects the base of the sprue to the gates. A tapered runner attached with a runner well is a modification from the traditional rectangular runner, since long flat thin runners provide more slag and doss to be trapped. The runner wells and extensions also aid in trapping the initially damaged metal entering the gating system. For obtaining smooth filling, a laminar flow of metal is essential where the metal flows in parallel layers. The Reynolds, number (Re), is used to characterize the flow of metal as a turbulent or laminar flow.[10] The Reynolds number is given by,

$$Re = (\rho Vd) / (\mu) \tag{6}$$

where ρ is the density of the metal, V is the velocity of the metal, d is the diameter and μ is the viscosity of the metal. At Re lower than 2000, viscous forces prevail, leading to a smooth and laminar flow while Re over 2000 is considered as turbulent flow, where the velocity and direction of flow of the metal changes erratically. [9,10]

The Weber number is a dimensionless quantity which helps to establish the relationship between the kinetic energy of a fluid and the stabilizing surface tension forces, given by

$$We = \rho L v^2 / \sigma \tag{7}$$

where ρ is the density of the molten metal, L is the radius (characteristic length) of the channel, v is the molten metal velocity and σ is the surface tension of the molten metal. When We = 1, the inertial and surface forces are roughly balanced. A Weber number in the range of 0–2.0 defines the range of flow conditions that are free from surface turbulence. Molten metal velocity has the greatest effect on the Weber number and as the Weber

number keeps increasing, the kinetic energy becomes more dominant leading to high splashing turbulent flow of metal.[52]

1.6.5. Gating. Gating systems for horizontally parted sand molds are traditionally designed using a gating ratio. The gating ratio is the ratio of the total cross-sectional area of the sprue, total runners, and total gates, (A $_{sprue}$: A $_{runners}$: A$_{gates}$). A gating system can be classified as a pressurized or non-pressurized gating system depending on where the choke is present. A choke is the smallest cross-sectional area and determines the rate at which the liquid metal enters the mold. [52] For a non-pressurized system, the choke is present at the base of the sprue. So, a non-pressurized system might have a gating ratio of 1: 3: 4. These kind of gating systems are commonly used for aluminum and turbulent sensitive alloys. The liquid metal at the base of the sprue comes at a very high velocity which is controlled by the sprue well. Since the runners and gates have an area greater than the choke, the velocity subsequently reduces, and the metal enters the gating smoothly in a laminar pattern with low Reynolds number. [9,10]

For a pressurized system, the choke is present at the gates. Thus, a gating ratio, something akin to 2:4:1 might be found for these kinds of systems. They are commonly used for metals like gray iron which are not sensitive to damage and turbulence. Due to the high velocity and turbulence, these alloys experience oxidation and mold erosion higher than the non-pressurized system. The violent mixing of the metal inside these systems also leads to slag and dross accumulation and gas porosity.[10]

Due to increased demand for better quality castings and to avoid the formation of bubbles, bifilms and reoxidation defects, new gating systems have been developed which are discussed below. The presence of an extended runner with a runner well, helps in

controlling the velocity of the metal with the high pressure head and also collect the incoming metal carrying slag and dross, But once the runner becomes full, it leads to a sudden rise in pressure into the gate leading to high velocity and splashing causing reoxidation inclusions and bifilm formation.[82] Another important type of gating system that has gained prominence over the last few years is the naturally pressurized vortex filling system as shown in Figure 1.23. [81, 82) In this system the runner is extended into a runner well where the vortex helps in reduction of the high velocities of the metal entering the mold cavity. [82) Though the vortex gating system aided in reducing the velocity of the
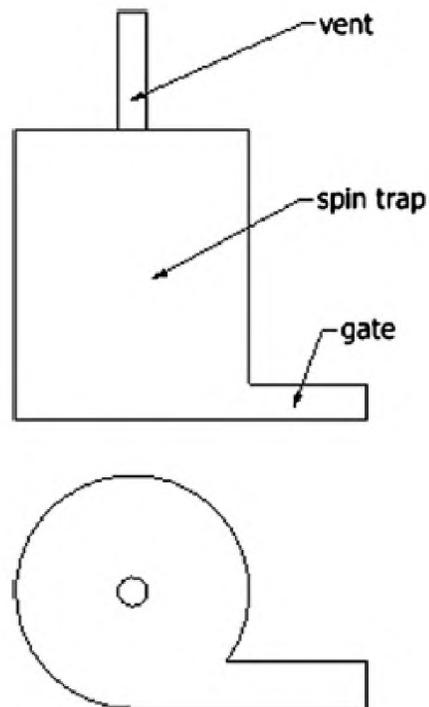
Figure 1.23. The vortex gate showing the presence of a gate and the velocity tracker which collects the incoming metal from the runner and traps all the slag and aids in velocity control [82,10)

metal, it leads to centrifugal formation of bubbles where into the middle of the system, where the bubbles coalesce into one major bubble and might force its way into the casting. To avoid this problem, a terminal spin trap is used for the castings as shown in Figure 1.24. In this type of gating system, where the runners are extended into the terminal spin traps, which act as a well for the incoming metal with high velocity, carrying slag, dross and other impurities. Moreover, the presence of the centrifugal spin trap also aids in the buildup of gradual pressure on the back of the runner. Thus, unlike the runner extension seen above, there is no immediate spurt in pressure, preventing any splashes of bifilm defects.
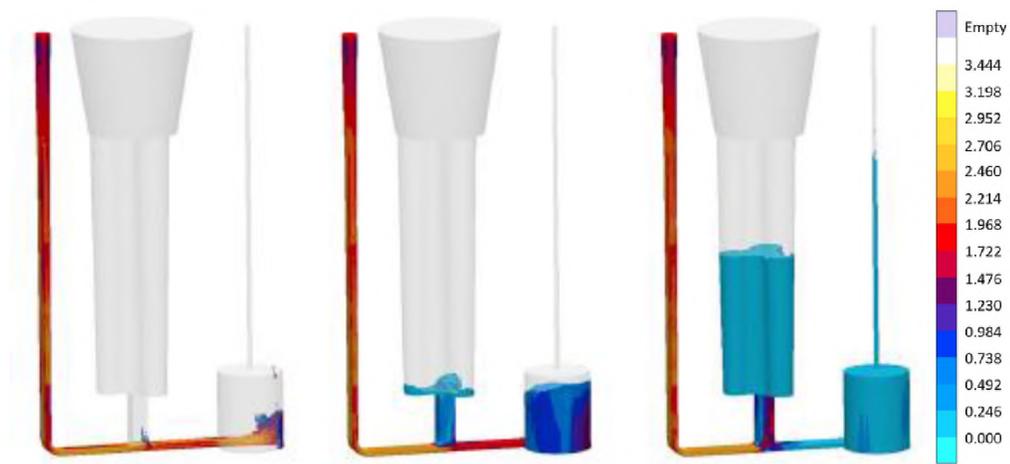
Figure 1.24. A gating system with a terminal trap. The terminal trap apart from controlling the incoming velocity, also collects the slag, dross and the inclusions carried by the incoming metal. This ensures the casting filled with new metal and a stable velocity as shown where the scale is absolute velocity in m/s [82]

Using a system with the vortex spin trap and using a bottom gated system, also eliminates the need of a filter unlike the traditional pressurized and non-pressurized gating systems. [10,82] Since the vortex trap acts as a reservoir to collect the incoming metal and control the velocity, it eliminates the need of filtration. The presence and use of a tapered rectangular sprue unlike the conventional tapered cylindrical sprue help to keep the sprue

fill up with metal faster, thus keeping it full to avoid any gases being aspired into the system or bubbling to take place.

1.6.6. Riser/Feeder. Risers are feeders are designed to ensure that the casting is fed with metal completely and to prevent hotspot formation. To feed the casting effectively, a riser must have a longer solidification time than the casting and prevention of heat loss is an important consideration. Risers can be either top risers or side risers depending on their placement. Since the riser must feed the casting completely, it is ensured that the volume of the riser is at least 1.2 times the volume of the casting and external sleeves is available in risers to prevent heat loss. [9,10]

Using the above methods and results from previous researchers [9,10,81,82], an off step pouring basin with an undercut followed by a rectangular down sprue to enable laminar flow of metal would be an optimum choice. The presence of a vortex terminal trap to collect the incoming metal, slag and dross, to ensure smooth filling of metal in the bottom gated system, would be an ideal system of choice for the steel maker to obtain quality castings. Since the slag and dross are collected by the terminal spin trap this eliminates the necessity to use a filter.

PAPER

I. FILTRATION EFFICIENCY OF INCLUSIONS IN LIGHTWEIGHT FeMnAl STEELS

K. Balasubramanian,[1] L.N. Bartlett,[1] R.J. O'Malley,[1]
S. Chakraborty[1], and M. Xu[2]

[1]Missouri University of Science and Technology, Rolla, MO and [2]Georgia Southern University, Statesboro, GA

Keywords: FeMnAl steel, non-metallic inclusions,
filtration, bifilms

ABSTRACT

The efficiency of ceramic foam filters in removing different inclusion populations in a Fe-30Mn-9Al-1Si-0.9C-0.5 Mo steel was investigated. A mold design was created utilizing fluid flow and solidification modelling software. The design utilized a common pouring cup attached to two different but balanced gating systems. One runner utilized a ceramic foam filter while the other runner was unfiltered. Three molds were poured in sequence from a teapot style ladle. Metallographic samples revealed extensive Al and Mn rich oxide bifilms in samples taken before the filter. Samples sectioned after the filter did not contain bifilms. AlN or complex AlN-MnS or AlN-MnO comprised more than 70% of all inclusions. Samples sectioned from the first two molds showed an inclusion removal efficiency of 38% and 39%, respectively. Larger inclusions greater than 3 μm were more efficiently filtered. The third mold with the greatest number of larger inclusions showed the highest inclusion removal efficiency of 55%.

1. INTRODUCTION

Lightweight high strength steel with aluminum contents between 4-12wt.%Al have found applications for military vehicles as well as in the automotive sector because of a combination of low density, high strength, and good toughness. Fully austenitic cast steels of composition Fe-30Mn-9Al-0.9C-1.0Si-0.5Mo offer almost a 15% lower density compared to quenched and tempered SAE 4130 cast steels with equivalent strengths and dynamic fracture toughness.[1] It should be noted that all compositions in the following study are in weight percent unless otherwise stated.

1.1. NON-METALLIC INCLUSIONS IN FeMnAl STEELS

Internal defects in FeMnAlC steels such as microporosity and the presence of faceted aluminum nitride inclusions are a major contributor for loss of toughness in these steels.[2] A high aluminum content of 5-12% is also responsible for the formation of solid oxide bifilms that can be entrained during pouring and filling and this has been linked to a significant loss in tensile strength, ductility and fatigue life in aluminum castings.[3] Studies by Schulte et al.[4] show that the population density of AlN inclusions directly affects the impact properties of a Fe-30Mn-9Al-1Si-0.9C-0.5Mo. In the solution treated and aged condition, Charpy V notch (CVN) toughness at -40°C decreased from 35J to 19J as the concentration of AlN increased from 12 inclusions/mm^2 to 210 inclusions/mm^2.[4] Clean steelmaking practices using argon cover can help reduce nitrogen pickup. However, high nitrogen in charge materials, exposure to air during metal transfer as well as during pouring and filling always results in a significant amount of AlN inclusions in these castings.

1.2. FILTRATION

There have been constant efforts in foundries to increase cleanliness and reduce inclusions in both high and low alloy steel castings. The use of foam ceramic filters (FCF) is currently one of the best engineering solutions for increasing metal cleanliness and reducing velocity and turbulence during mold filling. The cellular structure of foam ceramic filters results in deep bed filtration leading to attachment of inclusions within the porous network. The forces of adhesion, that is good wettability, and the presence of a large specific area within the foam filter improves the efficiency of non-metallic inclusion removal.[5] The porous cellular structure that is present in a FCF plays a major role since it provides a high surface area and torturous flow path that increases the coefficient of mass transfer between the metal and filter surface.[6] Filtration of alumina inclusions using ceramic filters has been studied by Apelian et al. for a steel composition of Fe-0.012C-0.04Ni between with between 12-20ppm of oxygen. It was shown that inclusions greater than 2.5μm were trapped by the filter.[7] In the study by Tian et al. on steels consisting of composition Fe-0.66Mn-0.005P-0.29C-0.095Cu-0.092Cr-0.001Mo, zirconia filters were shown to have up to a 90% removal efficiency for alumina inclusions.[8]

The filtration efficiency expression for liquid metal filtration can be expressed as:

$$\eta = (C_i - C_0)/C_i \qquad (1)$$

where η = inclusion removal efficiency

C_i = concentration of inclusions at inlet of the filter

C_0 = concentration of inclusions at the outlet of the filter.[7]

The use of FCFs in castings has been shown to increase the yield of the castings, reduce the rejection rate, and improve the machinability of the casting.[6] The use of filters gives improvement in the yield and quality of steel castings and understanding of how inclusions in FeMnAlC steels are filtered by these filters is of high priority. Although there has been some work published on the filtration of alumina inclusions utilizing foam filters, the effectiveness of these filters in inclusion removal of FeMnAl steel castings has not been investigated. The goal of this study is to determine the inclusion filtration efficiency of ceramic foam filters at removing different inclusion populations and oxide bifilms from a Fe-30Mn-9Al-0.9C-1Si-0.5Mo steel. In this regard, a mold was designed that allowed balanced filling of two identical Y-block castings in the same mold that were attached to two different but balanced rigging systems. One side of the gating systems included a 10 ppi (pores per inch) zirconia ceramic foam filter while the other side was unfiltered. In the current study the effectiveness of ceramic foam filters at removing different inclusion populations from the melt was evaluated directly from the filter inlet and outlet in the runner utilizing a scanning electron microscope with automated feature analysis. The effect of pouring order on the filtration efficiency was also determined in this study. Subsequent investigations will be performed to determine the effect of filtration on casting quality and mechanical properties.

2. METHODOLOGY

The solidification software MagmaSoft (5.3) was used to design the mold. The design of the mold and experimental procedure has been adapted from the paper by Chakraborty et al.[9] The design consisted of two modified Y-block castings, where one of

the runners is fitted with a ceramic filter (FOSECO STELEX ZR 10ppi filter) of dimensions 10cmX10cmX2.5cm, while the other did not have any filters. The dimensions of the vertically parted molds are 70cmX20cmX35cm. A drawing of the mold is shown in Figure 1.

The designs used similar castings, sprues, runners, and gates while the gating ratio used was different to accommodate the filter in one of them while balancing the filling into the castings. Hence the gating ratios of the two molds were 1:2:3.8 (with filter) and 1:2.6:3.8 (without filter). Figure 2 shows the absolute velocity of filling at different stages, namely 10%, 20%, 30% and 50% full. It is shown that the presence of a filter helps in slowing down the velocity at one runner, while the filling is faster in the other runner.
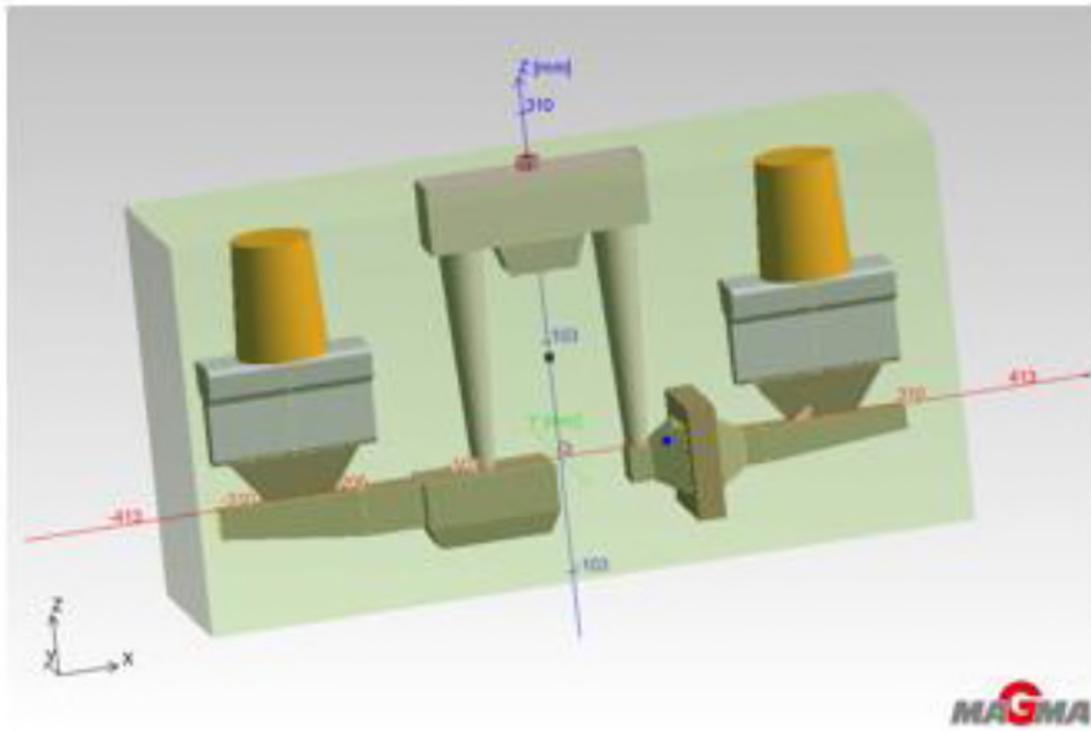
Figure 1. Drawing of the vertically parted mold design showing the two-bottom gated modified Y-block castings attached to two balanced gating systems. The gating system on the right contains the filter while the other gating system on the left is unfiltered

Flow through the ingates of the castings takes place at a velocity of less than 0.44 m/s which is lower than the critical velocity of 0.45 m/s recommended by Campbell to minimize any air entrainment and reoxidation defects.[10] Figure 3 shows the temperature at the end of filling for the steel. The steel was poured at a temperature of 1519°C. Figure 3 shows the temperature profile just after filling with all temperatures in the casting and rigging system above 1450°C. The liquidus temperature for this composition of steel was determined utilizing Thermocalc thermodynamic modeling software to be 1338°C. Figures 2 and 3 indicate that the filling of the casting happened at an absolute velocity which was less than the critical velocity and at the end of the pour all the parts of the casting had a temperature higher than the liquidus, therefore avoiding any problems regarding premature solidification.

Thermodynamic modelling for the Fe-30Mn-9Al-1Si-0.9C-0.5Mo steel composition was performed using the Thermo-Calc 2017a software. Figure 4 shows the phases that form as a function of equilibrium cooling. The steel was modeled with 0.007% N, 0.005% O, and 0.005% S in order to determine the stability of different inclusions. Figure 4 also shows stable precipitation of Al_2O_3 (corundum) and AlN at temperatures well above the liquidus. MnS forms below the liquidus temperature during solidification. It should be noted that sulfur tends to highly segregate to interdendritic regions and this can increase the stability of MnS during solidification of FeMnAlC steels.[11]

High purity induction iron, ferrosilicon, ferromolybdenum, electrolytic manganese, high purity aluminum and high purity graphite were melted in a coreless 90.7kg (200lb) ferrous capacity induction furnace under argon cover with a flow rate of 25 SCFH.
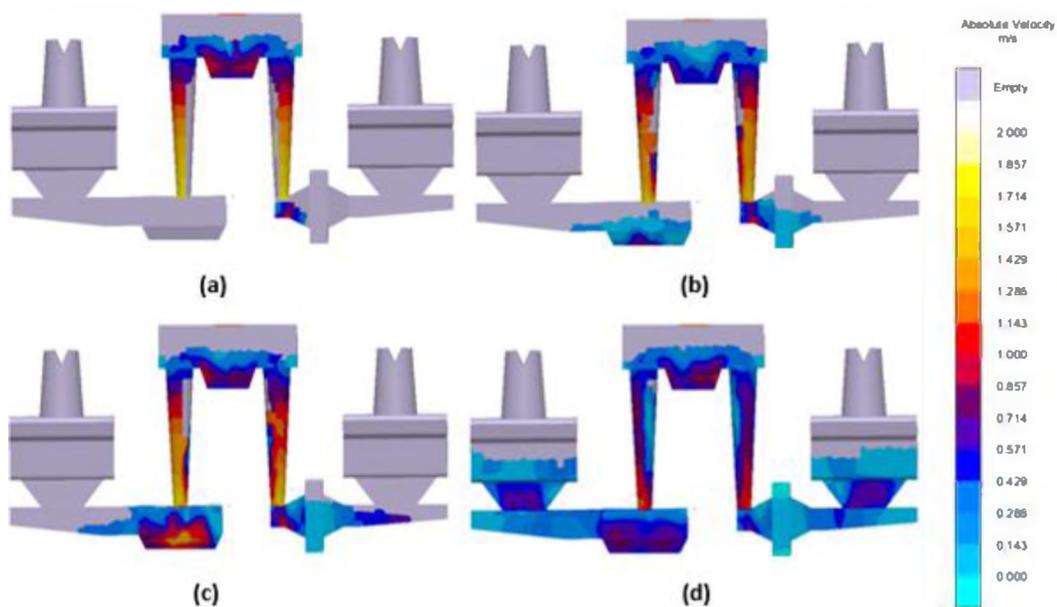
Figure 2. The velocity profile during filling at (a) 10% (b) 20% (c) 30% and 50% filled
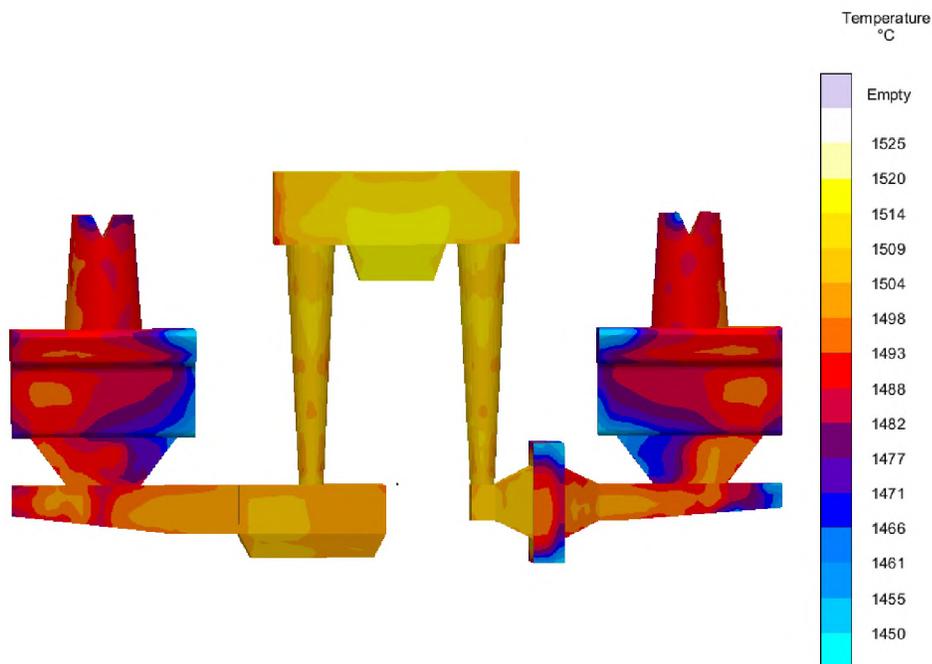
Figure 3. The temperature profile directly after filling shows that all temperatures are above the calculated liquidus temperature of 1338°C at all points in the design
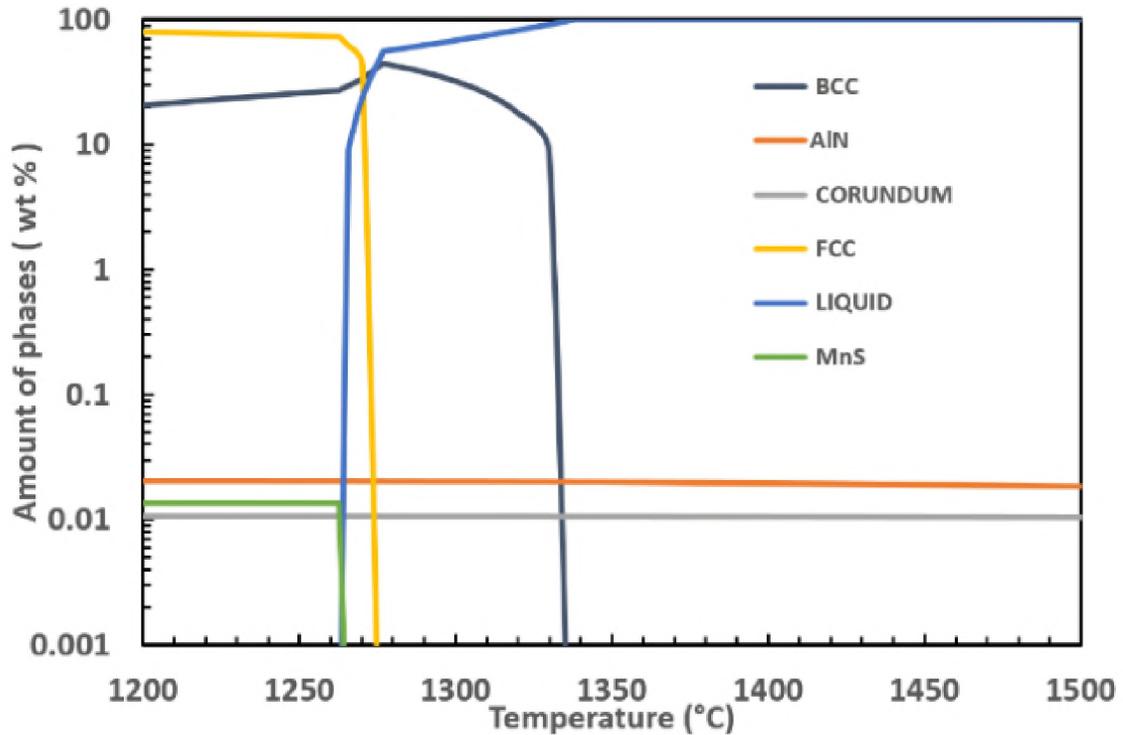
Figure 4. Thermodynamic modeling of the equilibrium solidification of a Fe-30Mn-9Al-1Si-0.9C-0.5Mo steel with 0.007% N, 0.005% O, and 0.005% S. AlN and Al_2O_3 are stable in the liquid well above the liquidus. MnS forms after the liquidus during solidification

The target chemistry was Fe-30%Mn-9% Al-1%Si- 0.9%C-0.5%Mo. The mass of the total charge was 160lb (72.56kg). The molten metal was tapped at 1630°C into a teapot style ladle which was used to pour the metal into the three molds. The first mold consisted of metal poured from the bottom one-third of the ladle while the second mold consisted of metal from the middle of the ladle. The last mold was poured from the metal at the top of the ladle.

Specimens were sectioned for microstructural and inclusion analysis at a distance of 10 mm from the inlet and outlet side of the filter as shown in Figure 5(b). The chemistry analysis was performed by optical emission arc spectroscopy and combustion analysis using the LECO CS 500 for carbon and sulfur and a LECO TC 600 for determining the

total oxygen and nitrogen contents. Specimens were sectioned before and after the filter in the same location for each of the three castings and three sets of samples were obtained from each of them, as shown in Figure 5(c), and observed under an optical microscope. A representative optical micrograph of a sample taken from the inlet side of the filter is shown in Figure 5(d) to contain a large bifilm defect. Polishing was performed utilizing standard metallographic techniques and inclusion analysis was performed using automated inclusion analysis and was conducted utilizing an ASPEX PICA 1020 scanning electron microscope (SEM). The chemistries of the inclusions and the matrix were also observed using energy dispersive X-ray spectroscopy (EDS). The bifilms were quantified using ImageJ software.

3. RESULTS

The computer filling simulation exhibited a filling time of 9 seconds. This was in close accordance with the actual filling time of the first mold which was recorded to be 9s. The filling time for molds two and three were 12s and 17s. This could be because of factors like less metallostatic pressure as the ladle was drained and slight differences in tilt speed during pouring. The simulation produced results in close accordance to the first mold poured.

The total oxygen, nitrogen and sulfur contents results are shown in Table 1 and were measured using inert gas fusion and combustion infrared detection techniques. The samples were taken in the runner area directly after the filter in all three castings as shown in Figures 5 (b and c) as well as from the unfiltered runner area in the same relative position (Figure 5(a)). Table 1 compares the results. Nitrogen was largely constant at 45ppm

regardless of pouring order in the samples taken in the unfiltered runner area. However, the filtered runners show a decrease in total nitrogen content when compared to the samples taken from the unfiltered runners. It is important to remind the reader that these molds were poured from a teapot ladle in which the first metal from the ladle may contain the cleanest metal while the last metal poured from the ladle will likely have the highest amount of possible slag as well as oxide and nitride inclusions. However, throughout the three molds all the samples taken in the unfiltered runner and after filtration showed oxygen levels less than 10ppm and this did not appear to be influenced by filtration. Total nitrogen decreased with pouring order from 34 to 22ppm in filtered specimens. Sulfur was also invariant of pouring order and filtration with a value around 32ppm as shown in Table 1.

3.1. CHEMISTRY ANALYSIS

Table 2 gives the target and measured chemistry of the steel in weight percent as measured by optical emission spectroscopy, OES, for all the elements except carbon and sulfur, which were measured by combustion infrared detection techniques in a LECO C/S analyzer. The certified standards used for calibration of the OES had chemistries similar to the composition of the steel. The measured chemistry is reasonably close to the target chemistry. It should be noted that the molybdenum level was slightly higher than the anticipated, 0.7% Mo when 0.5%Mo was expected and the carbon content was slightly lower, 0.8%C when 0.9%C was expected.
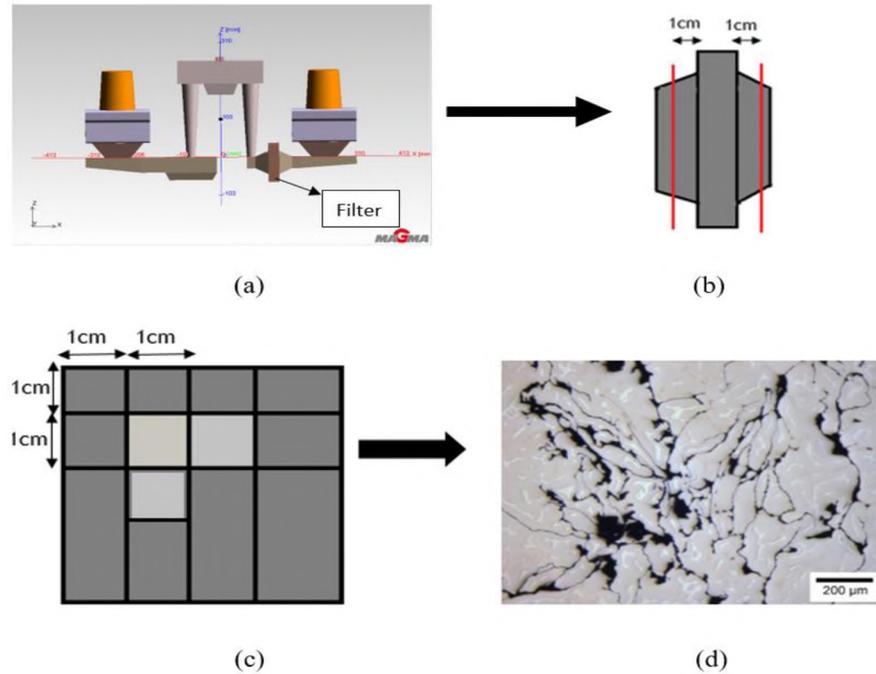
Figure 5. Experimental procedure for sectioning filter and obtaining specimens for AFA analysis. (a) The design showing the position of the filter (b) Representative image showing how the filter was sectioned (c) Representative image showing where the metallographic and inclusion analysis samples sectioned from each side of the filter. (d) Optical micrograph of one of the samples taken before the filter

Table 1. LECO analysis of N, O, and S (ppm) content from samples taken from unfiltered runners and after filters

	Unfiltered Runner			Runner After Filtration		
	Mold 1	Mold 2	Mold 3	Mold 1	Mold 2	Mold 3
Nitrogen	45 ± 5	45 ± 9	46 ± 2	34 ± 2	26 ± 2	22 ± 4
Oxygen	7 ± 3	6 ± 2	5 ± 1	6 ± 1	7 ± 2	5 ± 2
Sulfur	29 ± 5	33 ± 2	32 ± 4	32 ± 3	30 ± 5	33 ± 4

Optical micrographs of samples sectioned directly before the filter for all the three molds are presented in Figures 6 (a-c). The matrix consists of mainly austenite with less than 10 to 15% ferrite. The most notable feature in Figure 6 (a-c) is the presence of extensive oxide bifilms that are increasing in prevalence in the order of filling.

Table 2. Measured chemistry and target composition in weight percent as determined using OES and LECO C/S analyzer

	Fe	C*	Si	Mn	S*	Mo	Ni	Al
Target	Bal.	0.9	1	30	-	0.5	-	9
Measured	Bal.	0.82	0.99	29.10	0.002	0.70	0.15	9.4

These networks of oxide bifilms were found in of all the samples taken before the filters in all the molds. In some cases, they are associated with areas of porosity caused through thickness failure of inlet gating system resulting from bifilm separation. The microstructures of samples taken after the filter are shown in Figure 7. Bifilms were quantified by determining the average area coverage utilizing image analysis on optical micrographs.

3.2. BIFILM AND INCLUSION ANALYSIS

Bifilms were not observed in filtered specimens as shown in Figure 7. It should be noted that the areas presented in Figures 6 and 7 were sectioned in the same positions before and after the filter in each of the three gating systems as shown in Figures 5 (b and c). The composition of the bifilm defects was characterized utilizing an SEM with EDS and compared with the matrix austenite chemistries. Figure 8 shows the backscattered electron images of a network of bifilm defects from the area before the filter in mold 1. EDS analysis confirmed that the bifilms are mainly composed of aluminum and manganese oxides as shown in Table 3. Previous unpublished work by the authors show that nitrogen and possibly hydrogen gas may nucleate on the bifilms during solidification, causing

porosity and growth of coarse AlN plates during subsequent heat treatment, making these defects even more detrimental to casting quality.

(a)   (b)   (c)
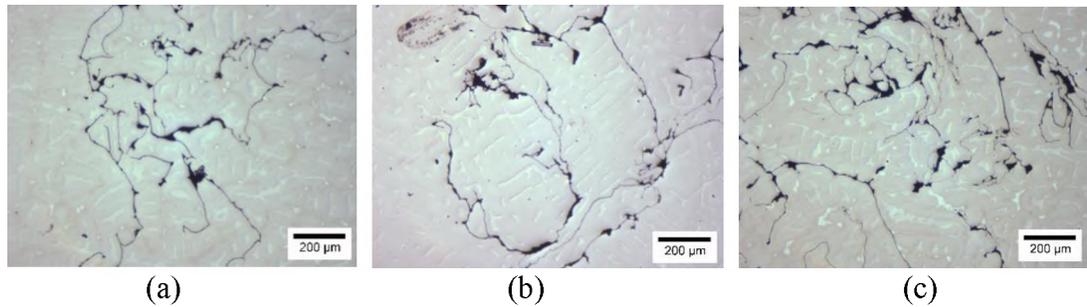
Figure 6. Optical micrographs of sections taken before the filter show a matrix of mainly austenite with less than 15% ferrite. Extensive bifilm defects and associated porosity are shown in the microstructure

(a)   (b)   (c)
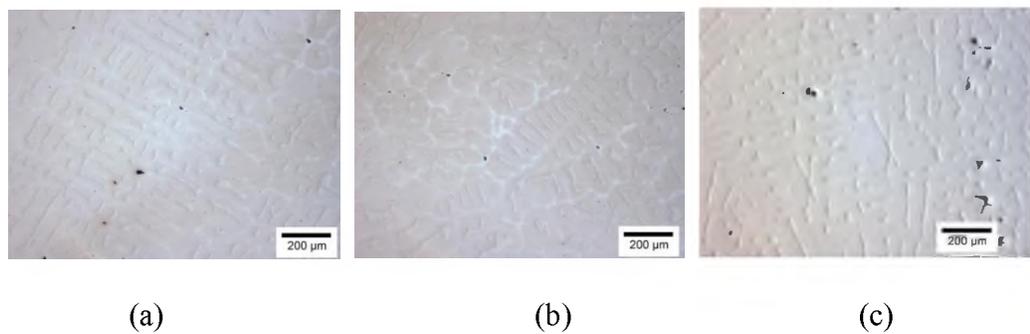
Figure 7. Optical micrographs of samples taken after the filter in (a) mold 1 (b) mold 2 (c) mold 3 show that bifilms have been effectively removed by filtration

Table 3. Comparison of bifilm chemistries compared with the matrix chemistry in samples sectioned before the filter

	Mn (wt. %)	Al (wt. %)	O (wt. %)
Mold 1	23±7	13±8	25±15
Mold 2	23±6	13±7	24±10
Mold 3	23±2	16±11	29±10
Austenite matrix	32±3	7±0.5	0.9±0.2
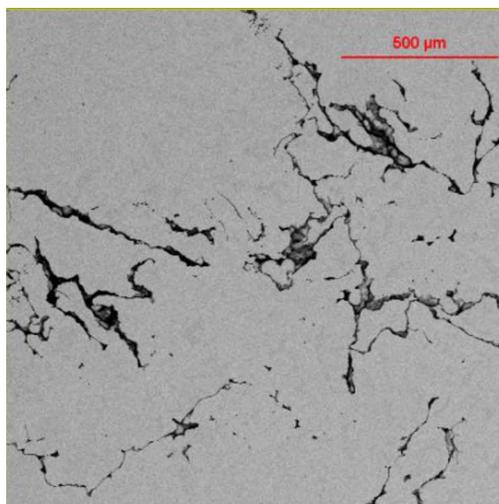
Figure 8. The backscattered electron image of a network of bifilms present in the sectioned sample taken before the filter from mold 1. It shows areas of bifilms that were determined to be mainly aluminum oxide

As seen from Table 3, the bifilms were composed of mainly alumina and possibly in combination with manganese oxides. However, the high amount of Mn in the matrix contributes to a background effect and thus the presence of Mn in these bifilms is difficult to resolve. Inclusion analysis of samples sectioned before and after the filter was accomplished utilizing an ASPEX PICA 1020 SEM with automated feature analysis. A backscattered electron detector (BSED) and a magnification of 500X was used for the analysis.

An emission current of 32-34μA with a dwell time of 12μs were considered for the analysis. Areas of bifilms and pores were excluded from the inclusion analysis based on size (greater than 10μm for bifilms) and chemistry. For example, pores and bifilms were found to have either high carbon levels, and since the diamond paste used for polishing can accumulate in the cracks in the bifilms and pores, or high concentrations of iron and manganese at or above the matrix composition and without any other elements in the case of porosity and bifilm cracks. Inclusions were also differentiated from the bifilms and

pores from the nitrogen and/or sulfur levels that were always greater than 4% in all inclusions. From Table 1, it is observed that the amount of total oxygen in chemistry samples was low (<10ppm). Additionally, EDS is not very accurate at determining oxygen. Thus, inclusions were classified depending on the amount of Al, Mn, S, and N. The representative chemistries of different inclusions by type is shown in Table 4. Most of the inclusions observed were aluminum nitride AlN, manganese sulfide MnS and complex inclusions consisting of an AlN core with a capping layer of MnS. Some representative backscattered electron, BSE, images of AlN and complex AlN-MnS are shown in Figure 9. Figure 9(a) shows singular AlN inclusion that has nucleated and grown in the liquid. As the steel solidifies, sulfur will be enriched in the liquid and MnS inclusions will precipitate below the liquidus, utilizing AlN as a nucleation site as shown in Figure 9(b and c).

Table 4. The average chemistry of the different types of inclusions obtained using EDS

	Al (wt %)	N (wt %)	Mn (wt %)	S (wt %)
AlN	56.2	22.9	20.1	0.70
AlN-MnS	33.4	16.2	43.9	6.2
AlN-MnO	37.2	21.3	40.4	0.86

Automated inclusion analysis was performed on samples sectioned from identical locations from each of the mold gating systems before and after the filter as shown in the drawings in Figure 5 (b and c). The following nomenclature will be adopted to identify the respective samples; mold 1, before filter (M1BF), mold 1, after filter (M1AF), mold 2,

before filter (M2BF), mold 2, after filter(M2AF), mold 3, before filter(M3BF), mold 3, after filter (M3AF).

(a)   (b)   (c)
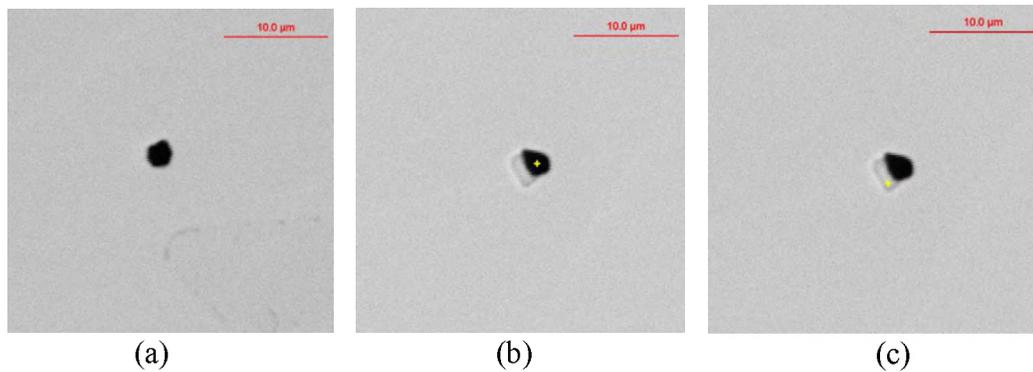
Figure 9. SEM images of different inclusions found in the steel (a) An image of an aluminum nitride inclusion (b and c) A complex AlN-MnS inclusion with the AlN at its core and (c) a MnS inclusion around the AlN

Figure 10 shows the inclusion density by type for specimens sectioned before the filter. It was found that the AlN inclusions formed most of the inclusions followed by AlN-MnO and AlN-MnS. MnO and MnS were observed to precipitate on AlN. MnS inclusions had an inclusion density of less than 5/mm^2. It should be noted that the MnS inclusions will form below the liquidus temperature as observed from Figure 4 and are thus unaffected by filtration.

Complex oxysulfides of Al and Mn and Ti-Mo carbides were found in trace amounts in all the three molds. However, these inclusions accounted for only 1-1.5% of the total amount of inclusions and was therefore excluded from the analysis. Figure 11 shows the inclusion density by type for samples sectioned after the filter in all three molds. The density of AlN decreased in the filtered samples by 27-28% in the first two molds and by 38% in the last mold poured.
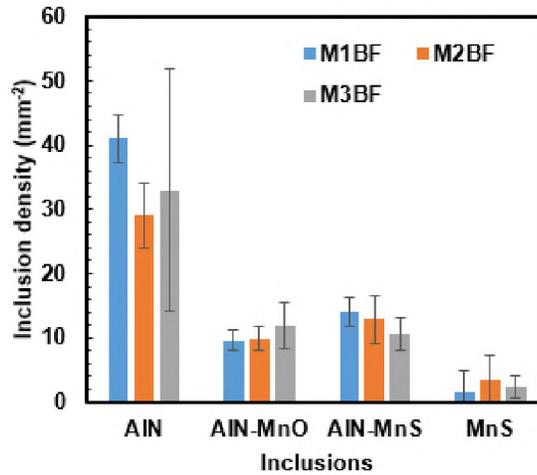
Figure 10. Inclusion density of inclusions by type, taken from the three molds before the filter, indicating a high density of AlN inclusions
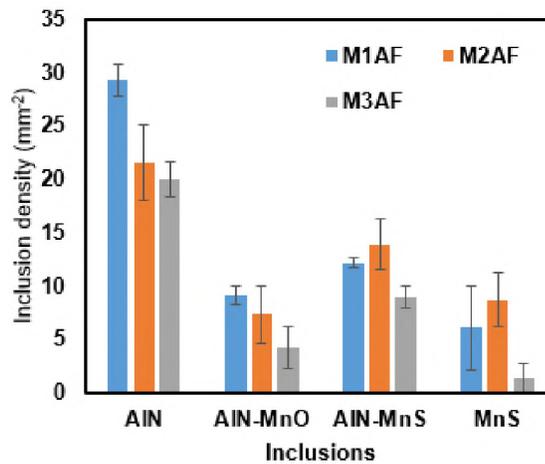
Figure 11. Inclusion density of inclusions by type, taken from the three molds after the filter, indicating a reduction in AlN inclusions and a slight increase in the number of MnS inclusions

The percentage of MnS increases slightly; however, MnS forms after filling of the gating system and during solidification and thus for analysis of the filtration effectiveness, MnS is excluded from the analysis. The inclusions forming in the liquid, and thus subject to filtration, were considered to be AlN and complex AlN-MnS and AlN-MnO inclusions.
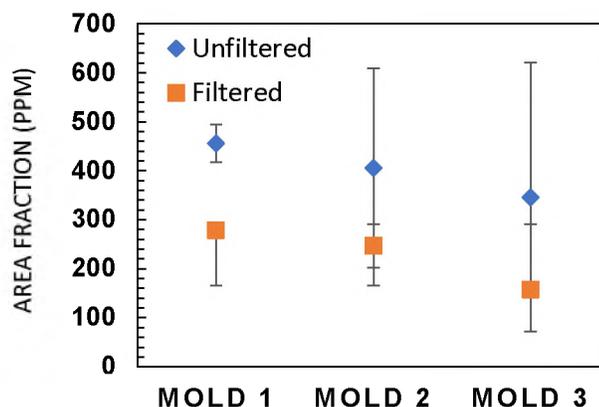
Figure 12. The area fraction of inclusion coverage as a function of filtration and mold pouring order shows a reduction in the amount of inclusions in filtered specimens by as much as 54% in mold 3

The total area fraction of inclusion coverage in the filtered and unfiltered samples as a function of mold pouring order is given in Figure 12. Mold 1 showed the highest area fraction of inclusions before filtration at 456 ppm followed by mold 2 and mold 3 at 405 and 345 ppm, respectively. The samples taken after the filter were much cleaner and showed an average decrease in inclusion area of 174 ppm. The efficiency of inclusion removal by the filter was greatest in the last mold poured with a 54% overall reduction in the area fraction of inclusions. Figure 13 (a-c) show size distribution plot between the average inclusion size and the inclusion density for inclusions that are stable during filling.

All the three molds show a reduction in the inclusion density between the unfiltered and filtered samples. From Figures 13 (a and b), it can be noted that most inclusions were between 2-3μm. The inclusion removal efficiency for inclusions greater than 3μm was found to be 30.3% and 28.6% for the molds 1 and 2, while for the third mold it was 58.2%. The area fraction of the aluminum nitride inclusions as a function of the average size of inclusions for the three molds considering filtered and unfiltered sections are represented in Figures 14 (a to c).

(a)

(b)

(c)
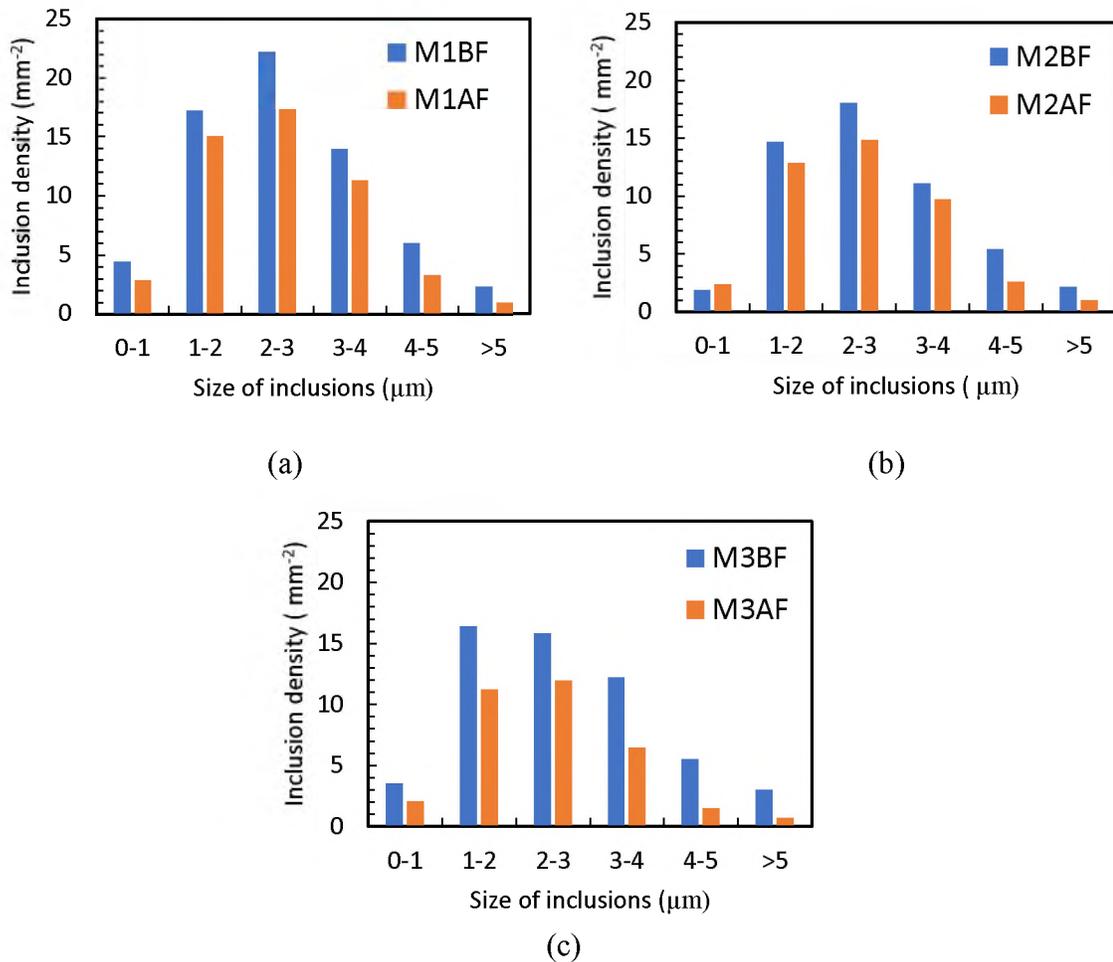
Figure 13. Inclusion density as a function of the size distribution the unfiltered and filtered samples in (a) mold 1 (b) mold 2 and (c) mold 3

The area fraction of AlN was shown to decrease in filtered samples taken from each of the molds. The results are similar to those presented for the total number of stable inclusions in the melt presented in Figure 12. Larger AlN inclusions, >2-3μm, were removed from the melt more efficiently by the filter than smaller AlN inclusions. The filtration is most significant in the third mold, as shown in Figure 14 (c) as there is a higher percentage of larger sized aluminum nitride inclusions in the unfiltered sections.
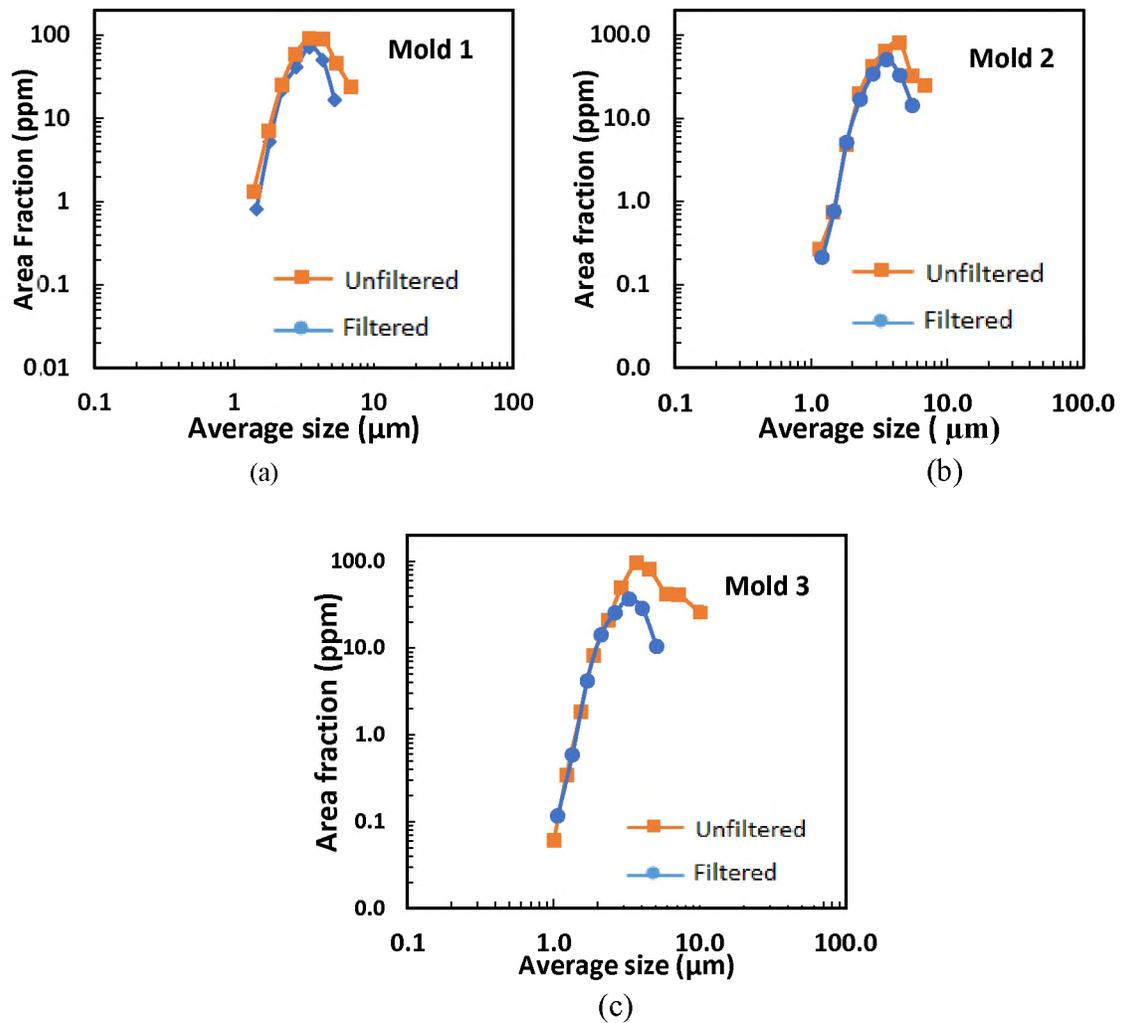
Figure 14. Size distribution of aluminum nitride inclusions as a function of area fraction for filtered and unfiltered samples in (a) mold 1 (b) mold 2 and (c) mold 3

It is also observed that the filtered areas from mold 3, have a maximum inclusion size of 6-8 μm, indicating that the larger sized AlN inclusions have been mostly removed by the filter.

4. DISCUSSION

Figure 15 shows the measured N, O, and S contents from samples taken from unfiltered runners and from samples taken just behind the filter as described in Figure 5. The amount of sulfur and oxygen was not much different in the unfiltered and filtered runners and that did not appear to vary with pouring order. The sulfur concentration corresponds directly to the amount of sulfide inclusions (MnS and complex AlN-MnS) in the castings. Thermodynamic modeling in Figure 4 shows that MnS is stable below the liquidus near the end of solidification and this is consistent with the work of Vaz Penna et al. who show MnS precipitation after the liquidus in a Fe-30Mn-9Al-1C- 1Si-0.5Mo steel with 40 to 400 ppm S.[12] Thus, MnS did not form until after filling and during solidification and therefore the consistency of the sulfur concentrations in Figure 15 between the filtered and unfiltered runner areas is understandable. This is consistent with the work of others who have shown that inclusions in these steels mainly consist of AlN and AlN-MnS complex inclusions in which MnS is often found to precipitate heterogeneously on AlN during solidification.[1,2,4,11] The amount of measured total oxygen in Figure 15 is low in all the samples and was less than 10 ppm.

This is consistent with the inclusion analysis presented in Figures 10 and 11 that show less than 10 inclusions/mm^2 were complex oxide inclusions. In general, endogenous oxide inclusions such as alumina and manganese spinel are not as prevalent as AlN in castings poured from FeMnAlC steels that are induction melted and this has been reported by several studies.[1, 2,4,11]

Samples taken from the unfiltered runner show no real difference in the amount of nitrogen as a function of pouring order as shown in Figure 15. However, filtered specimens

show a substantial decrease in total nitrogen, decreasing from around 45 ppm N to 35 ppm

N in mold 1 to less than 22 ppm N in mold 3. The amount of nitrogen in these steels

appears to be directly correlated to the amount aluminum nitride inclusions. This is

consistent with the inclusion analysis presented in Figures 11 and 14 that shows a reduction

in the area fraction and number of AlN and complex AlN inclusions with filtration.
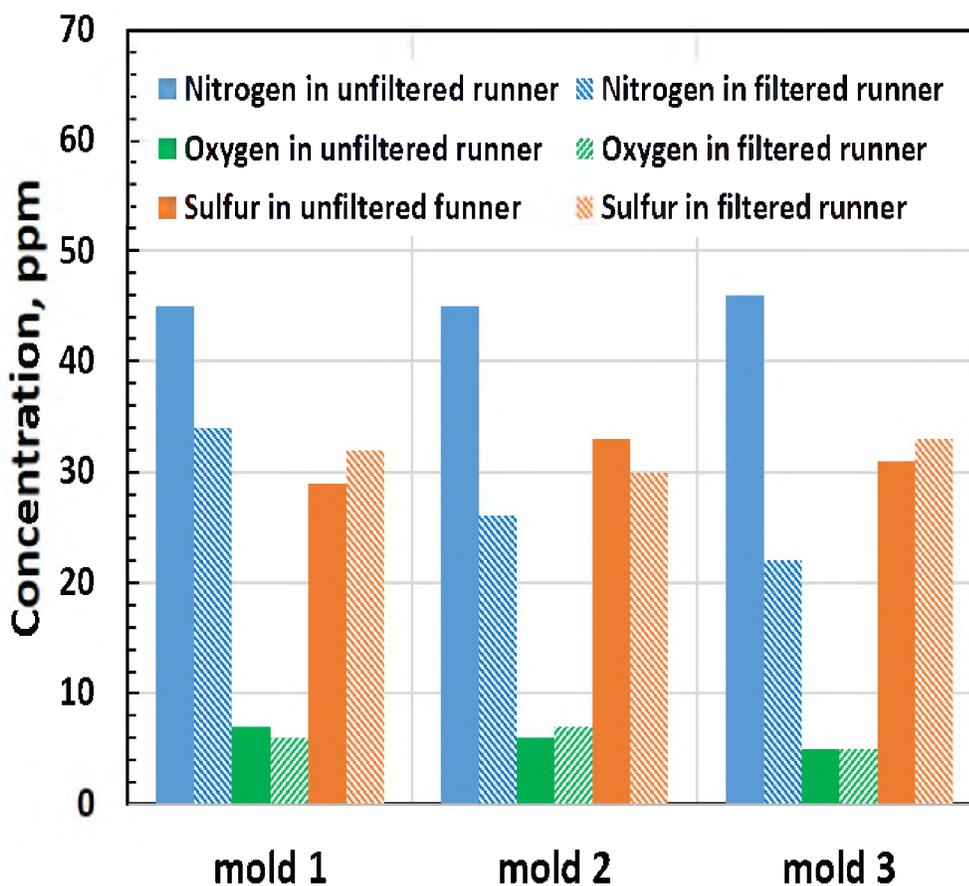
Figure 15. LECO analysis of N, O, and S concentration content from samples taken from
the unfiltered runners and in the runners after filters as a function of mold pouring order

The total nitrogen contribution from the inclusions was determined from samples

sectioned after the filter and compared to the measured nitrogen in the unfiltered and

filtered runners. The method used for calculating the nitrogen content based on inclusion was obtained from the work by M Harris et al.[13]

The areal average elemental composition of inclusions is calculated for each element as follows:

$$\%m = \frac{\Sigma(\%x)(A_{inclusion})}{A_{total}}$$

(2)

where %m is the areal average mass percent of a given element, %x is the amount of respective element in an individual inclusion, $A_{inclusion}$ and A_{total} are the area of the individual inclusion and total area of all measured inclusions. The mass balance calculation was performed using the compositional data obtained from the EDS inclusion analysis and the following equation.[13]

$$M_{ppm} = \frac{\%m\,A_f\,\rho_i\,w_i}{100\rho_m}$$

(3)

In the above equation, M_{ppm} is the mass fraction in ppm of a given element in the steel sample contained within the inclusions, A_f is the total inclusion area fraction, ρ_i and ρ_m are the densities of the inclusions associated with the given element and the density of the matrix, respectively. w_i is the mass fraction of the given element in the associated inclusion compound.[13]

As shown in Figure 16, nitrogen decreases after filtration and the filtered nitrogen contents are in very good agreement with the nitrogen contribution from the inclusions. The efficiency of solid inclusion filtration increases with pouring order as shown from Figures 13 and this is supported by the measured nitrogen contents in Figures 15 and 16. The measured amount of total nitrogen observed in the filtrated steels is also somewhat

lower than previous induction melted Fe-30Mn-(3-9) Al-(0.9-1.8) C steels in which the total nitrogen content that varied between 50 and 150 ppm.[2] It should be noted that results indicate that the steel in the current study was very clean even in the unfiltered condition with total inclusion densities before filtration ranging from 50 to 70 inclusions/mm^2 as shown in Figure 1.
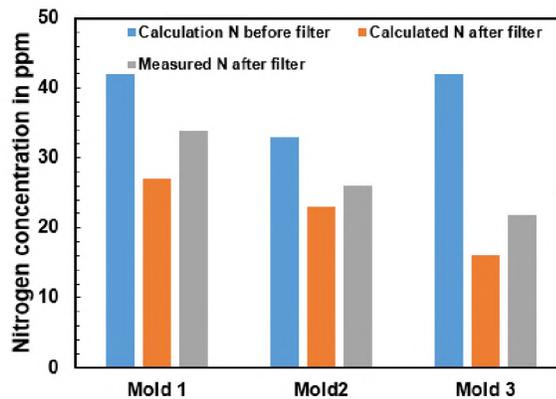
Figure 16. Calculated total nitrogen contribution of inclusions from specimens sectioned before and after the filter as compared to the measured total nitrogen after filtration

The total inclusion density of the current steel can be compared with the results of Bartlett et al.,[2] who showed total inclusion densities ranging from 70 to 146 inclusions/mm^2 in induction melted Fe-30Mn-(3-9)Al-(0.9-1.8)C steels. The optical microstructural analysis of the samples in Figures 6 and 8 revealed extensive bifilm networks in samples taken before the filter with high amounts of porosity. The percentage of area covered by bifilms in samples taken before and after the filters in molds one, two and three were 1.78, 2.04 and 2.46%, respectively. Bifilms were not observed in samples taken after the filter. The velocity of the metal was the highest at the base of the downsprue and before the filter expansion area as shown in Figure 2. In some regions, the velocity reaches as high as 2m/s,

which is above the critical value 0.45m/s. This leads to mixing of the metal with the air and the formation of a surface skin of the metal oxide that folds onto itself with along with a volume of entrapped air, leading to formation of aluminum oxide bifilms and associated porosity. This phenomena of bifilm formation and air entrainment has been widely reported in aluminum castings[14-16]. The high amount of aluminum in these steels makes these alloys particularly susceptible to bifilm formation and EDS elemental analysis of the bifilm defects in the current study shows that they are made of primarily aluminum oxide and perhaps in some cases Al-Mn-O spinel as shown in Figure 8 and Table 3. The filter was effective at removing the bifilm defects from the steel as shown in Figure 8. This is an encouraging result that has not been previously documented for high Mn and Al steels. It should be noted that the bifilms may have contributed to some inclusion removal because of their large area to volume ratio and a possible "inclusion netting" mechanism. However, inclusions were not observed to be attached or associated with bifilms when observed both optically and with an SEM. Additionally, the high initial velocity in front of the filter of greater than 1 m/s, as shown in Figure 2, may tend to push inclusions through these networks suggesting that most of the inclusions were captured by the filter. Further studies are planned to determine the mechanism of inclusion attachment within the filter.

Inclusions in the FeMnAlC steel consisted mainly of AlN and complex AlN-MnS and AlN-MnO inclusions. Very few oxide inclusions were observed, other than bifilm defects, and this is consistent with previous studies that report that inclusions in these steels are mainly AlN, and complex AlN-MnS and AlN-MnO type inclusions as previously noted for industrially induction melted and cast Fe-30Mn-9Al-(0.6-1.6)Si-0.9C-0.5Mo steels.[1,2] The presence of mainly AlN and complex AlN-MnS and AlN-MnO inclusions in this study

are consistent with previous studies of similar compositions of Fe-30Mn-XAl-0.9C steels with Al contents between 3 and 9%Al.[1,2,4,17] A comparison of the inclusion removal of samples taken from before and after the filter for all the three molds is shown in Figure 12. The density of AlN decreased in the filtered samples by 27-28% in the first two molds and by 38% in the last mold poured. The filtration efficiency has been calculated using Equation 1 and the area fraction of inclusions before and after filtration as per the method used by Apelian et al.[7] Filtration efficiency of all the nitride based inclusions that form in the liquid (AlN, AlN-MnO and AlN-MnS namely) was between 38 and 39% for the first two molds poured and increased to 55% in the last mold poured. It is shown in Figure 13, that although the incoming inclusion densities are largely similar, the last molds poured tended to have a higher percentage of larger inclusions, >3μm, and these larger inclusions tend to be filtered out more efficiently. The inclusion removal efficiency for inclusions greater than 3μm was found to be 30.3% and 28.6% for the first two molds, while for the third molds it was 58.2%. A study for a similar mold design and inclusion filtration study was recently performed by Chakraborty et al. on a SAE 316 steel that was deoxidized by aluminum, generating a large amount of solid alumina inclusions.[9] The efficiency of solid nitride inclusion filtration in the current study in mold 1 and mold 3 was higher by 20% and 10%, respectively, than in the study by Chakraborty et al.[9]

From Figures 10 and 11, it was observed that aluminum nitride inclusions had the highest inclusion density among all inclusions. The analysis of aluminum nitride inclusions across the three sets of molds becomes of paramount importance since it plays a major role in determining the impact toughness of the steel.[4] It was also observed that the filter displayed an efficiency of 37% removal of AlN inclusions in the first mold followed

by 45% and 61% removal of AlN inclusions in the second and third mold respectively. Figure 13 shows that the samples taken after the filter had a higher amount of smaller sized inclusions than large sized inclusions The difference in the bar graphs in Figure 13 show that since the larger inclusions float to the top and since mold three was poured at the end, it consisted of a high number of larger (>3 μm) sized inclusions. A similar trend is observed in the filtration of alumina inclusions by Chakraborty et al.[9] This is understandable since the smaller sized inclusions would have passed through the pores of the ceramic filter while the larger sized inclusions are more easily filtered out.

5. CONCLUSION

The filtration of inclusions from the melt of a Fe-30Mn-9Al-1Si-0.9C-0.7Mo steel was studied as a function of pouring order and utilizing a novel mold design consisting of two castings connected to two separate but balanced rigging designs. One of the gating systems utilized a zirconia 10 ppi foam filter in the runner system while the other one was unfiltered. The three molds were prepared using no-bake sand and the metal was poured using a tea pot ladle. Results showed a decrease in the number and area fraction of inclusions with filtration as well as elimination of bifilm defects in samples sectioned directly after the filter in the runner system. Samples taken before the filter were covered with bifilms on their surface, which were mainly composed of aluminum and manganese oxides. Samples taken after the filter showed an elimination of bifilms. These results show that filters are extremely effective at removal of bifilm defects from high manganese and aluminum steels. AlN inclusions contributed to approximately 50% of the total inclusion population, while AlN-MnS and AlN-MnO contributed about 20% of the total inclusions.

The filtration efficiency of inclusions from the melt increased from 38% to 39% in mold 1 and 2, to 55% for mold 3. The filter displayed an efficiency of AlN removal from 37% to 61% from mold 1 to mold 3. Mold 3 exhibited the highest amount of large size inclusions in the size distribution analysis and showed the highest inclusion filtration rate. These results show that ceramic foam filters are very effective at decreasing bifilm defects and at filtration of large inclusions from the steel and should be used when a high degree of cleanliness and toughness is desired. Future work will quantify the effect of filtration on casting quality and toughness and verify the inclusion capture mechanism within the filter.

ACKNOWLEDGEMENTS

REFERENCES

1. Laura Bartlett, David Van Aken "High Manganese and Aluminum Steels for the Military and Transportation Industry", The Minerals, Metals and Materials Society, Vol 66, No 1, (2014)

2. L.N.Bartlett, D.C.Van Aken "Effect of Aluminum and carbon on dynamic fracture toughness of FeMnAlC steels", American Foundry Society, AFS Transactions, Paper 13-1344, (2013)

3. R.Gopalan and Narayan. K. Prabhu "Oxide Bifilms in aluminum alloy castings: A review", Materials Science and Technology,Vol 27, Issue 12, Pages 1757-1769, (2011)

4. A.M.Schulte, S.N.Lekakh, D.C.Van Aken, V.L.Richards " Phosphorus mitigation in cast lightweight Fe-Mn-Al-C steel'" 114th MetalCasting Congress, Orlando, Florida, March (2013)

5. A.N. Leonov, M.M.Dechko " Theory of design of foam ceramic filters for cleaning molten metals", Refractories and Industrial ceramics, Vol 40, Nos 11-12, (1999)

6. V.N.Antsiferov, S.E.Porozova " Foam Ceramic Filters for molten metals: Reality and Prospects", Powder Metallurgy and Metal Ceramics, Vol 42, Nos 9-10, (2003)

7. D.Apelian, R.Mutharasan, S. Ali "Removal of inclusions from steel melts by filtration", Journal of Materials Science 20, Pp, 3501-3514, (1985)

8. Chenguo Tian, "On the removal of non-metallic inclusions from molten steel through filtration", Thesis: Mining and Metallurgical Engineering, MNpill University, May (1990)

9. S. Chakraborty, L. Bartlett, R. O'Malley, M. Xu, "Efficiency of solid inclusion removal from the steel melt by foam ceramic filter: Design and Experimental Validation",122nd AFS MetalCasting Congress, American Foundry Society, (2018)

10. Campbell J., "Complete Casting Handbook", Elsevier Ltd., Oxford, UK (2011)

11. R. Vaz Penna, L.N. Bartlett, and T. Constance, "Understanding the Role of Inclusions on the Dynamic Fracture Toughness of High Strength Lightweight FeMnAl Steels," International Journal of Metal Casting, October, (2018) In Press

12. Gunter Gigacher, Wilfred Krieger, Piotr R Scheller, Corinna Thomser, "Non-metallic Inclusions in High Manganese Alloy steels" Steel Research International, Vol 76, Issue 9, pp.644-649, (2005)

13. M. Harris et al., "Evolution of Non- Metallic Inclusions in Foundry Steel Casting Processes Processes," Proceedings of the 69th Annual Technical and Operating Conference, Steel Founders Society of America (SFSA) (2015, Chicago Illinois), Steel Founders society of America (SFSA) (Dec 2015)

14. D. Dispinar, and J. Campbell, "Porosity, hydrogen, and bifilm content in Al alloy castings," Materials Science and Engineering, 528 pp. 3860-3865 (2011)

15. G. Bozchaloei, N. Varahram, P. Davami, S. Kim, "Effect of oxide bifilms on the mechanical properties of cast Al–7Si–0.3Mg alloy and the roll of runner height after filter on their formation" Materials Science and Engineering A, Vol 548 pp. 99-105 (2012)

16. B. Farhoodi, R. Raiszadeh, and M. Ghanaatian, "Role of Double Oxide Film Defects in the Formation of Gas Porosity in Commercial Purity and Sr-containing Al Alloys," Journal of Materials Science and Technology., Vol 30, pp. 154-162 (2014).

17. L. Bartlett, A. Dash, D. Van Aken, V. Richards, and K. Peaslee, "Dynamic Fracture Toughness of High Strength Cast Steels," Transactions of the American Foundry Society, pp. 17-33 (2013)

II. QUANTIFYING THE EFFECT OF FILLING CONDITIONS ON 8630 STEEL CASTING QUALITY

K. Balasubramanian,[1] L.N. Bartlett,[1], M. Xu[2]

[1]Missouri University of Science and Technology,
Rolla, MO and [2]Georgia Southern University, Statesboro, GA

Keywords: vortex gate, non-metallic inclusions, air entrapment, simulation

ABSTRACT

Gating systems play an important role in determining the quality and mechanical properties of castings. Recently developed naturally pressurized gating systems have been proclaimed by some to completely eliminate defects in steel castings, however, this has not been quantitatively studied. In the current study, the efficiency of different gating systems on reduction of inclusions and the corresponding improvement in notch toughness in quenched and tempered SAE 8630 high strength steel castings was studied using a combination of fluid flow and solidification modeling software and coupled with experimental studies on industrially produced test castings. A novel mold design allowed for the simultaneous comparison of four different "best practices" gating systems. These systems included two horizontally gated castings with a pressurized system and a non-pressurized system as well as two naturally pressurized countergravity systems. The test castings were identical modified Y-block castings and were modeled to have critical microporosity of less than 0.06% and Niyama criterion greater than five. This was done to minimize variation in solidification and to eliminate the effect of microporosity on

toughness. Inclusion analysis revealed presence of mainly alumina and complex alumina and manganese sulfide inclusions. The naturally pressurized system provided the cleanest casting with the highest Charpy V notch, CVN, toughness. Eutectic type II MnS that formed during solidification negatively affected notch toughness and this obscured the effect of pre-existing alumina inclusions. The pressurized system was shown to have the highest inclusion fraction.

1. INTRODUCTION

Over the last few decades many investigations have been conducted by researchers to develop "best practices" gating systems that improve steel casting quality [1]. Since the liquid melt enters a casting system through the rigging or gating system these systems play a significant role in either increasing or degrading casting quality.

Research has shown that a well-designed gating system can help decrease molten metal turbulence, reduce the slag, dross, and air entrainment within the casting and also capture detrimental inclusions that might enter the casting cavity. [2] Various other defects such as blows, cold shuts, ripple marks etc. can also be directly related to the gating system and metal flow during mold filling. [3] When the metal filling is turbulent, it can lead to air entrainment, oxide bifilm formation, and reoxidation inclusions as well as sand inclusions from mold erosion. It has been shown that reoxidation inclusions resulting from pouring and mold filling can comprise up to 83% of the inclusions in low alloy steel castings and 48% of inclusions in stainless steel castings. [4] The presence of excessive amounts of filling related inclusions is often detrimental to machinability, casting surface quality, and mechanical properties. Control of reoxidation inclusions is important as it is estimated that

up to 20% of the manufacturing costs associated with the production of steel castings are associated with repair and rework that results from these filling related defects.

Various types of flows that can occur in gating systems can entrain air into the molten metal such as the metal falling from a height, formation of breaker waves, or waves returning from the runner after hitting an obstacle. These cases lead to the entrainment of oxygen which subsequently causes formation of oxides that get entrapped in the liquid metal as reoxidation inclusions.[5] Therefore, gating systems must be properly designed to limit metal turbulence during filling and exposure of the molten metal with air. For obtaining smooth filling, laminar flow of the molten metal is essential. The Reynolds, number (Re), is used to characterize the flow of metal as a turbulent or laminar flow.[6] The Reynolds number is given by,

$$Re = (\rho V d) / (\mu) \tag{1}$$

where ρ is the density of the metal, V is the velocity of the metal, d is the diameter and μ is the viscosity of the metal. At Re lower than 2000, viscous forces prevail, leading to a smooth and laminar flow while Re over 2000 is considered as turbulent flow, where the velocity and direction of flow of the metal changes erratically. [1,6]

However, it has been shown that surface turbulence (predicted by the Weber number) and the amount of time the liquid metal is in contact with the air have more of an effect on air entrainment and reoxidation than Re alone. The Weber number is a dimensionless quantity which helps to establish the relationship between the kinetic energy of a fluid and the stabilizing surface tension forces and is given by Equation 2.

$$We = \rho L v^2 / \sigma \qquad\qquad (2)$$

where ρ is the density of the molten metal, L is the radius (characteristic length) of the channel, v is the molten metal velocity and σ is the surface tension of the molten metal. As the Weber number increases, the kinetic energy becomes more dominant leading to high splashing an turbulent flow of the metal.[7] It is shown that molten metal velocity has the greatest effect on the Weber number and therefore one way to decrease turbulent flow and reduce the amount of filling related defects is to decrease metal velocity, however, cold shut formation and misruns can occur when the flowrate is below a critical level. Thus, design of gating systems has a direct impact on proper filling of castings.(5) Campbell gives a critical ingate velocity of 0.5 m/s where the molten metal is safe from entrainment problems.[8] However, in practice it is often hard to achieve this in an industrial foundry and ingate speeds between 0.5 and 1.0 m/s are often recommended.[8]

Most steel foundries use adaptations of the gating system shown in Figure 1 for a horizontally parted mold, which has been widely accepted for more than 50 years. This design has a number of features to control molten metal velocity, eliminate oxide damaged metal, and minimize turbulent flow. For example, rectangular pouring basins are preferred over conical pouring cups because they minimize air aspiration, allow for stabilization of the molten metal flow, and allow entrained air bubbles to rise in the basin without being washed into the downsprue.

Tapering the downsprue reduces air aspiration and a sprue well helps to minimize the turbulence due to high velocity and molten metal changes in direction. Curved, rectangular runners and gates also minimize air aspiration and promote laminar flow. Runner extensions and runner wells are utilized to decrease the gate velocity and provide

removal of the first metal into the mold which likely contains high amounts of reoxidation defects from the initial pouring event.
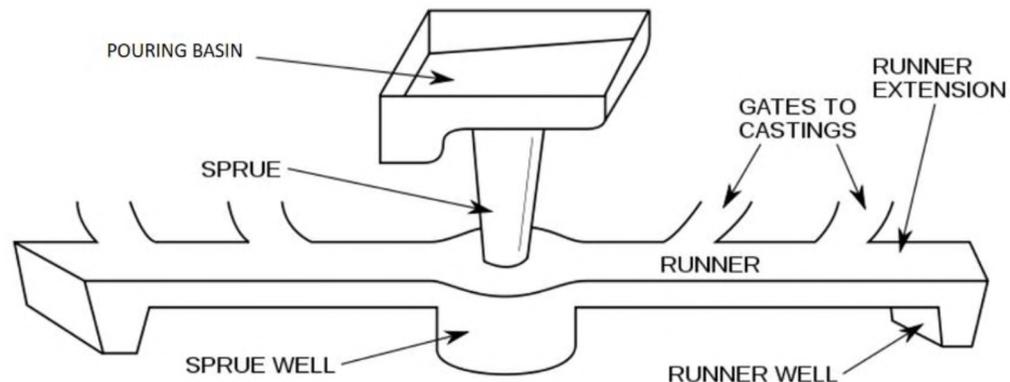
Figure 1. Horizontally parted gating systems that are typically used in the steel casting industry [9]

The work that has been done thus far on investigating the pouring conditions, and their impact on formation of oxide inclusions have suggested that, minimizing the velocity of the incoming metal has a sizeable impact on reduction of air entrainment defects with the goal to limit the gate velocity to 0.5 m/s or less .[10] Historically, both pressurized and non-pressurized gating systems have been employed in design of horizontally gated sand molds. However, these castings use the gravity filling method and in practice, it is often difficult to avoid high gate velocities, metal splashing, and surface turbulence.

With the demand for cleaner quality castings constantly arising, new bottom-gated, or countergravity, systems are being developed to prevent air entrainment and enable better filling results.[6] The vortex gate, vortex spin trap, and the trident so called "Naturally Pressurized" countergravity gating systems have recently been developed and use centrifugal spin traps which help to reduce velocity and eliminate damaged metal from

entering the casting.[11]   The vortex gate leads directly into the casting and utilizes a filter to reduce turbulence due to metal spin. This system effectively reduces the incoming metal velocity; however, it centrifuges the bubbles into the casting that can lead to oxide defects and blows. The trident gate was found to be more effective and has a complex design system that incorporates the use of two filters and a bubble trap and has proven its capabilities in aluminum alloys, however, the use of filters adds an additional cost that most foundries are not willing to encumber.(12) Vortex spin trap gating systems with extended runners were found to be as effective as trident gates at reducing metal velocity and are less expensive and complex to implement because they do not use filters.

Although these novel gating systems have shown great promise in computer simulations, there has been limited studies that link the design, modeling, and actual performance of these gating systems in industrial steel castings. Competition in the foundry industry and the need for higher quality products with complex designs has made computer modeling of molten metal flow and solidification simulations almost essential with the goal of minimizing critical gate velocity (13). However, the use of these software packages cannot accurately predict filling related defects and as such as reoxidation inclusions and bifilms. The goal of this study is to use a combination of computational computer modeling coupled with experimental validation to optimize and compare the filling conditions of four different "best practices" gating systems during the pouring of SAE 8630 steel castings. A novel mold design was designed to simultaneously evaluate two countergravity vortex spin trap gating systems in comparison to traditionally side gated pressurized and nonpressurized systems. The cleanliness of the resulting castings was then

evaluated using scanning electron microscopy, SEM, with automated feature analysis (AFA) and correlated to Charpy V notch toughness.

2. DESIGN OF MOLDS AND TEST CASTINGS

The commercially available filling and solidification software, MagmaSoft (5.3.1) was used for designing the molds. The mold design is shown in Figure 2 (a) and (b). The test castings are shown in gray in Figure 2 and were designed to be modified y-block castings of length 180 mm and a height of 85 mm. The castings were designed in such a way to accommodate a flat surface for obtaining samples to understand the effect of filling conditions on surface quality and provide an evaluation surface for floatation of reoxidation inclusions. For the study of CVN impact toughness, the length and width of the narrow section of the y-block was designed to accommodate sectioning of eight ASTM E23 standard sized CVN bars in two layers of four bars each. The size of the castings was identical between different gating systems to minimize the effect of solidification on the microstructure and mechanical properties. The goal of the current study is to study the effect of filling conditions on steel cleanliness and CVN toughness. Therefore, other defects such as shrinkage and microporosity should be minimized. It is also important to "catch" filling related damage in the evaluation area of the castings and minimize floatation of inclusions into risers. Keeping these two requirements in consideration, the castings and gating systems were meticulously designed to ensure that most of the inclusions that entered the gate from the filling process remained in the castings while at the same time, producing sound metal with low levels of microporosity, <0.08%, in the evaluation area. Table 1 shows the nomenclature for the different gating systems that will be used as

abbreviations. As shown in Figure 2, for the traditionally gated non-pressurized, NP, pressurized, P, and the naturally pressurized system with a side riser, SR, these conditions were satisfied by using a vented top chill (shown in blue) and a side riser (shown in red) to produce a high thermal gradient and low microporosity. The second naturally pressurized system incorporated a top riser to observe the filling of the molten metal into the casting cavity during the pouring operation. However, the solidification conditions in the test area were almost identical to the others. The top riser system was also provided with a sleeve as observed in Figure 2(b). All four of the different gating systems were connected to a single offset pouring basin which was designed using the guidelines suggested by John Campbell.[7] The pouring basin had an undercut which helped in controlling the velocity

(a)   (b)
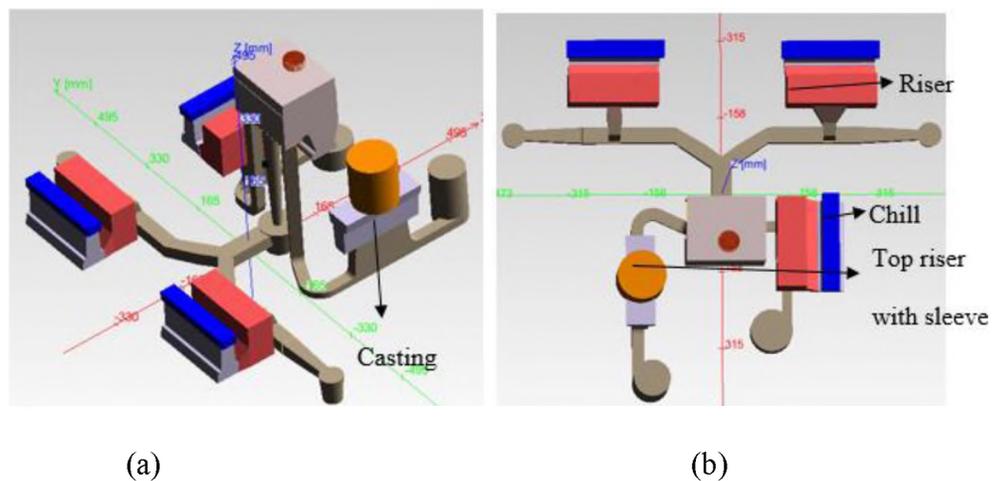
Figure 2. The complete design of the four gating systems in (a) isometric view (b) top view

of the incoming metal. The pouring basin was also provided with a curved radius to ensure the easy flow of metal into the downsprue, minimizing any air entrainment defects. The pouring basin had three downsprues attached to it. The central conical downsprue from

the pouring basin lead to a sprue well and subsequently into a runner with a Y-split into a traditional pressurized, P, and nonpressurized, NP, system. These systems were designed according to recommendations from the American Foundry Society Steel Technical Division and incorporated runner extensions and runner wells to catch the first metal into the mold. The gating ratio for the pressurized system was found to be 1:3:1.4 and the non-pressurized system was found to be 1:3:8.

Each of the naturally pressurized systems are fed by different sprues that gradually transitioned into flat rectangular runners with vortex spin traps at the end of runner extensions. The Y-block castings were countergravity filled from a bottom fan gate with an enlargement taper at the interface of the casting to prevent hydraulic jumps. The downsprues were designed in such a way that all the sprues were completely full before 25% of filling was completed to avoid air entrainment defects and obtain a clean casting. The velocity through each ingate was minimized as much as possible.

Castings were designed to have similar solidification characteristics and a low level of microporosity, <0.06%-0.08%. Since the goal of the project concentrated on studying the formation and influence of inclusions caused by reoxidation in different gating systems, it was important to eliminate the presence of macro and microporosity in castings. While the castings were devoid of macroporosities, the microporosity was ensured to be less than 0.08% as shown in Figure 3. The Niyama criterion has been shown to be a good predictor of microporosity in steel castings and was designed to be above six for all the castings to obtain casting with a high amount of soundness. In Figure 4(a), it is observed that the top risered casting had a Niyama criterion above six near the shoulders from where the Charpy bars are intended to be taken. Figure 4(b) shows the casting of the naturally pressurized

side riser system where the top section of the entire casting had a Niyama criterion greater than six. From the scale it must be noted that the uncolored regions display a Niyama number greater than 6, while the colored regions have a Niyama of less than 6. The castings of all other gating systems show similar Niyama trends as what is shown in Figure 4(b). Once the solidification criterion was successfully satisfied, the gating systems for the different gating systems were designed. The runner and gating systems for the castings were designed to obtain an ingate velocity of less than 0.5 to 0.8 m/s and to reduce air entrapment defects. The air entrapment result was used in the pouring simulation stage to evaluate the presence of wave formation, eddy currents and any fragmentation that was caused from the filling of the liquid metal. Figures 5(a-d) shows the progressive filling of metal into the naturally pressurized top riser system, TR, at 30%, 35%, 50% and 75% respectively. At 30% it is observed that the incoming metal hits the base of the gate but because of the curvature provided there is no swirl, or any metal fallback observed. At 35% filling of the casting, the metal starts entering the casting with a velocity of less than 0.5m/s and with a flat and quiescent filling profile. Since different gating systems fill up at slightly different speeds, the naturally pressurized top riser system fills up in 8.5 seconds while the pressurized and the non-pressurized systems take close to 12 seconds for filling. The velocity at the base of the gates in the pressurized and the non-pressurized systems was around 0.8m/s but the filling velocity inside the casting was found to be 0.5m/s as shown in Figure 6(a). The air entrapment in the gating system shown in Figure 7(a) was found to be 6-8% while the air entrapment in the casting was found to be less than 3%. The naturally pressurized vortex spin trap systems incorporated a cylindrical overflow attached to a runner extension.
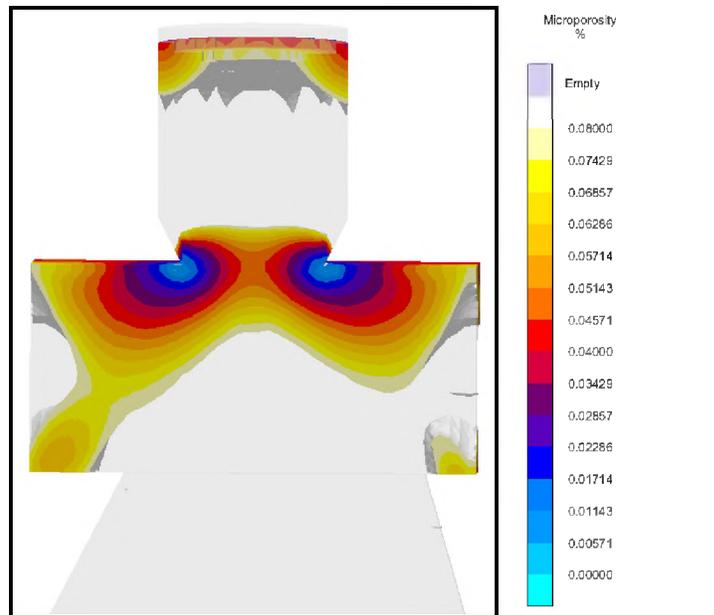
(a)
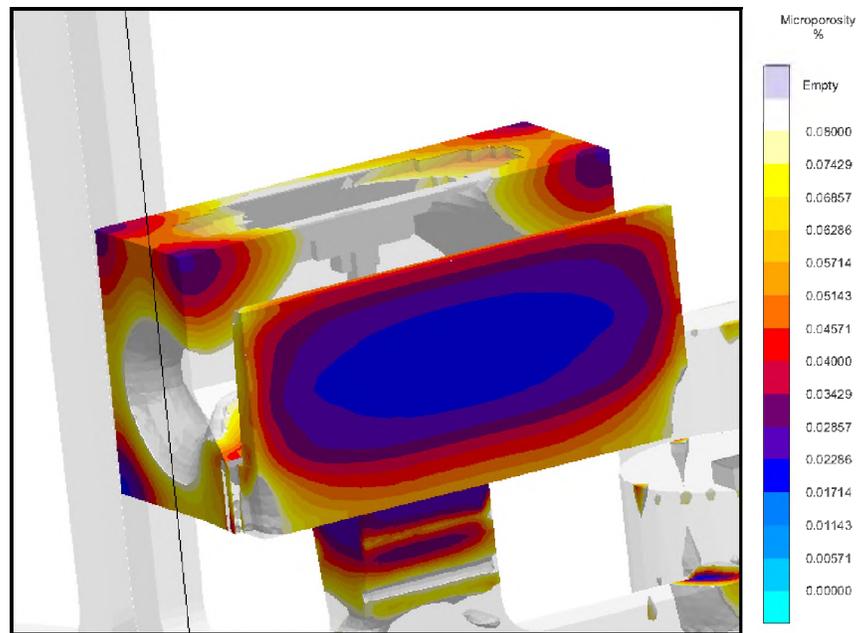
(b)

Figure 3. The castings were designed to ensure a microporosity less than 0.08%. (a) TR system with a low microporosity in the top sections (b) The clipped SR casting had a microporosity lower than 0.08%. The microporosity displayed by the NP and P systems were similar to the SR casting
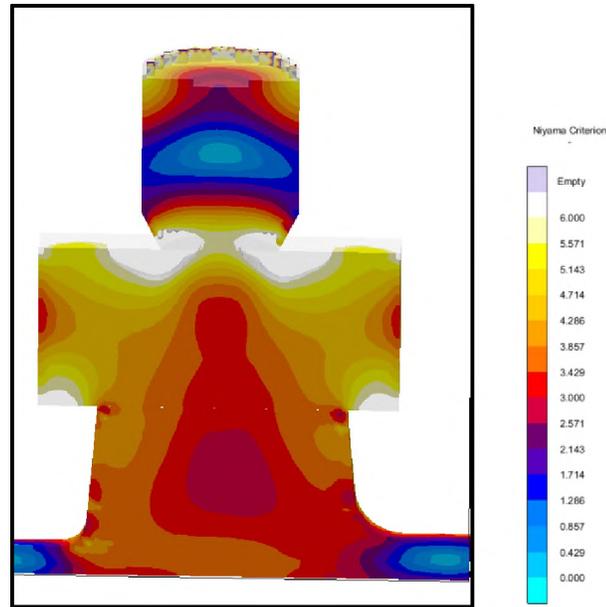
(a)
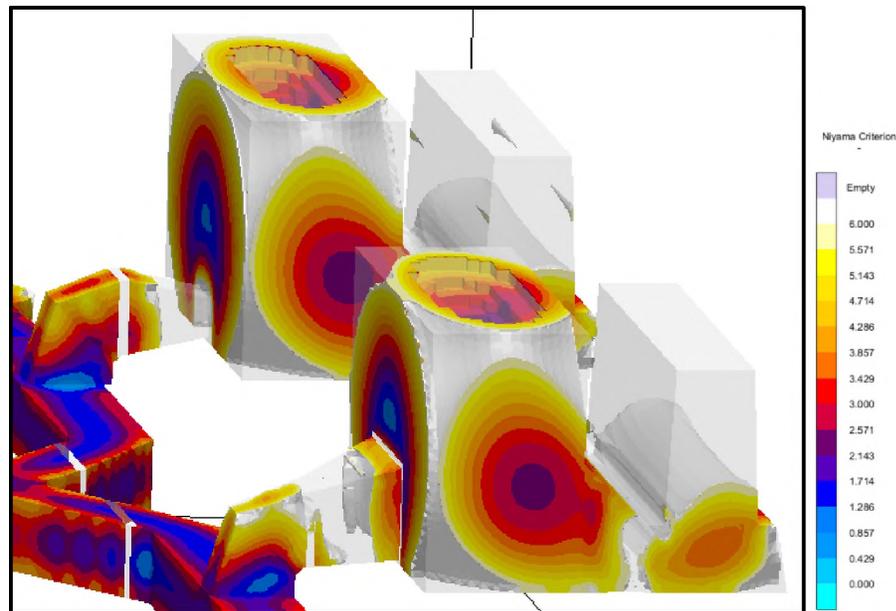
(b)

Figure 4. The castings were designed to have a Niyama number of greater than 6 for obtaining quality castings without shrinkage defect. (a) the casting from top riser system (b) casting from the pressurized and non-pressurized system. The transparent regions indicate a Niyama value greater than 6

The high velocity incoming metal in the runner initially bypasses the bottom gate and the vortex spin trap works as anticipated for reducing the velocity of the metal into the gate as shown in Figure 3. The velocity of the metal flow inside the casting was found to be 0.5-0.6m/s as shown in Figure 6(b). The air entrapment in the gating system was found to be 6-10% while the air entrapment in the casting was found to be less than 3% as shown
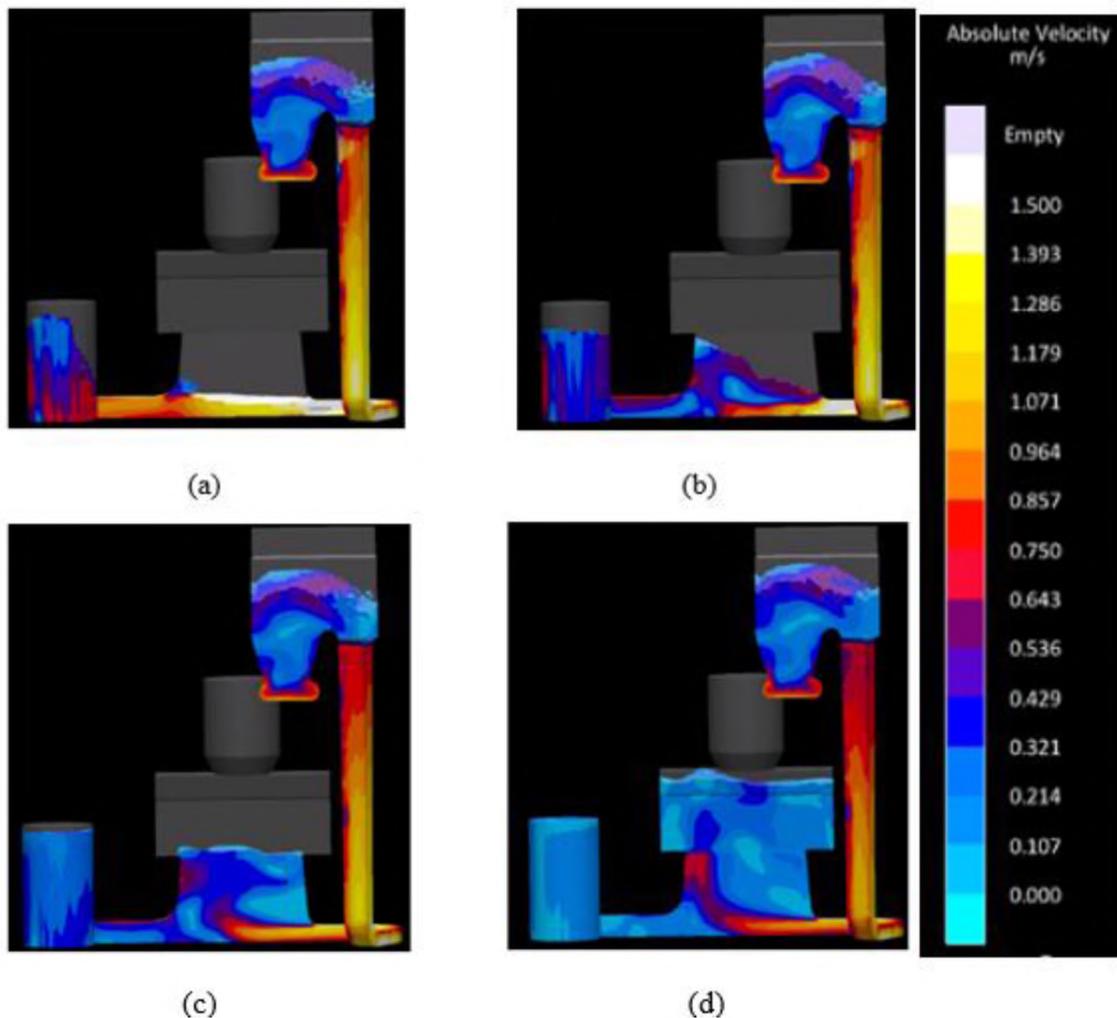
Figure 5. The velocity profile during filling for the top riser naturally pressurized gating system at (a) 30% (b) 35% (c) 50% and (d) 75% of complete filling of the mold observed between a scale of 0-1.5m/s. observed between a scale of 0-1.5 m/s. Molten metal is shown to enter the casting at less than 0.5 m/s and with a flat and quiescent filling profile
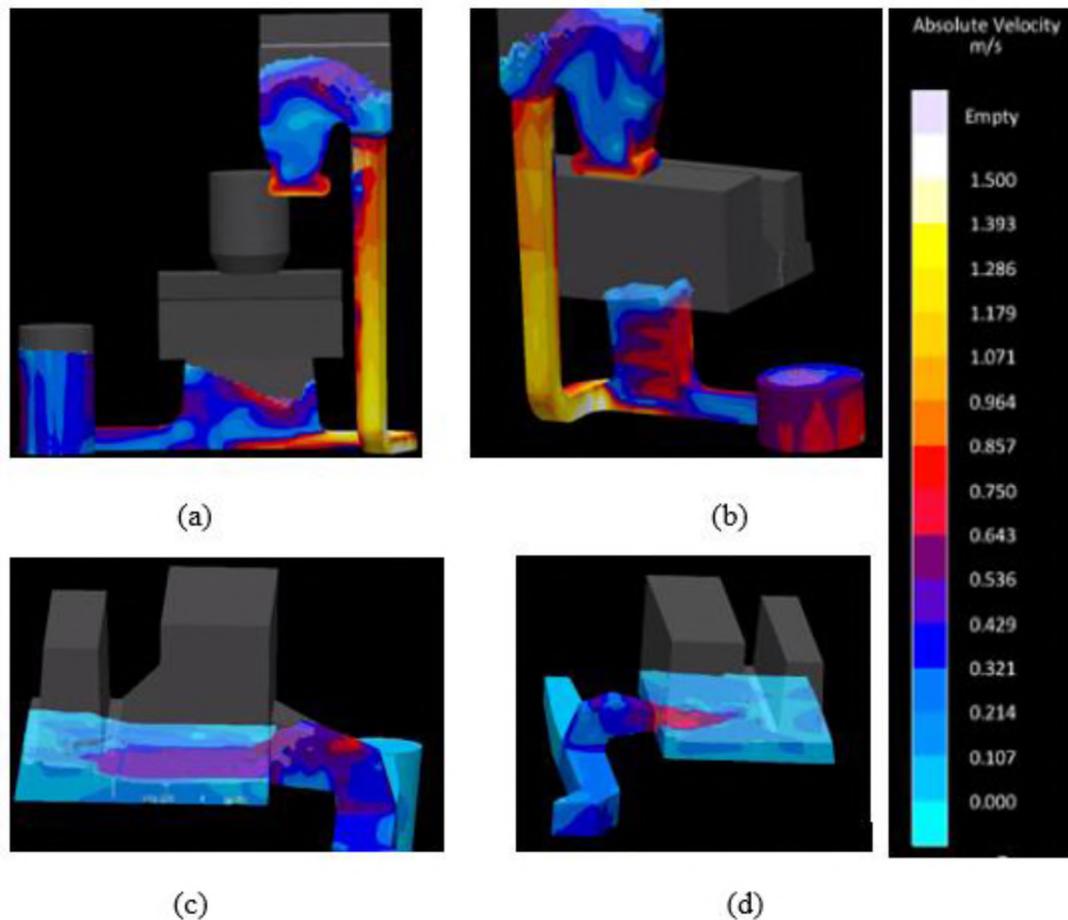
Figure 6. The velocity profile of filling when the molten metal enters the casting in (a) the naturally pressurized top riser system (b) the naturally pressurized side riser system (c) the pressurized system and (d) the non-pressurized system. In (c and d), gate velocity was slightly higher in the traditional pressurized and non-pressurized systems and increased from less than 0.5 m/s to 0.8m/s

in Figure 7(b). Air entrapment less than 15% is considered a well-designed gating in castings and the design shows good agreement with the expected values for a good quality casting.

In the pressurized system, the velocity of the metal into the casting was found to be less than 0.7m/s and in the non-pressurized system, the velocity less than 0.5m/s as shown

in Figure 6(c and d). The air entrapment in the castings of both the pressurized system and non-pressurized system was less than 6% as shown in Figure 7(c) and 7(d), respectively.
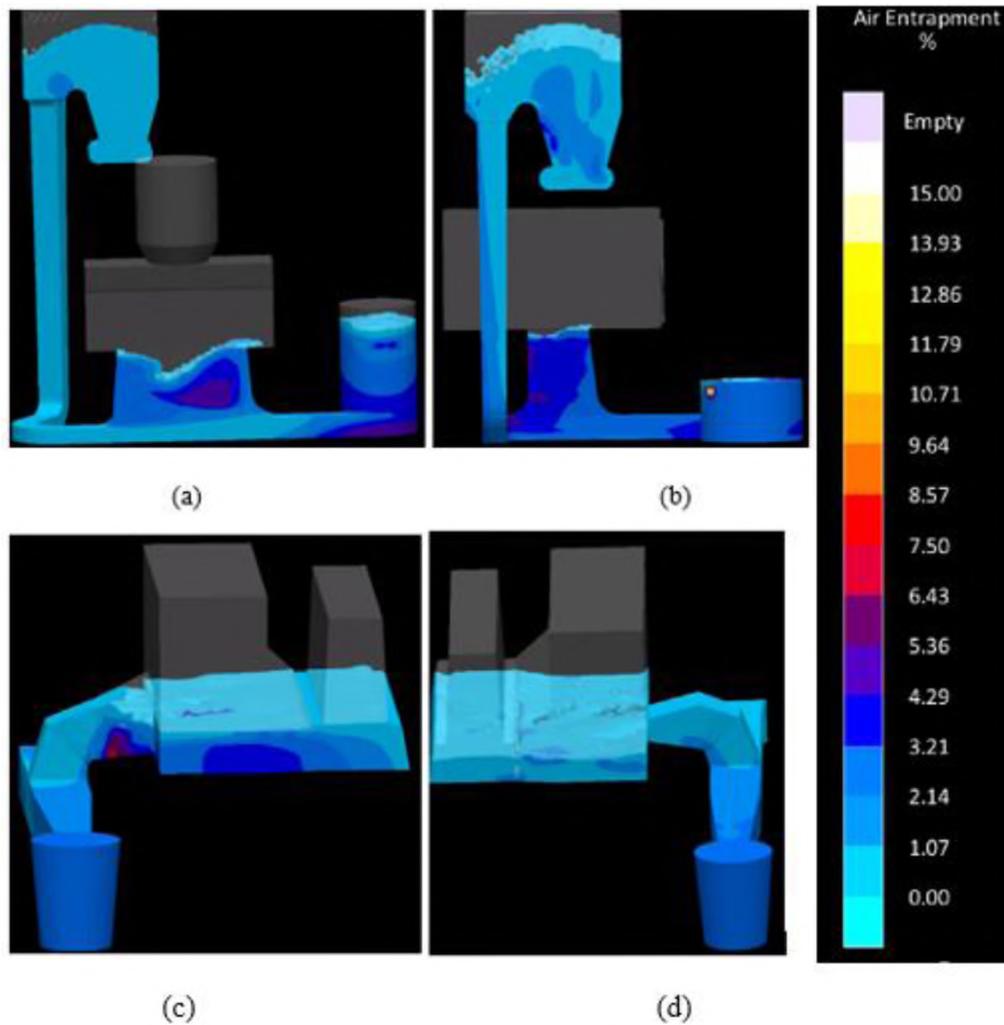
Figure 7. The air entrapment for filling when the metal enters the casting in (a) TR system (b) SR system (c) NP system (d) P system taken between a scale of 0-15%. All the castings were designed to have air entrapment lower than 15%

3. EXPERIMENTAL PROCEDURE

The molds for this study were 3D printed using furan bonded alumina ceramic sand. The complete dimensions of the mold box was 990mm in length, 700mm in width and

550mm in height. As shown in Figure 8, the cope box on these quad molds consisted of the risers and the traditionally gated casting cavities while the drag box contained the runners and the gates. The parting line was irregular and the naturally pressurized casting cavities were printed separately as cores and glued into place. Openings were provided in the cope box for inserting the chills. Alumina tubes were inserted into holes in the steel chills as vents to prevent misrun.

To understand the industrial conditions and replicate actual industrial practices, an SAE 8630 steel alloy was poured by a partner foundry into two quad molds. The steel was melted in a 1000lb induction furnace. The melt was protected from oxidation by surface protective argon liquid, the EGAL process, during steelmaking. The steel was tapped into a 1000lb teapot style ladle and the ladle temperature was recorded to be 1605°C (2921°F). The steel was aluminum killed in the ladle prior to pouring. Immersion samples were obtained in the ladle just prior to pouring and the temperature in the ladle just before the pour was recorded as 1605°C. The filling time for each mold was measured to be 11 seconds. The top of the castings was sectioned for inclusion analysis. The locations of samples for inclusion analysis are shown in Figure 10. Samples were sectioned from a depth of approximately 7.5mm from the top surface of the castings, as shown in Figure 10(a). Five samples, numbered 1, 2, 3, 4 and 5 according to their positions as shown in Figure 10(b) were obtained for the castings with side risers and four samples were taken for inclusion analysis in the casting with the top riser as shown in Figure 10(c). Since the inclusions tend to float to the top, it was decided that analysis near the of the top surface would be the ideal location for inclusion analysis. The remaining casting was sectioned, 15mm from one end and 25mm from the top (shown as a yellow box), to obtain samples

for chemistry analysis as seen in Figure 10(b). The position of the samples was kept constant throughout the castings. A LECO TC500 was used for oxygen and nitrogen analysis while a LECO CS600 was used for carbon and sulfur analysis. The vortex overflows that were designed in both the naturally pressurized systems were also sectioned to study the inclusion population. The sectioning of the overflows of the top riser system is seen in Figure 11(a). The overflow from the top riser system was sectioned vertically in half and from one of the halves, three samples were obtained.
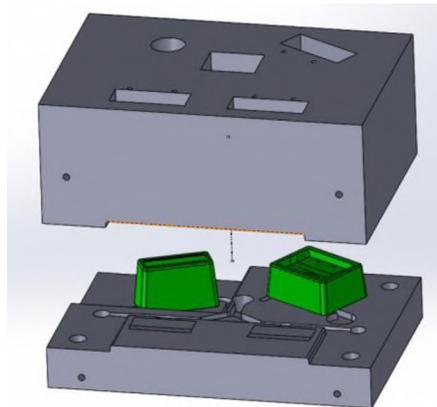
Figure 8. CAD drawing of the mold assembly shows the cope box containing the risers and the casting cavities while the drag box contains the runners and the gates

Figure 9. Image of the mold directly after pouring at the industrial partner foundry shows a full pouring basin and no spillage

The three samples were named OA11, OA12 and OA13 respectively from top to bottom for the top riser system. Similarly, the sectioning of overflows of the naturally pressurized side riser system is seen in Figure 11(b). Since this overflow was smaller than the other was, two samples were obtained, namely OB11 and OB12.
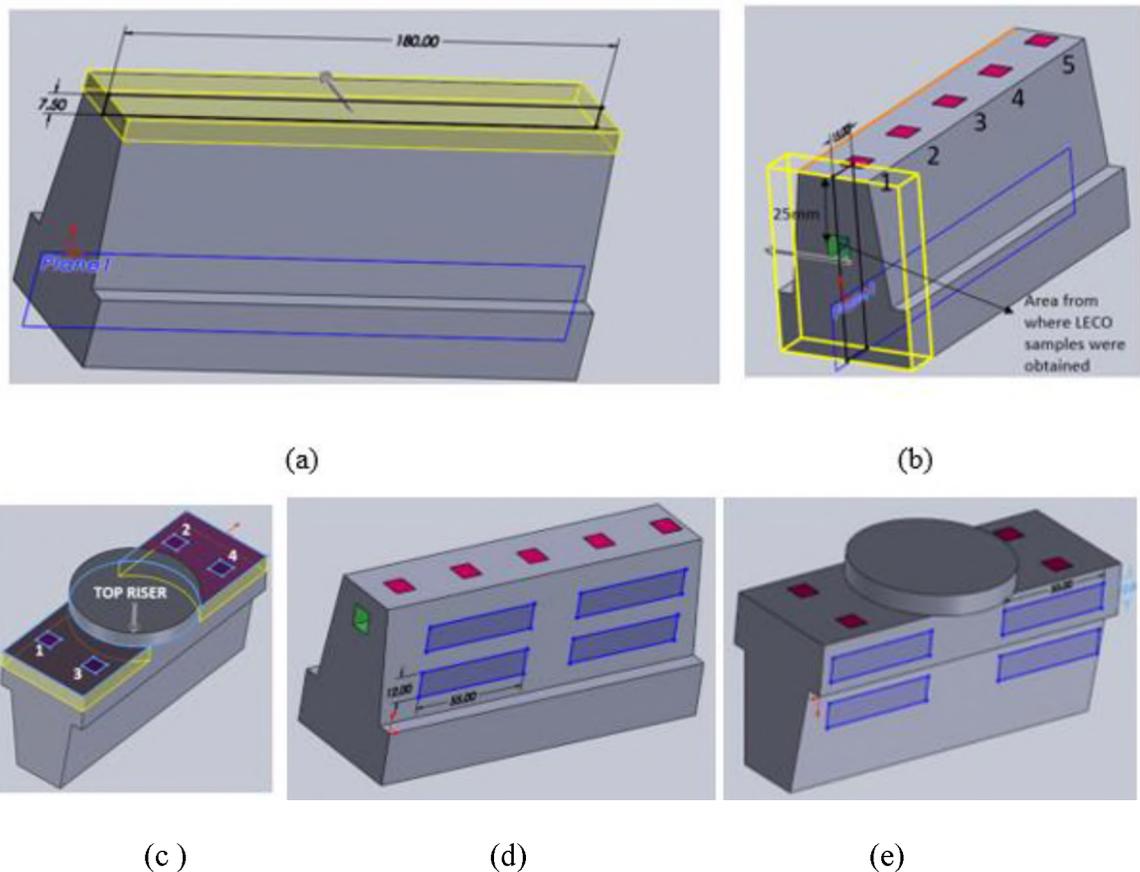
Figure 10. CAD drawing of castings showing the location of chemistry samples, inclusion analysis samples, and CVN test bars. (a) 7.5 mm from the top of the side risered castings were sectioned and 5 samples were sectioned for inclusion analysis according to their positions directly beneath as shown in (b). LECO chemistry analysis of total C, S, O, and N was obtained at a depth of 15 mm into the casting. (c) Specimens for inclusion analysis were taken from the shoulders of the TR system. (d) Locations of the CVN bars taken from the SR, NP and P systems in two different layers, 1 and 2. (e) Locations of CVN bars taken for the TR system below the shoulders of the casting

The samples were metallographically polished and inclusion analysis was performed. Inclusion analysis of samples was accomplished utilizing an ASPEX PICA 1020 SEM with automated feature analysis. A backscattered electron detector (BSED) and a magnification of 500X was used for the analysis. An emission current of $32\mu A$ with a dwell time of $12\mu s$ was considered for the analysis. To understand and compare the impact toughness of various gating systems, Charpy V-notch tests were performed at room temperature as per ASTM E23. The pressurized, non-pressurized and naturally pressurized side riser system's castings were sectioned into two layers of 18mm each as shown in the Figure 10(d). From the first layer 4 samples were obtained, namely 1, 2, 3 and 4 and from the second layer, four samples were obtained, namely 5, 6, 7 and 8. From Figure 4(a), it was observed that the naturally pressurized top riser system had a low Niyama criterion the mid-section. To avoid this shrinkage affecting mechanical properties, samples from this particular system were obtained as shown in Figure 10(e) from the shoulders of the casting. These test bars were initially machined to dimensions of 12mmX12mmX55mm. The bars were normalized by soaking at 900°C for 30 minutes in protective atmosphere and cooled. The bars were then austenitized at 870°C for 30 minutes, quenched in room temperature water, and subsequently tempered at 600°C for 30 minutes and water quenched immediately. The bars were then machined as per ASTM E23 standards and tested at room temperature using a Tinius Olsen model 84 pendulum type impact testing machine. The area directly under the fracture surface of selected specimens were metallographically polished to understand the relationship between area fraction of inclusions and impact toughness.
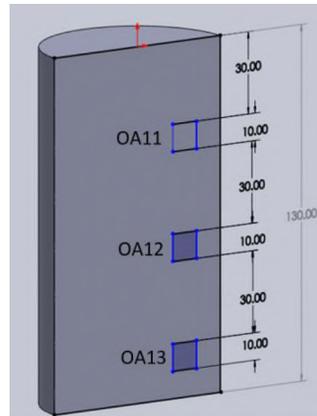
(a)
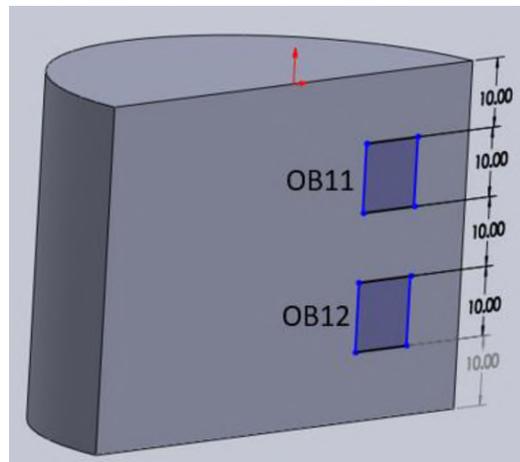
(b)

Figure 11. CAD drawing showing the position of samples obtained for inclusion analysis from the vortex overflows in the naturally pressurized systems. These are named OA11, OA12 and OA13 for the top riser, TR, system as shown in (a). (b) Two samples were obtained for inclusion analysis and named OB11 and OB12 from the side riser, SR, system

4. RESULTS

For the results and discussion section, the following abbreviation would be used for the different gating systems.

Table 1. Abbreviation of different gating systems and the molds

TR	Naturally pressurized Top Riser system
SR	Naturally pressurized Side Riser system
NP	Non-Pressurized system
P	Pressurized system
1	Samples/data obtained from mold 1
2	Samples/ data obtained from mold 2

4.1. CHEMISTRY ANALYSIS

The immersion samplers that were obtained from the ladle before the pour were analyzed using the optical emission spectroscopy (OES). Table 2 gives the measured chemistry for all the elements except carbon and sulfur which were measured using combustion infrared detection techniques in a LECO C/S analyzer. For analyzing the carbon, oxygen, sulfur and nitrogen levels, samples were sectioned from the casting as shown in Figure 8(b) and the results are shown in Table 2.

Table 2. Steel chemistry in weight percent as determined using OES and LECO*

Fe	Al	C	Cr	Cu	Fe	Mn	Mo	Ni	Si	O*	N*	S*
Bal	0.01	0.33	0.60	0.07	97.1	0.71	0.18	0.58	0.31	.003	0.006	0.006

A comparison of the total oxygen, nitrogen, and sulfur levels for mold 1 and mold 2 are given in Figures 12(a) and 12(b), respectively. The oxygen and nitrogen levels in all of the four gating systems were relatively constant in mold 1. The oxygen content varied

around 55-60 ppm while the nitrogen content was found to be between 75-78 ppm. However, for mold 2 while nitrogen levels remained constant and were similar to the levels in mold 1, the total oxygen levels showed a significant variation. The pressurized, P, system exhibited the highest oxygen content at 70 ppm while the nonpressurized system with the top riser, TR, showed the lowest amount of total oxygen at 43ppm. The sulfur levels in the pressurized system were the highest in both of the molds, however, the average sulfur content was around 50 to 65 ppm in all of the castings except for the pressurized system in mold one which had significantly higher sulfur at 78 ppm.
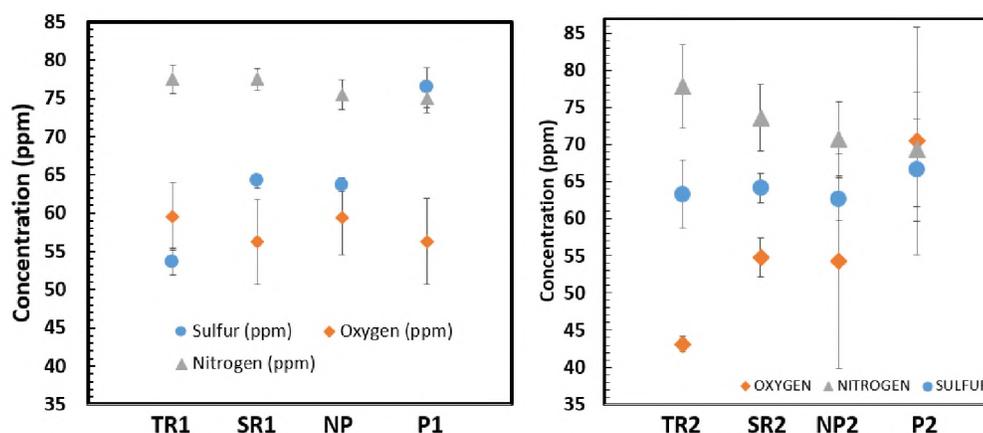
Figure 12. Total oxygen, sulfur, and nitrogen (in ppm) for samples taken from the castings of different gating systems. (a) The naturally pressurized top riser (TR) and side riser (SR) systems and traditional nonpressurized (NP) and pressurized (P) gating systems for (a) mold 1 and (b) mold 2

Optical micrographs of the polished specimens sectioned underneath the top surface of the castings are shown in Figure 13. Inclusions were present in clusters in the different gating systems in both the molds. The optical micrographs that were observed for the TR, SR, NP, and P systems of mold 1 are shown in Figures 13 (a), 13(b), 13(c) and 13(d) respectively.
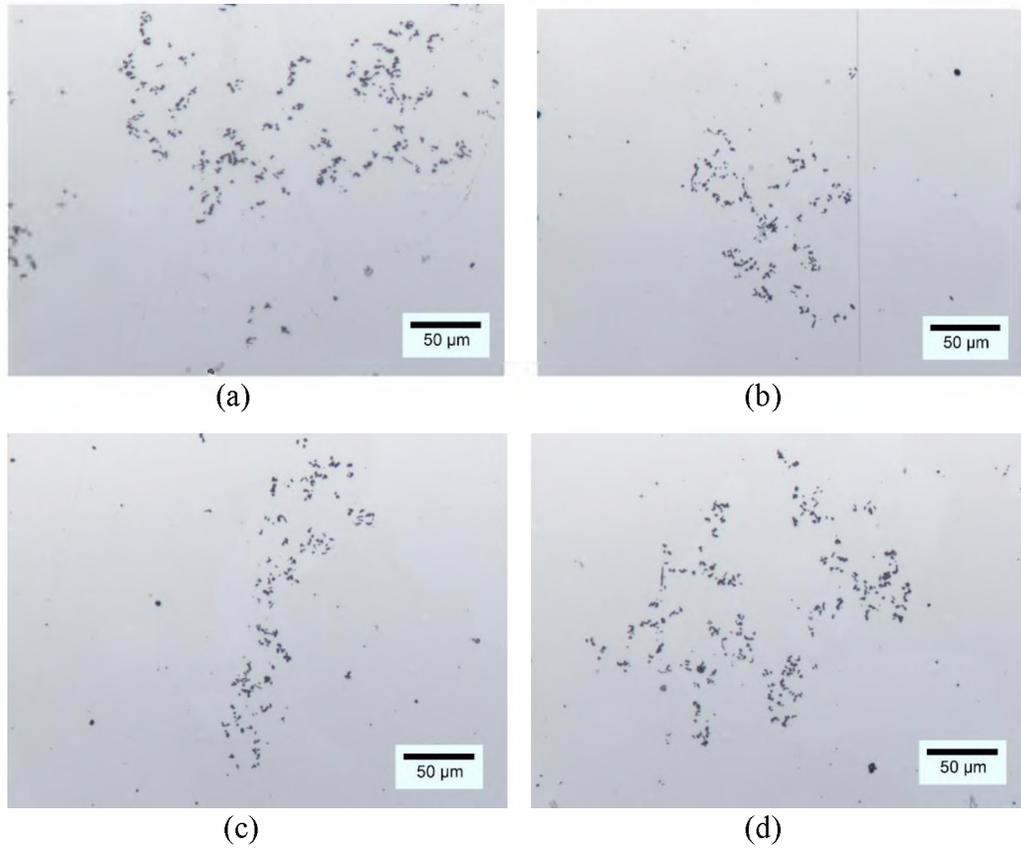
Figure 13. The optical micrographs taken from the different gating systems in mold 1 reveal the presence of inclusions present in clusters throughout the samples. (a) Naturally pressurized top riser (b) Naturally pressurized side riser (c) Non-pressurized system (d) Pressurized system

4.2. NON-METALLIC INCLUSION ANALYSIS

Inclusion analysis of samples was accomplished utilizing ASPEX PICA 1020 SEM with automated feature analysis. Inclusion analysis revealed that most of the inclusions found in the samples were manganese sulfide (MnS), alumina (Al_2O_3) and complex Al_2O_3 – MnS inclusions. Some representative backscattered electron, BSE, images of inclusions are shown in Figure 14.
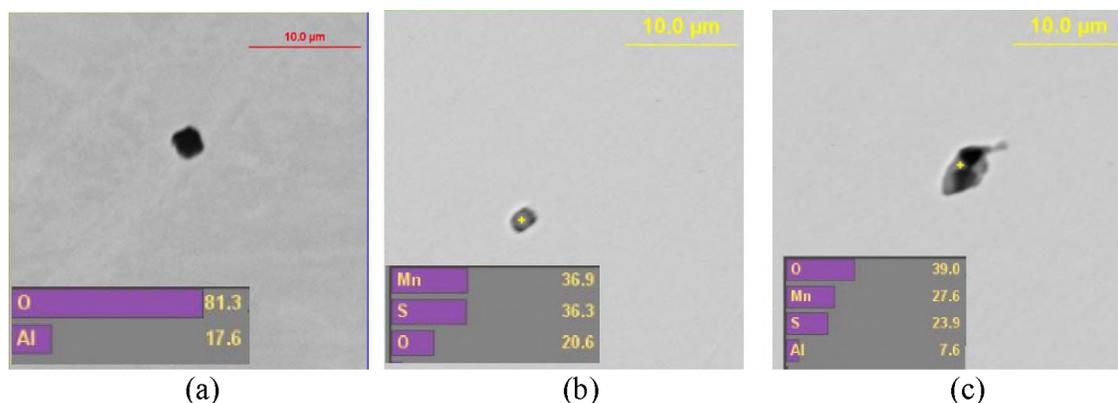
Figure 14. Backscattered electron images of different inclusions and their corresponding chemistries observed in the 8630 steel castings. (a) An alumina inclusion, (b) type 1 MnS, (c) an image showing a complex alumina-manganese sulfide inclusion

Inclusion analysis was performed on samples that were sectioned just below the surface of the castings. Figure 15 shows the area fraction of alumina inclusions with respect to different positions in the casting as denoted in Figure 10. In both the molds, the non-pressurized system had an area fraction of alumina between 200-400 ppm. The naturally pressurized SR systems, apart from position five in mold 1, had an average area fraction between 180 to 250 ppm. The pressurized system in the second mold had high area fraction, ranging from 180 ppm to a maximum alumina area fraction of coverage of 1450 ppm.

Figure 16 shows the area fraction of alumina inclusions between the naturally pressurized top riser, TR, systems of mold 1 and mold 2. It can be observed that except for a single position where the area fraction was 1200 ppm of alumina, the remaining positions had a lower area fraction between 120-300 ppm. The total average area fraction of the alumina, MnS and the complex Al_2O_3-MnS inclusions across different positions is shown in Figure 17(a) and 17(b) for mold 1 and mold 2, respectively. The overall comparison of alumina inclusions in mold 1 showed that the area fraction was between 200-300 ppm. The

complex Al$_2$O$_3$-MnS and MnS was highest in the nonpressurized TR system in both the molds. In mold 2 it was observed that the nonpressurized TR system and the pressurized system exhibit very high standard deviations owing to the high value of alumina area fraction as shown seen in position 3 of Figure 16 and positions 3 and 4 of Figure 15(b).

(a)   (b)
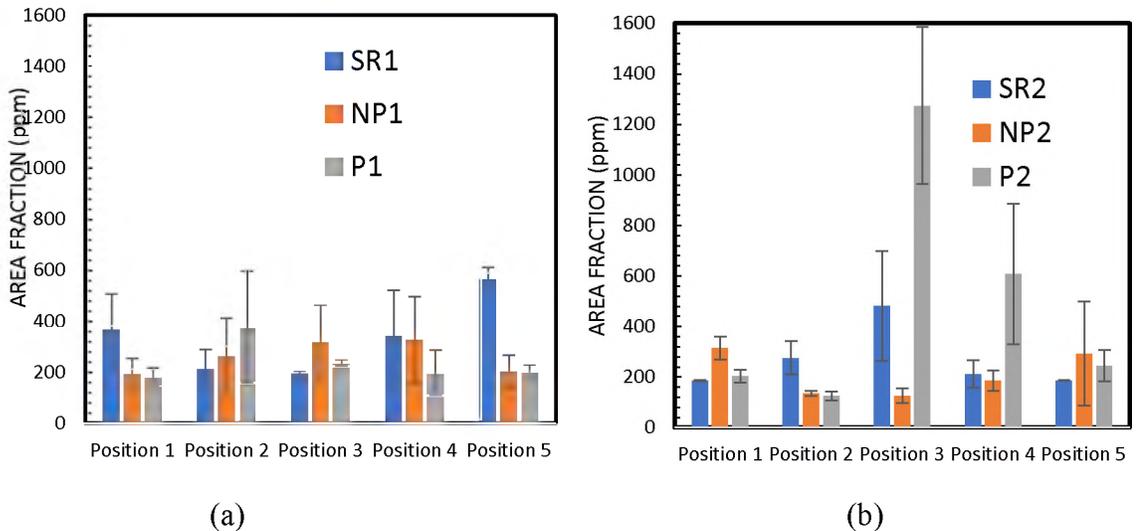
Figure 15. The area fraction of alumina inclusions with respect to the different positions from the top sections of castings from (a) mold 1 and (b) mold 2. The gating systems in mold 1 had an area fraction between 180-500 ppm. The pressurized system of mold two had high inclusion density compared to the rest of the systems

The SR and the NP systems in both the molds showed consistent values for all the inclusions across both the molds. The size distribution of the combined alumina and alumina + MnS inclusion can be seen in Figure 18(a) and 18(b) for mold 1 and mold 2 respectively. Both the molds exhibit similar trends with respect to the size distribution of inclusions and 60-70% of the total inclusions were found to be between 0-3μm. The TR system had the maximum percentage of inclusions above 3μm.
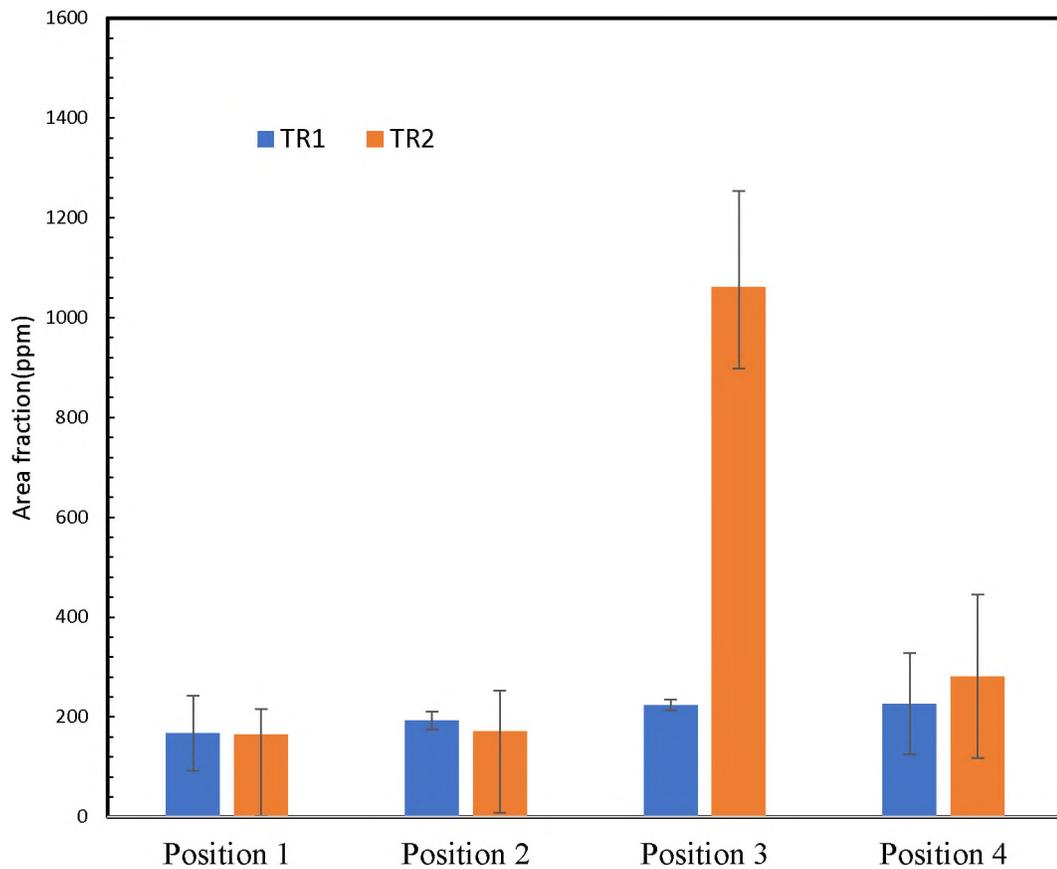
Figure 16. The area fraction of alumina inclusions comparison between the two molds for the TR gating system across different positions. An area fraction between 120-300ppm was found consistently for all positions except one peak of 1200ppm

The analysis of the overflows for mold 1 is shown in Figure 19 for the naturally pressurized top riser and the side riser system. There were no trends with respect to the positions, but the overflows showed a higher area fraction of alumina inclusions than the castings compared from Figure 19 for both the TR and the SR systems.

(a)   (b)
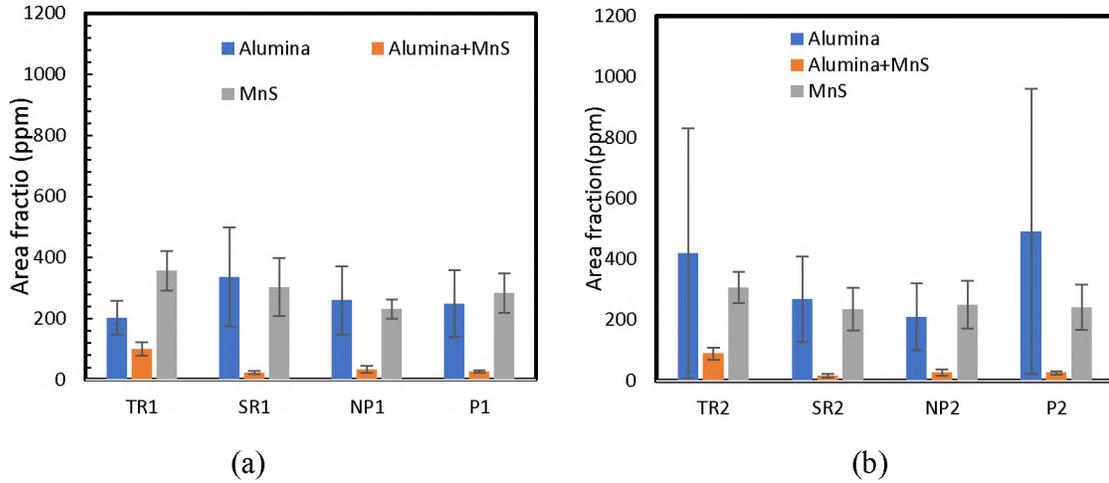
Figure 17. The overall average area fraction of alumina, Al_2O_3-MnS complex inclusions and the MnS inclusions for (a) mold 1 and (b) mold 2 respectively. The NP and SR system showed consistent values while the TR exhibited highest values for the complex and MnS inclusions respectively

(a)   (b)
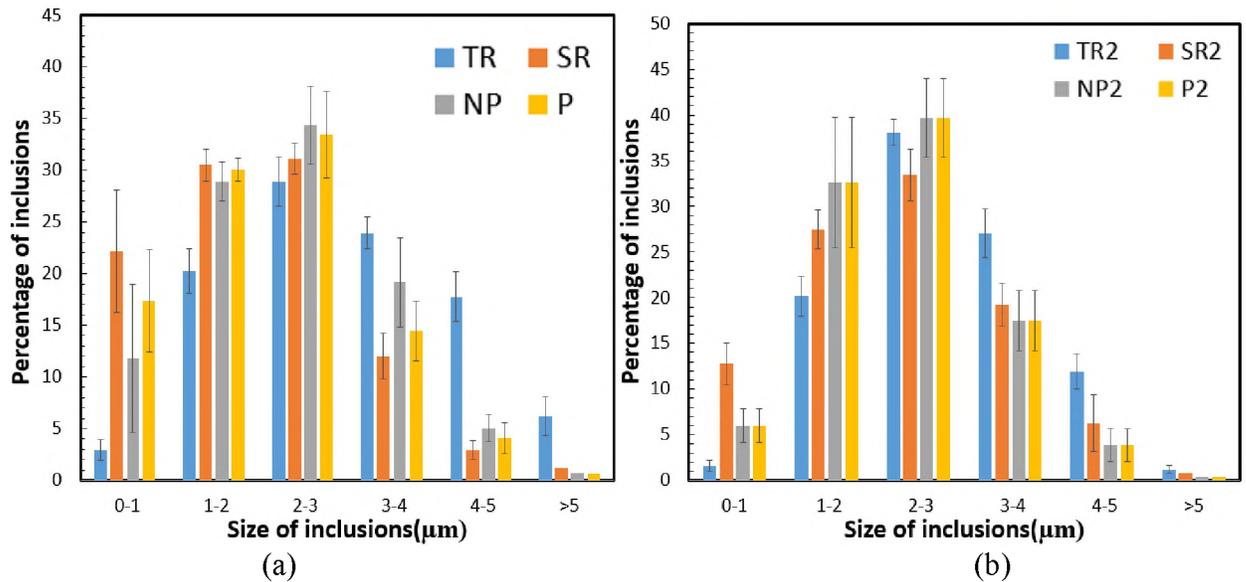
Figure 18. Comparison of size distribution of alumina and the complex inclusions for all the four systems in (a) mold 1 and (b) mold 2. It is seen that 60-70% of all inclusions are <3 μm. Mold 2 has higher size of inclusions than mold 1 which is attributed to inclusion floatation in teapot ladle

4.3. MECHANICAL PROPERTIES

The Charpy bars were tested for hardness (HRC scale) and the CVN impact toughness at room temperature. The comparison of CVN and toughness for mold 1 and mold 2 is shown in Figure 20(a) and 20(b) respectively. The tempered hardness varied somewhat between 35 and 38 HRC. In both the molds, it was observed that hardness and toughness were inversely proportional to each. In both the molds, the TR system exhibited the highest impact toughness while the SR and the NP systems displayed an average of 44 J of toughness.

Fractography was performed on the fractured surface of the bar taken from the pressurized system of mold 1 to understand the nature of the fracture. The specimens all displayed ductile fracture, however, as observed from Figure 21, the presence of large areas of type II eutectic manganese sulfides were noted on the fracture surface on most all of the fracture surfaces and these were the major inclusions observed on the fracture surface and likely contributed to the low energy ductile rupture observed in Figure 21.
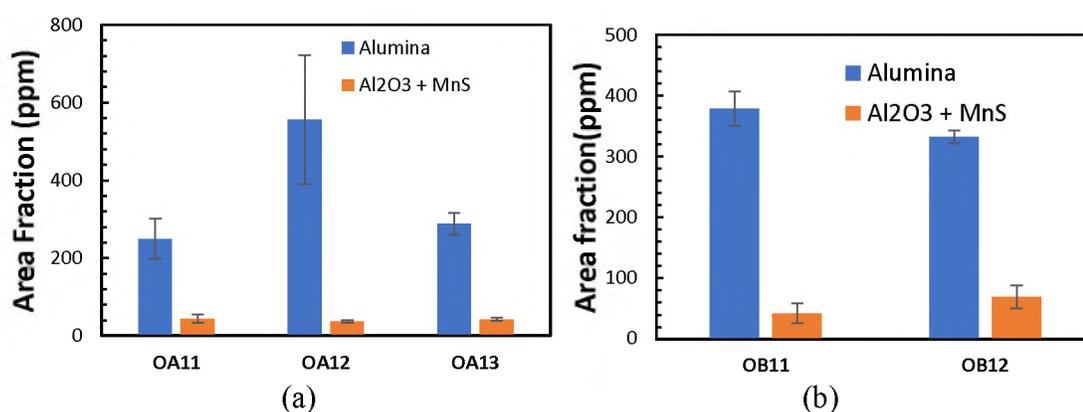
Figure 19. Inclusion analysis in overflows. (a) The area fraction of alumina and the complex inclusions plotted for the different sections of the overflow for the TR system (b) positions in the SR systems

(a)
(b)
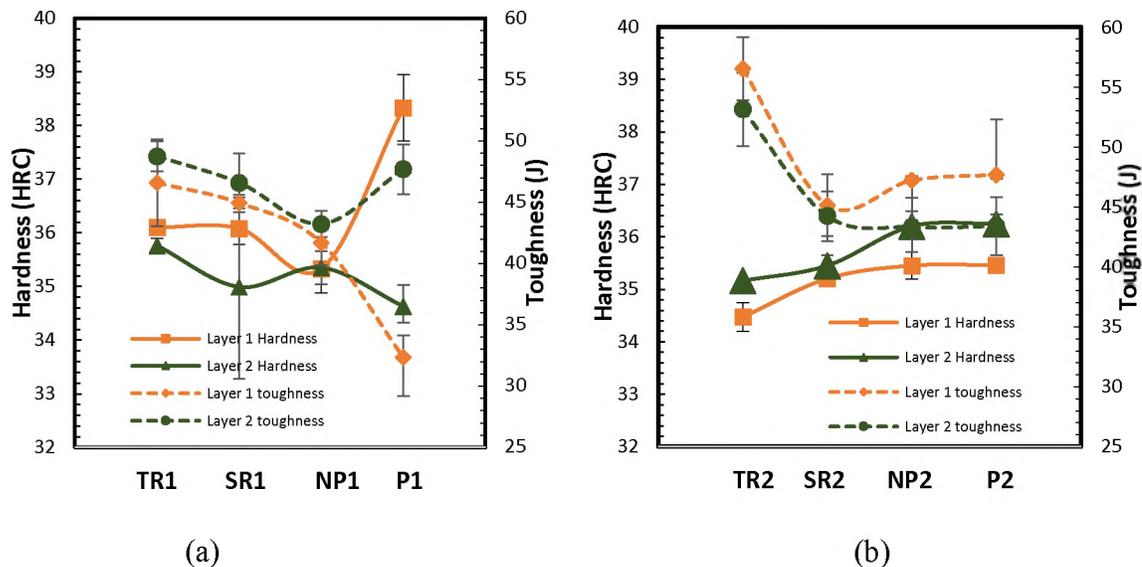
Figure 20. The hardness and toughness properties were compared for the bars obtained from the two layers of the castings from each gating system in (a) mold 1 and (b) mold 2. The hardness and toughness properties were inversely proportional, and the TR system exhibited the highest impact toughness in both the molds

(a)
(b)
(c)
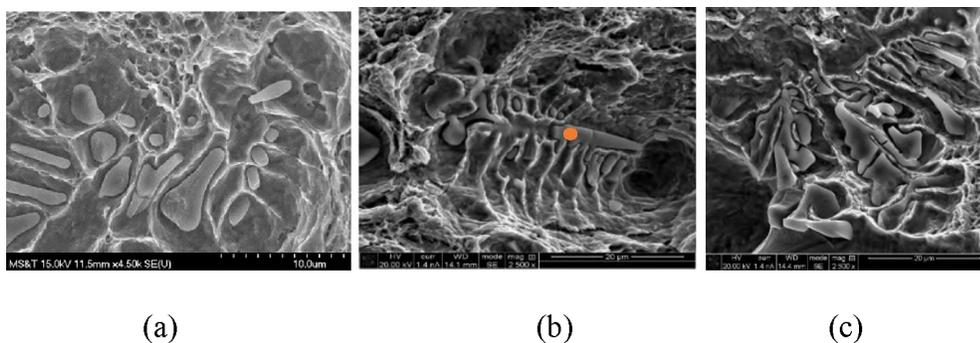
Figure 21. From the pressurized system of mold 1, fractography was performed on the bars which showed the presence of type II eutectic manganese sulfides formed in the chain or fan structure. (b) EDS analysis showed the MnS inclusions were composed of roughly 45%Mn and 27% sulfur by weight

5. DISCUSSION

The simulation for the entire system showed a filling time of 12 seconds while the actual mold filled in 11.4 seconds during the pour showing the accuracy of the simulation

in predicting mold filling. The non-pressurized system was observed to have the best casting surface quality. It has been shown that the filling methods have large impact on the final surface quality of the castings and that a quiet turbulence-free filling method provides a better surface quality to the casting with reduced defects [14, 15]. It must be noted that there were no major defects on any of the surfaces and the chill used on the top of these systems were not zircon washed. The hot metal coming in contact with the chill and some small amount of reaction with the chill might have played an effect on minor surface irregularities. Analysis of the casting chemistries from Figure 12 showed that the nitrogen levels remained relatively constant between 70-75 ppm, while the sulfur content showed a variation in mold 1, with the pressurized system at 75ppm and the TR systems showing around 55ppm. The remaining two systems in mold 1 and all the systems in mold 2 showed around 65ppm of sulfur.

To track the source of sulfur, the immersion sampler obtained from the ladle was sectioned and analyzed for chemistry which showed the concentration (ppm) of nitrogen to be 69.2 ± 4.95, oxygen to be 34.05 ± 6.71 and sulfur to be 63.38 ± 4.62. This shows that there was no sulfur pickup from the mold. The rise in oxygen levels when compared between the immersion sampler and the castings shown in Figure 12, indicates that the oxygen pickup may have been because of reoxidation. The total oxygen contribution from the inclusions was determined from chemistry samples and compared to the measured oxygen in the top section of the castings. The software used for finding the measured oxygen from the inclusion analysis was obtained from the work by M Harris et al.[16] As shown in Figure 22, the total average oxygen content is in very good agreement with the oxygen obtained from the inclusions in mold 1. The two peaks found in the TR system and

the P system in mold 2 was because of the high alumina content in the third position of TR system and third and fourth position of P system respectively as observed in Figure 16 and Figure 15(b).

The optical microstructural analysis as shown in Figure 13, indicated that the alumina inclusions were found in clusters. In the work by Yin et al, it is seen that there exists a strong long-range attraction force between alumina inclusions in low-carbon aluminum-killed steels.[17]. T.B.Braun et al.[18], showed that, the clusters of alumina inclusions are formed because of the collision and coalescence of individual alumina inclusions as a result of convective currents in the melt. To understand the types of inclusions and their formation, thermodynamic modelling for the 8630-steel composition was performed using the JMatPro software. The steel was modelled with 0.006 wt% oxygen, 0.0075 wt% nitrogen and 0.007wt% of sulfur to understand the formation and stability of the inclusions. Figure 23 shows the phases that formed as a function of equilibrium cooling. It is observed that the liquidus of the system was 1435°C. Stable precipitation of alumina as observed at steelmaking temperatures. MnS formed below the liquidus temperature during solidification.

The inclusion analysis shown in Figure 15, indicates that there was no definite pattern of inclusions acquired with respect to positions. In mold 1 except position 2 of the pressurized system and position 5 of the SR system, the rest of the positions for all the systems exhibited an area fraction between 160-240ppm. In mold 2, the area fraction of inclusions remained almost constant except two of the positions in the pressurized system displaying huge deviations. Figure 18 shows that the third position in mold 2 showed an area fraction of 1200 ppm of alumina.

(a)   (b)
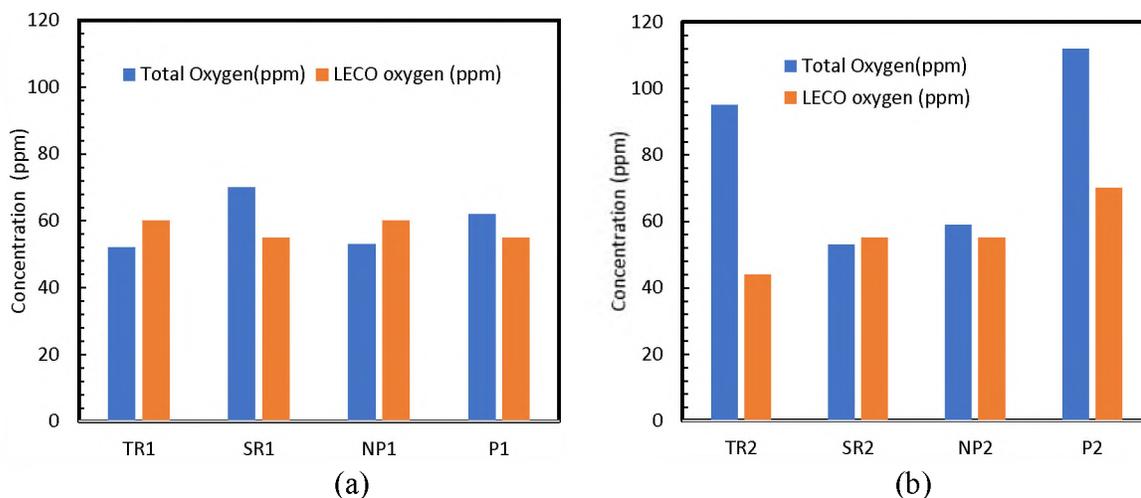
Figure 22. Calculated total oxygen contribution of inclusions from specimens obtained from the top section of the castings as compared to the measured oxygen from LECO analysis
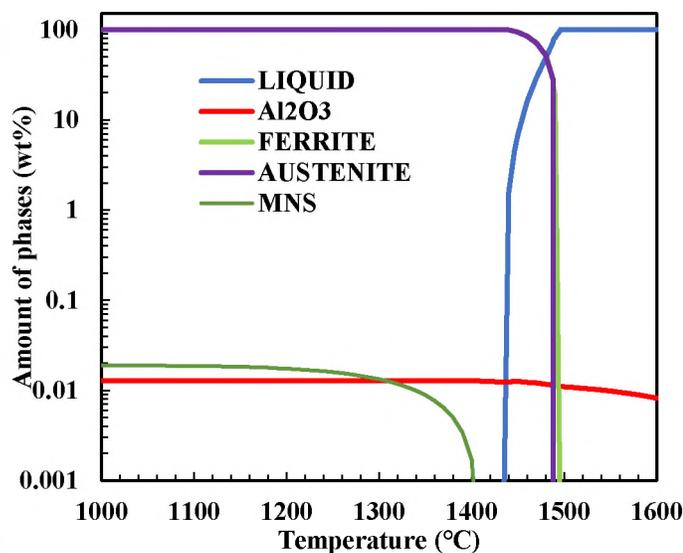
Figure 23. Thermodynamic modeling of the equilibrium solidification of 8630 steel with 0.0075% N, 0.006% O, and 0.007% S. Al_2O_3 is stable in the liquid well above the liquidus. MnS forms after the liquidus during solidification

Using Magmasoft 5.4.1. alumina inclusion tracers with density 3g/cc were used to simulate and predict the formation and accumulation of reoxidation inclusions. As observed in Figure 24(a) (marked by a black circle), for the TR system, the accumulation

of inclusions takes place in the locations where the sample 3 was obtained as shown in 8(d). Similarly, in 24(b), a high concentration of inclusions is obtained from the same location where sample 3 and 4 were acquired. Comparing the above data with Figure 15(b) and 16, it is seen that the simulation results correlate well with the inclusion analysis indicating high alumina concentration in the same locations for the TR and P systems. This validates the presence and accumulation of inclusions in certain areas compared to the others. In both the images, the white areas show the accumulation of alumina inclusions. However, it must be remembered that, these areas may not be the final location of inclusions. There are possibilities for movement of inclusions once solidification begins and the presence of the white areas indicating area fraction of alumina are subject to relocation.

Figure 18(a and b) shows the size distribution of the alumina and the complex inclusions across the different gating systems for the two molds. Mold 2 was found to have larger sized inclusion than mold 1. This indicates that the cleaner metal enters the first mold from the bottom half of the teapot ladle while the second mold collects metal from the top half of the teapot ladle. Due to inclusion floatation, mold 1 has cleaner metal than mold 2. This leads to the accumulation of higher sized inclusions in mold 2. Moreover, the TR system had a higher percentage of larger sized inclusions, than the other systems. Since the TR systems was provided with a top riser while the remaining three systems had a side riser, the movement of larger sized inclusions towards the top riser, leads to the accumulation of larger sized inclusions near its evaluation area.

(a)   (b)
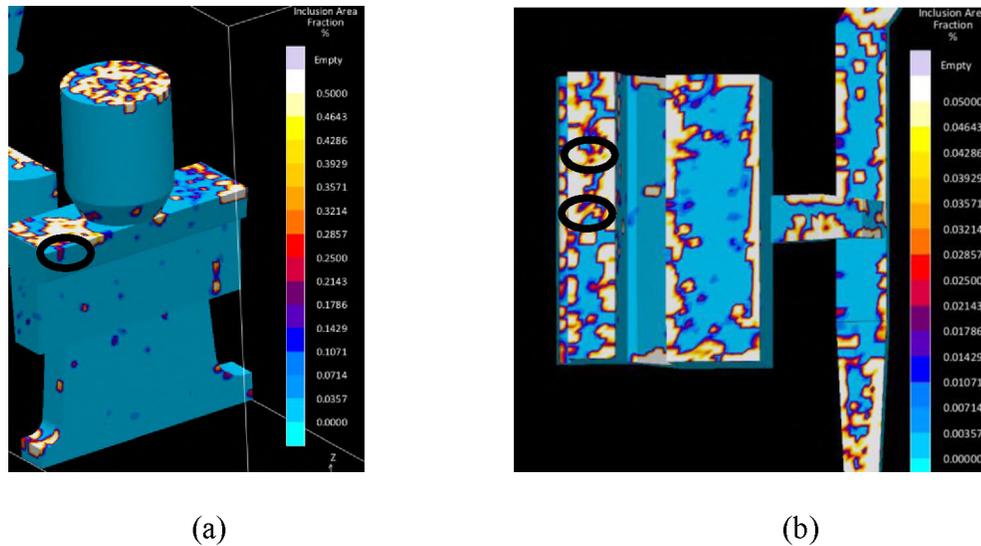
Figure 24. Magmasoft inclusion tracer analysis showing the position of reoxidation inclusions after filling. (a) The accumulation of alumina inclusions observed in the TR system where sample 3 was obtained for analysis (b) The alumina inclusion accumulation in pressurized system where samples 3 and 4 were obtained for analysis indicated using black circles on the castings

Figure 19(a) and (b) show the area fraction of alumina inclusions in the spin traps in the vortex overflows or spin traps. It was observed that the area fraction of alumina inclusions in the overflows were higher than that in the castings. The area fraction of alumina inclusions in the overflow of SR system was on average 8% higher than that in the casting while the overflow of the TR system showed a 65% increase in alumina inclusions in the vortex spin trap than in the casting. The spin traps were designed primarily to trap the incoming metal containing slag, dross, and other inclusions to prevent them from entering the casting. The high area fraction shows that the terminal spin traps functioned efficiently. The overflow from the TR system showed a higher inclusion content than the SR system and this could be attributed to the inclusion floatation. The plot showing the hardness and toughness values for the different systems is shown in Figure 20 and it can be observed in both the molds that the TR system had the highest toughness. Except for

the pressurized system of mold 1, in both the molds, layers 1 and 2 respectively, did not

show a statistically significant difference in the impact toughness. The TR system from

mold 2 showed a maximum toughness of 56±4 J while the pressurized system from mold

1 showed the least toughness of 43J. The difference in the variation in toughness of layer

1 and layer 2 of the P system, could be a function of hardness. In an earlier study performed

by Stephens [19], for 8630 steel, a hardness of 32.5HRC and a CVN toughness of 32 J was

obtained at 25°C. In the current experiment, a maximum toughness of 52 J is observed and

an average toughness of 45±6 J at an average hardness of 35HRC taken across all the

systems. As seen in Figure 21, the presence of the eutectic type II manganese sulfides was

the main factor leading to loss in fracture toughness. To understand the relationship

between the MnS inclusions and toughness, a polished section was obtained directly

beneath the fracture surface of the test bars. In Figure 25, the MnS inclusion density

obtained from the sections underneath the Charpy bars is plotted against the corresponding

toughness. An inverse relationship between the inclusion density of manganese sulfides

and toughness of the inclusions is observed as shown in Figure 25. The TR system shows

the least MnS inclusions across both the layers and hence the highest toughness among all

the systems. The consistency in the amount of MnS density across both the systems and

the associated toughness shows that the toughness was dependent on the MnS inclusions

in all the gating systems across both the molds. From literature [20-22], among the three types

of sulfides, the type II which are formed as a chains or fan like structures in interdendritic

regions during solidification and are the most detrimental to the mechanical properties of

steel. The toughness of notched bars was reduced as much as 50% with the presence of

these eutectic sulfides. Type II sulfide inclusions cover large areas of the surface which

leads to high stress concentration and easy crack initiation and propagation causing premature ductile failure in steels and a corresponding loss in strength and toughness.
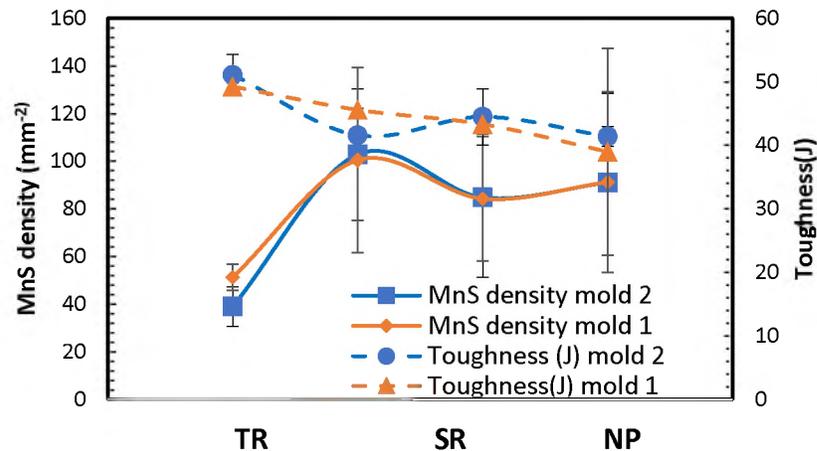
Figure 25. Notch toughness plotted along with the density of manganese sulfide inclusions for (a) mold 1 and (b) mold 2. It was observed that the toughness and the inclusion density display an inverse trend for both the molds

6. CONCLUSION

To understand the effect of filling on steel castings and quantify them, four gating systems, namely, a non-pressurized system with a side riser, pressurized system with a side riser, a naturally pressurized top riser and a naturally pressurized side riser system were designed using MagmaSoft 5.3.1. The solidification parameters like macro and microporosity, Niyama criterion and hotspots were simulated. The runners and gates were designed to minimize ingate velocity to less than 0.8m/s and air entrapment less than 15%. The two naturally pressurized systems were provided with vortex overflows to collect the incoming new metal and to reduce the velocity of liquid metal for smoother filling. A common pouring basin was designed to unite the system and the castings were chilled and

vented. Alumina and manganese sulfide were the major inclusions found. Alumina inclusions were mainly found in clusters throughout the castings from all the four systems. The overall comparison of inclusions from samples obtained from the top layer of the castings showed that the top riser performed the best, followed by the non-pressurized system. The pressurized system exhibited high area fraction of alumina inclusions. Sectioning of overflows revealed that the area fraction of inclusions in overflows were higher than in the castings proving that the overflows collected most of the damaged incoming metal and slag effectively. The naturally pressurized system with a top riser was shown to have the highest toughness among all the systems. The type II eutectic MnS were the major reason for low energy ductile fracture. The naturally pressurized gating systems with overflows provided castings with better surface quality and lower inclusions. The naturally pressurized systems provide better quality metal and would be a good fit for producing cleaner castings with good mechanical properties for 8630 steel.

ACKNOWLEDGEMENTS

program at Missouri S&T as well as their contribution to the modeling work within this

manuscript.

REFERENCES

1. John Campbell "Castings" Butterworth-Heineman (2003)

2. Xue X, Hansen S.F, Hansen P.N, Water Analog Study of Effects Gating Designs on Inclusion Separation and mold filling control, AFS Transactions, vol. 101, pp.199-209, (1993)

3. Lin H.J, Hwang W. S., Three-Dimensional Fluid Flow Simulation for Mold Filling, AFS Transactions, vol. 97, pp 855-862, (1989)

4. Griffin, J. A., and Bates, C. E., "Ladle Treatment, Pouring and Gating for the Production of Clean Steel Castings," SFSA Research Report, No. 104, 1991

5. M. Masoumi, H. Hu, J. Hedjazi, M. A. Boutorabi "Effect of Gating Design on Mold Filling", AFS Transactions, pp 05-152, (2005)

6. John Campbell, "Mini Casting Handbook", Revised and Enlarged Second Edition book, 2018.

7. J. Campbell, Complete Casting Handbook, 2ndEdition, Elsevier, Oxford, UK 2015.

8. J. Campbell, Complete Casting Handbook, Elsevier Ltd. (2011). p. 74.

9. https://commons.wikimedia.org/wiki/File:Casting_gating_system.svg

10. Seyyed Hojjat Majidi "Effect of Pouring Conditions and Gating System Design on Air Entrainment during Mold Filling" International Journal of Metalcasting. AFS Transactions (2018)

11. A.Dojka, J.Jesierski, " Optimized gating system for steel castings", *J. of Materi Eng and Perform* **27,** 5152–5163 (2018)

12. Jan Jezierski, Rafal Dojka, Krzystof Janerka "Optimizing the Gating System for Steel Castings", Metals, 8(4), pp 266 (2018)

13. C Reilly, N.R Green,M.R. Jolly " The Present State Of Modeling Entrainment Defects In The Shape Casting Process" Applied Mathematical Modelling, Volume 37, Issue 3, pp 611–628 (2013)

14. C.Jorden, J.L.Hilll, T.S.Piwonka," Computer Designed Gating systems" Metal Casting Technology Centre, The University of Alabama

15. G.D.Chandley, M.C.Felmings, "Gating Premium Quality castings"

16. M. Harris et al., "Evolution of Non- Metallic Inclusions in Foundry Steel Casting Processes," Proceedings of the 69th Annual Technical and Operating Conference, Steel Founders Society of America (SFSA) (2015, Chicago Illinois), Steel Founders society of America (SFSA) (Dec 2015)

17. Sei Kimura, K. Nakajima, and S. Mizoguchi "Behavior of Alumina-Magnesia Complex Inclusions and Magnesia Inclusions on the Surface of Molten Low-Carbon Steels", Metallurgical and Materials Transactions B 32(1):79-85, (2001

18. T.B.Braun, J.F.Elliott,, M.C.Flemings, "The Clustering of Alumina Inclusions"

19. Ralph.L.Stephens, "Fatigue and Fracture Toughness Of Five Carbon or Low Alloy Cast Steels at Room Or Low Climate Temperature", Steel Founders' Society of America, Research Report No. 94A, October (1982)

20. Philips Charles Belding, "Control of non-metallic inclusions in steel", Master of Science Theses, Oregon state Unversity, June (1971).

21. Lyman, Taylor (Ed). Metals Handbook. Cleveland, Ohio, American Society for Metals, 1332p, (1948)

22. Breznyak, G. Das, M. T. Groves and J. F. Wallace. The effect of sulfur and phosphorous on the dynamic properties of cast steel. Rocky River, Ohio, Steel Founders' Society of America, (1968).

III. QUANTIFYING THE EFFECT OF FILLING ON HIGH MANGANESE AND ALUMINUM STEEL CASTING QUALITY

K. Balasubramanian,[1] L.N. Bartlett,[1], M. Xu[2]

[1]Missouri University of Science and Technology, Rolla, MO and [2]Georgia Southern University, Statesboro, GA

Keywords: naturally pressurized gating systems, non-metallic inclusions, air entrapment, bifilms, solidification simulation

ABSTRACT

High manganese and aluminum steels, or FeMnAl steels, have excellent combinations of strength and toughness and display up to a 17% reduction in density when compared with quenched and tempered low alloy martensitic steels. Military applications for FeMnAl steel castings require good ballistic performance and a low level of casting defects. However, filling related defects such as inclusions and oxide bifilms are problematic in these steels because of the high aluminum content and because these defects can sharply reduce mechanical properties. In the current study, the effect of different gating systems on reducing the amount of filling related defects in nominal composition Fe-29%Mn-8.2%Al-0.91%C-0.88%Si-0.49%Mo steel castings was studied using a combination of computer modeling of fluid flow and solidification, automated inclusion analysis, and evaluation of mechanical properties in test castings. Four different gating systems were evaluated in the same mold and included a traditional-styled non-pressurized system and pressurized system and two naturally pressurized systems, one with a side riser

and one system with a top riser. Parameters such as critical velocity of metal flow, air entrapment, microporosity and Niyama criterion were considered and a design was developed with a common pouring basin using solidification software. Optical and electron microscopy revealed the presence of alumina bifilms that were entrained into the castings during filling in each of the gating systems. Notch toughness was evaluated using standard sized Charpy V notch bars that were broke at room temperature and showed a decrease in notch toughness and an increase in variability with an increase in the percentage of bifilms. The results showed that a well-designed traditional-style nonpressurized gating system with runner extensions, a runner well, and keeping the gate velocity less than 0.7 m/s produced the cleanest castings with the highest average notch toughness of 160J and the least mechanical property variance.

1. INTRODUCTION

FeMnAl steels, are high toughness steels that are based on high manganese austenitic Hadfield steel and have additions of up to 12%Al.[1] These FeMnAl steels have reduced densities because of the added aluminum content that usually ranges between 4-10% and dilation of the austenite crystal structure with the addition of manganese between 20-30%. Most studies of cast FeMnAl steels have centered around a composition of Fe-30Mn-9Al-0.9C-1.0Si-0.5Mo. For this composition, a 15% reduction in density is observed when compared to quenched and tempered SAE 4130 steel castings with similar strength and dynamic fracture toughness.[2]

The presence of inclusions and oxide bifilms are one of the major reasons for the loss of toughness in these steels. Brittle and faceted aluminum nitride, AlN, inclusions are

stable at steelmaking temperatures in these alloys and this can decrease the ductility and toughness when these inclusions are present in significant amounts. The work done by Schulte et al. on a Fe-30Mn-9Al-1Si-0.9C-0.5Mo steel casting showed that the presence of AlN inclusions decreased the Charpy V-notch (CVN) breaking energy from 35J to 19J as the concentration of AlN increased from 12 inclusions/mm^2 to 210 inclusions/mm^2.[3] The high aluminum content in these alloys is also problematic with regard to the formation of solid oxide films that form as the surface of the melt reacts with oxygen in the atmosphere. This leads to the formation of solid oxide bifilm defects, which can be entrained in the steel during steelmaking and pouring, leading to a loss in strength, fatigue life and ductility in castings. Bifilms are formed when the molten metal is exposed to the atmosphere and forms a solid film which folds over itself and gets entrained in the melt, often containing a layer of trapped gas. [4, 5] Surface turbulence is an important contributor for bifilm formation because poorly designed molds provide the possibility for hydraulic jumping and splashing of metal. This provides the opportunity for the liquid metal to divide into droplets, exposing the melt and causing the formation of new bifilms by air entrainment.[6] Bifilms have been known to an adverse effect on the mechanical properties of aluminum castings and the work done on AA356 castings by Liu and Samuel, established a linear relationship between the percentage elongation and log area percentage of oxide films[7]. These bifilms can also serve as nucleation sites for gas porosity such as hydrogen during solidification and can act as sites of failure when stress is acted upon it. [8]

Gating systems play an integral role in determining the final quality of the casting, since the liquid metal enters the casting through the gate. A well-designed gating system

helps to decrease the turbulence in the flow of the liquid metal, reduces the slag, dross and air entrapment and captures inclusions in the gating system instead of the casting [9]. The various defects like cold shuts, ripple marks etc. that are usually formed in castings can be directly related to how the fluid metal behaves during mold filling [10]. During pouring of the liquid metal from the ladle into the mold, prevention of air entrainment is extremely important. During mold filling, the formation of breaker waves, low pressure areas created by liquid metal moving past sharp corners and the metal rebounding off obstacles leads to air entrainment. These subsequently leads to the oxide formation which occurs either as inclusions or bifilms in the steel castings. The pouring basin, the sprues, the runner and the gates must be designed and optimized to reduce or eliminate air entrapment to reduce reoxidation inclusion formation.[11] The work that has been done thus far on investigating the pouring conditions, and their impact on formation of oxide inclusions have suggested that, minimizing the velocity of the incoming metal has a sizeable impact on reduction of air entrainment defects.[12] Pressurized and non-pressurized systems, in which the choke in the system is present either at the gates or at the base of the sprue, respectively have traditionally been used in foundries for more than 50 years. Despite the advent of fluid flow and solidification modeling, their application is still largely based on ideal gating ratio calculations and rules of thumb. Although computer aided fluid flow and modeling and solidification software has come a long way in recent years, these software packages cannot accurately predict the amount or location of reoxidation inclusions during filling and the databases of different alloys and thermodynamic data is limited. Novel naturally pressurized gating practices have been introduced in the recent years to reduce filling related defects and improve mechanical properties, however, their application often

requires the trade-off of decreasing casting yield. [13] The vortex spin gate and the trident gate systems are two such bottom gated systems which have vortex surge cylinders or centrifugal traps which lower the velocity of the metal through the gate and aid in capturing the first metal into the gating system which is likely highly damaged from air exposure.[14] The presence of a terminal spin trap at the end of a runner extension not only aids in reducing the velocity of the incoming metal for smoother filling but also collects the slag and dross carried by the liquid metal. This enables cleaner metal to fill the castings. [14] These naturally pressurized systems have not been evaluated in FeMnAl steels. The goal of this study is to quantitatively evaluate the effect of different gating systems, namely a pressurized system, a non-pressurized system, and two naturally pressurized systems on casting cleanliness and notch toughness of nominal composition Fe-29Mn-8.2Al-0.91C-0.88Si-0.49Mo steel castings.

2. DESIGN OF TEST CASTINGS

The design and solidification software Magmasoft (5.3.1) was used for the designing the molds. The material used for the simulation from the database is GX120Mn13 (1.2%C and 13%Mn) which is the closest available to the target composition, Fe--29Mn-8.2Al-0.91C-0.88Si-0.49Mo. The test castings are shown in gray in Figure 1 and were designed to be modified y-block castings of length 180 mm and a height of 85 mm. The castings were designed in such a way to accommodate a flat surface for obtaining samples to understand the effect of filling conditions on surface quality and provide an evaluation surface for floatation of reoxidation inclusions. For the study of CVN impact toughness, the length and width of the narrow section of the y-block was designed to

accommodate sectioning of eight ASTM E23 standard sized CVN bars in two layers of four bars each. The size of the castings was identical between different gating systems to minimize the effect of solidification on the microstructure and mechanical properties. Table 1 shows the nomenclature for the different gating systems that will be used as abbreviations. The goal of the current study is to study the effect of filling conditions on steel cleanliness and CVN toughness for FeMnAl steel. Therefore, other defects such as shrinkage and microporosity were minimized. It is also important to "catch" filling related damage in the evaluation area of the castings and minimize floatation of inclusions into risers. Keeping these two requirements in consideration, the castings and gating systems were meticulously designed to ensure that most of the inclusions that entered the gate from the filling process remained in the castings while at the same time, producing sound metal with low levels of microporosity, <0.08%, in the evaluation area. The y-block castings were designed to have a flat surface for inspection of surface quality and the presence of bifilms and inclusions. The design consisted of four different gating systems as shown in Figure 1, namely a traditional pressurized system with a side riser, a traditional non-pressurized system with a side riser, a naturally pressurized side riser system and a naturally pressurized top riser system. As shown in Figure 1, for the traditionally gated non-pressurized, NP, pressurized, P, and the naturally pressurized system with a side riser, SR, these conditions were satisfied by using a vented top chill (shown in blue) and a side riser (shown in red) to produce a high thermal gradient and low microporosity. The second naturally pressurized system incorporated a top riser to observe the filling of the molten metal into the casting cavity during the pouring operation. However, the solidification conditions in the test area were almost identical to the others. The detailed explanation of

the mold design has been provided in the author's earlier paper, where the same mold design was utilized for analysis of 8630 steel composition. [15] The pouring basin had an undercut which helped in controlling the velocity of the incoming metal. The pouring basin was also provided with an offset having a curved radius to ensure easy flow of metal into the down sprue eliminating any air entrainment defects. The parameters considered for the design was velocity of steel flow to be less than 0.8m/s as shown in Figure 2, a Niyama criterion greater than $6(C\text{-}s)^{0.5}/mm$, micro porosity less than 0.08% and absence of any hotspots or macroporosity. As shown in the author's earlier paper, it is important to mention that the solidification parameters like Niyama criterion and microporosity displayed similar trends for FeMnAl steel as seen in 8630 castings.

(a)   (b)
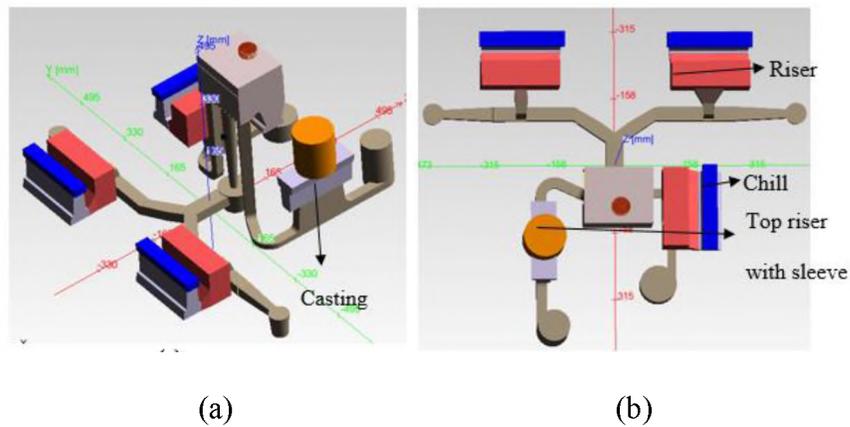
Figure 1. The complete design of the four gating systems in (a) isometric view (b) top view

While the pressurized, non-pressurized and the naturally pressurized side riser systems, had a Niyama value greater than $6(C\text{-}s)^{0.5}/mm$ throughout the castings, the top riser system as seen in Figure 2(b), had a Niyama greater than $5(C\text{-}s)^{0.5}/mm$ in the mid-

section of the casting and greater than $6(\text{C-s})^{0.5}/\text{mm}$ near the shoulders. Niyama values greater than $6(\text{C-s})^{0.5}/\text{mm}$ are shown by the uncolored region.

(a)   (b)
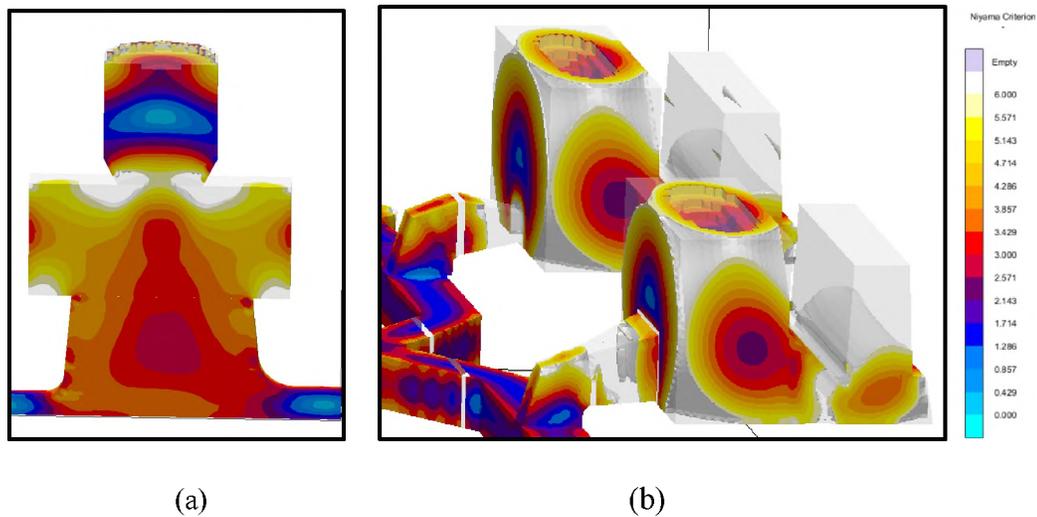
Figure 2. The castings were designed to have a Niyama number of greater than $6(\text{C-s})^{1/2}/\text{mm}$ for obtaining quality castings with low levels of microporosity. (a) The casting from top riser naturally pressurized system (b) Castings from the pressurized and non-pressurized systems

The velocity at the base of the castings in the naturally pressurized systems and at the gates in the pressurized and non-pressurized systems was found to be lower than 0.8m/s. The naturally pressurized systems were provided with overflows while the pressurized and the non-pressurized systems were provided with runner wells. The overflows aid in controlling the velocity of the metal and in collecting the incoming inclusions and slag, so that new metal without any impurities enters the castings. An elevated gate was attached to either of the split runners leading into the gates. The gating ratio for the pressurized system was found to be 1:3:1.4 and the non-pressurized system was found to be 1:3:8. Air entrapment was considered while designing the gating systems and the castings were designed in such a way that the overall air entrapment in the gates

and the castings was maintained below 15% for all the four gating systems. The naturally pressurized side riser system and the pressurized and the non-pressurized systems were also chilled from the top to ensure a high thermal gradient and greater riser feeding distance. A low carbon steel insert that was zircon-coated was used as the chill. The chills were vented by drilling holes through them and inserting ceramic alumina tubes. The naturally pressurized top riser system was provided with a sleeve and remained an open riser.

3. EXPERIMENTAL PROCEDURE

The molds for this study were 3D printed using furan bonded ceramic sand at the University of Northern Iowa. The complete dimensions of the mold box was 990mm in length, 700mm in width and 550mm in height. The cope box consisted of the risers and the traditionally gated casting cavities while the drag box contained the runners and the gates. The parting line was irregular and the naturally pressurized casting cavities were printed separately as cores and glued into place. Openings were provided in the cope box for inserting the zircon-washed chills. Alumina tubes were inserted into drilled holes in the chills as vents to prevent misrun. These vents were then packed tightly around the holes using no-bake sand.

A 1000-pound furnace was used for melting the charge. The target composition was Fe-29Mn-8.2Al-0.91C-0.88Si-0.49Mo. The steel was poured into two molds sequentially using a tea pot ladle. Immersion samples were taken at every stage of charge addition and from the ladle. The temperature in the ladle just before the pour was 1561°C. The filling

time for each mold was measured to be approximately 11 seconds. Once the molds were

shaken out, they were sectioned for further analysis.
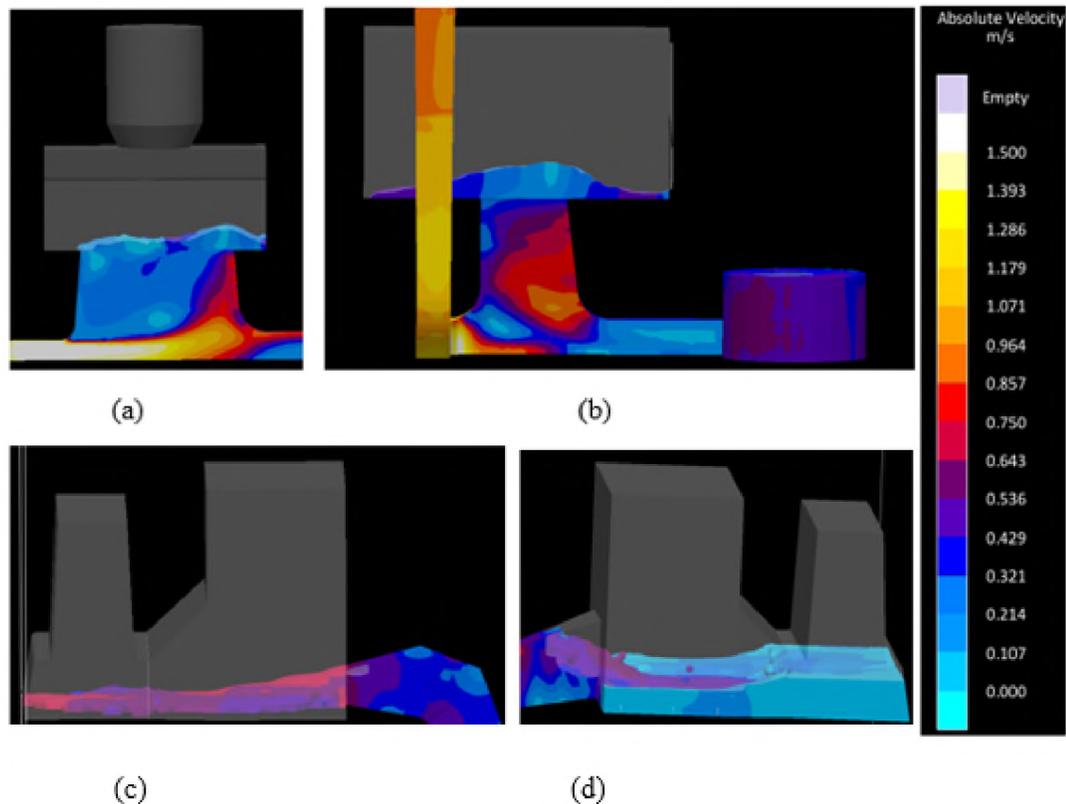
Figure 3. The velocity for filling when the metal enters the casting at various filling times in the(a) naturally pressurized top riser system (b) naturally pressurized side riser system (c) pressurized system (d) the non-pressurized system. All the castings were designed to have ingate velocities less than 0.8m/s

The top surface of the castings of all the four gating systems were analyzed for any

defects related to surface irregularities caused during solidification. The top surface of the

castings were sectioned for inclusion and bifilm analysis. The sample preparation methods

for the naturally pressurized top riser, naturally pressurized side riser, non-pressurized and

the pressurized system is shown in Figure 4. The locations for inclusion and bifilm analysis

were sectioned at a depth of 7.5mm from the top surface of the castings, as shown in Figure

4(a), where the yellow section shows the sectioned region. Five samples, numbered 1, 2, 3, 4 and 5 according to their positions as shown in Figure 4(b) were obtained from the top section. For representative purposes, the positions are marked in Figure 4(b). The authors would like to remind the readers that the five samples for inclusion analysis were obtained from the bottom side of the sectioned 7.5mm layer. Since the inclusions have a tendency to float to the top, it was decided that the analysis of this top surface would be the ideal location for inclusion analysis. From one end of the remaining casting, a block was sectioned for obtaining samples for chemistry analysis. The position of the 5 samples from the top skin and location of chemistry samples was kept constant throughout the castings for an even comparison of inclusion distribution and chemistry across the gating systems. LECO TC500 was used for oxygen and nitrogen analysis while a LECO CS600 was used for carbon and sulfur analysis. In the top riser system, because of a lower Niyama criterion in the mid-section as observed in Figure 4(c), samples were sectioned from either of the shoulders beside the top riser. Four samples were obtained for the analysis as seen in Figure 4(c), where the yellow region shows the sectioned part. These samples were polished using standard metallographic procedures and analyzed for inclusions and bifilms.

Due to the high volume of bifilms found on the top surface of the castings, the percentage area coverage of bifilms was used as a measure to determine cleanliness. To understand the effect of casting cleanliness on the impact toughness of the castings obtained from the different gating systems, standard Charpy tests were performed at room temperature as per ASTM E23 standards. As shown in Figure 4(d), for the pressurized, non-pressurized and naturally pressurized side riser systems, two layers of bars were obtained from the mid-sections of the castings. From the first layer, 4 bars were obtained,

namely 1, 2, 3 and 4 and from the second layer, four bars were obtained, namely 5, 6, 7 and 8.

(a)   (b)

(c)   (d)   (e)
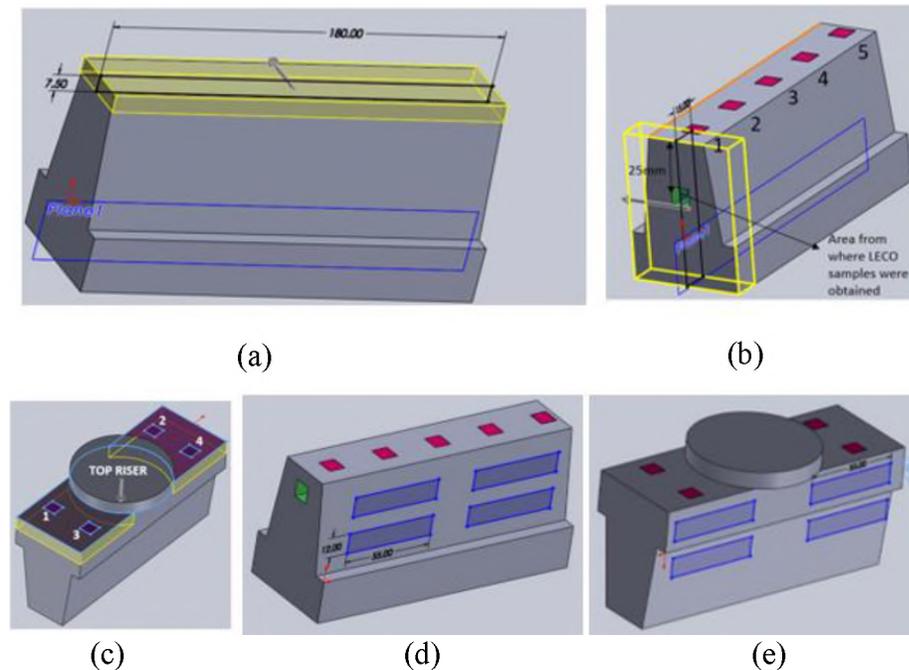
Figure 4. Experimental CAD drawing of castings showing the location of chemistry samples, inclusion analysis samples, and CVN test bars. (a) 7.5 mm from the top of the side risered castings were sectioned and 5 samples were sectioned for inclusion analysis according to their positions directly beneath as shown in (b). LECO chemistry analysis of total C, S, O, and N was obtained at a depth of 15 mm into the casting. (c) Specimens for inclusion analysis were taken from the shoulders of the TR system. (d) Locations of the CVN bars taken from the SR, NP and P systems in two different layers, 1 and 2. (e) Locations of CVN bars taken for the TR system below the shoulders of the casting

From Figure 2(a), the naturally pressurized top riser system had a low Niyama criterion in the mid-section. To avoid this shrinkage from affecting the mechanical property, bars from this system were obtained as shown in Figure 4(e) from the shoulders of the casting. Rectangular specimens were machined from the resulting castings and solution treated in a protective atmosphere at 1050°C for two hours and then rapidly quenched in water. The bars were then machined to dimensions of 10mmX10mmX55mm

according to ASTM E23 standards. Ten hardness values were taken on the ends of each machined bar using an INSTRON Rockwell tester. Charpy tests were conducted room temperature using a TINIUS OLSEN Model 84 impact testing machine. Representative fractured bars were retained for inclusion analysis and fractography using scanning electron microscopy.

4. RESULTS

For the results and discussion section, the abbreviation shown in Table 1 would be used for the different gating systems.

4.1. CHEMISTRY

The immersion samplers that were obtained from the ladle before the pour were used to analyze the chemistry using optical emission spectrometry (OES). Table 1 gives the measured chemistry which were measured using OES and combustion infrared detection techniques in a LECO C/S analyzer.

Table 1. Abbreviation for the different gating systems and the molds

TR	Naturally pressurized Top Riser system
SR	Naturally pressurized Side Riser system
NP	Non-Pressurized system
P	Pressurized system
1	Samples/data obtained from mold 1
2	Samples/ data obtained from mold 2

Table 2. Target and measured chemistry in weight percent as determined using OES and LECO*

Element	Al	C*	Cr	Cu	Fe	Mn	Mo	Ni	Si	O	S
Target	8.2	0.91	-	-	61.72	29	0.49	-	0.88	-	-
Ladle	7.88	0.9*	0.06	0.03	60.25	29.36	0.34	0.003	1.11	0.0015	0.005

The certified standards used for calibration of the OES had chemistries similar to the composition of the steel. Combustion analysis was performed for analyzing the concentrations of carbon, sulfur, nitrogen and oxygen. The results are shown in Figure 5 for mold 1 and 2 respectively. The sulfur levels in both mold 1 and mold 2 were constant between 50-60ppm. The oxygen levels were less than 5 ppm in mold 1 for the TR, NP, and P systems while it was 26.5ppm for SR systems with high standard deviation. For mold 2, the oxygen levels were between 30-45ppm with high standard deviations for all the four gating systems. The nitrogen concentration for the TR systems in both the molds remained constant at 15ppm while for the other gating systems, it was generally higher in mold 2 than mold 1 as observed in Figure 5(b).

4.2. BIFILM ANALYSIS

The samples obtained from the top skin of the casings were metallographically polished and observed under the optical microscope for inclusions and bifilms. They were

found to have a dense network of bifilms as shown in the Figure 6(a).Since the bifilms

interfere with the automated inclusion analysis, providing very little area for inclusion

(a)   (b)
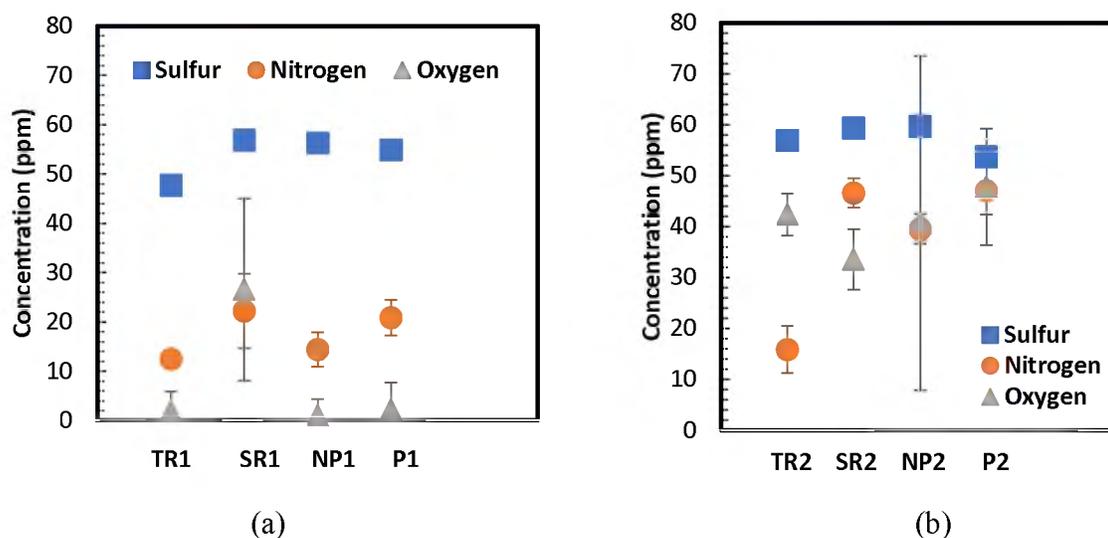
Figure 5. Measured concentrations of oxygen, sulfur, and nitrogen (in ppm) for samples taken from the castings of different gating systems for (a) mold 1 and (b) mold 2

characterization, only optical microscopic bifilm evaluation was performed on these

samples. Fifteen images were randomly captured for every sample at a magnification of

5X and it was ensured that the areas of 2 samples did not overlap. Using ImageJ software,

a threshold is applied as shown in Figure 6(b) and the percentage area cover of the bifilms

is calculated. The average of the fifteen values of percentage area cover of bifilm was

obtained per sample. As seen in Figure 4(a) and 4(b), there were 5 samples obtained from

the top SR, NP, and P gating system and 4 samples from the top of TR system. Figure 7(a

and b) show the percentage of bifilm area coverage as a function of location for each gating

system. It must be remembered that the values shown in Figure 7, are average values

obtained from fifteen images taken from that sample. It was observed that in mold 1, the

SR system showed consistently high bifilm area around 3-4% throughout all the positions.

The TR system showed 1-2% bifilm cover while the P and the NP displayed 1-2% except for position 1 and 4, where high film cover was observed. Except the SR system, mold 1 and mold 2 were found to have comparable area cover of bifilms for all positions.
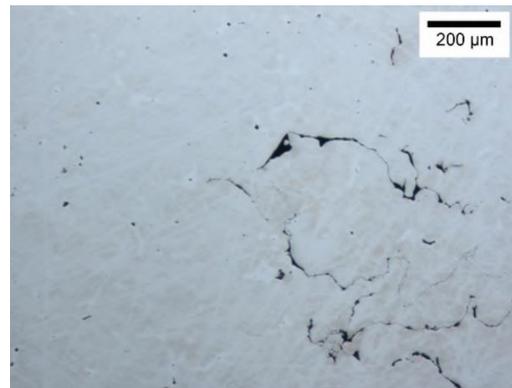
(a)
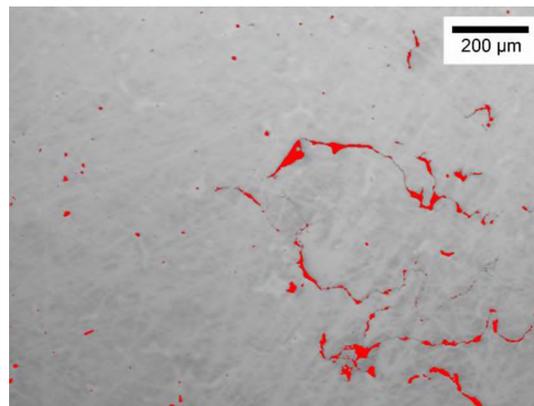
(b)

Figure 6. Bifilm analysis on images using ImageJ. (a) An image captured from the top riser system of mold 1, showing the presence of bifilms (b) Using ImageJ software, a threshold is created to identify the bifilms from the matrix and thus the percentage area cover of bifilms per sample is calculated

Figure 8 shows the cumulative area % of bifilm cover for all the positions. The TR system for mold 1 and mold 2 showed a bifilm cover of 1.5%. A huge variation in SR system was observed since mold 1 had an average of 3% across the 5 samples while the

mold 2 SR system showed around 1.4%. The NP system of mold 1 and mold 2 showed a variation of 0.3% in their bifilm areas and a high standard deviation was observed for the NP system of mold 1. The pressurized system in mold 2 had a bifilm cover of 1.8% while the mold 1 had an average of 1% bifilm cover.
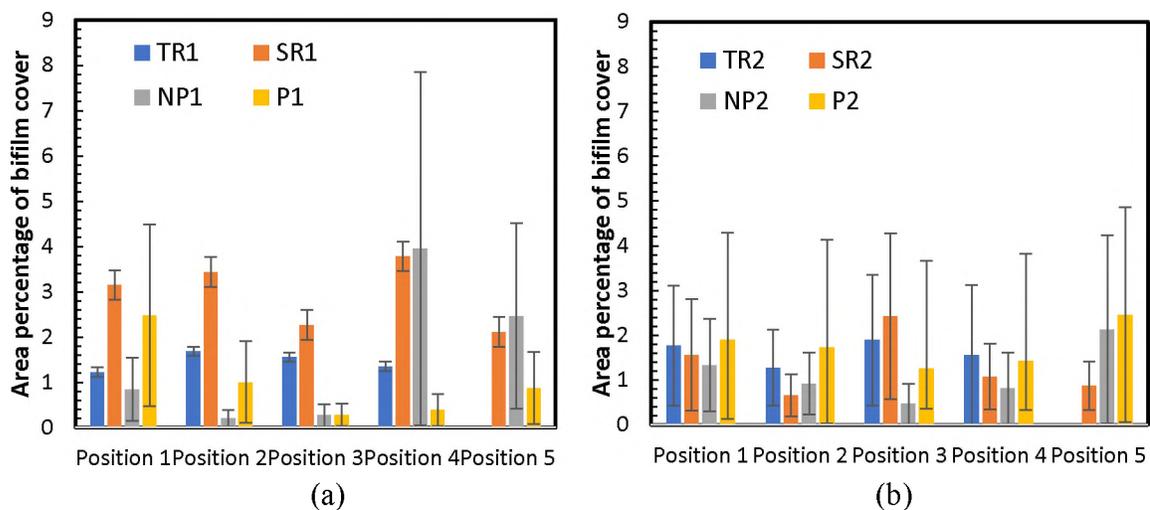
Figure 7. The percentage area of bifilm cover obtained as a function of position in the casting as referenced in Figure 4 for (a) mold 1 and (b) mold 2
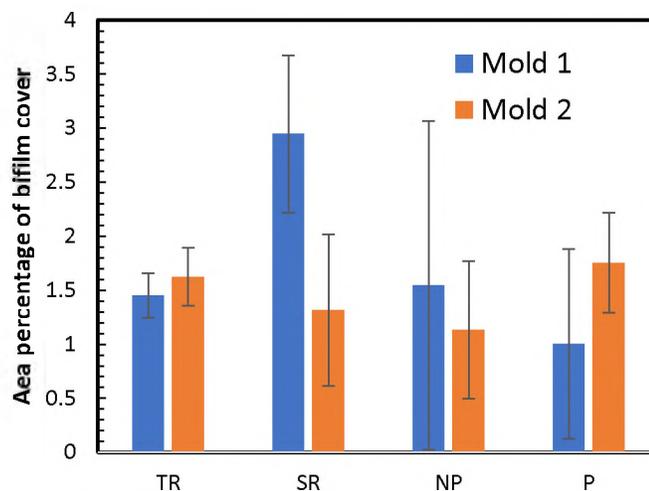
Figure 8. The percentage area of bifilm cover obtained as an average of all the samples obtained from the different positions of top layer of the castings as referenced in Figure 4 of various gating systems for mold 1 and mold 2

4.3. MECHANICAL PROPERTIES

From the bars, machined to ASTM standards, ten values of hardness were obtained from every bar using the Rockwell B scale and Hardness measurements are shown in Figure 9 (a and b) for mold 1 and mold 2, respectively.

It can be observed from Figure 9(a), that the hardness of the castings from mold 1 was between 93-97 HRB. For mold 2, the hardness of the castings was slightly higher and ranged from 97-100HRB. It was observed that the standard deviation of the hardness values was very low indicating the consistency in values. It must be remembered here that the values represent the average of four bars taken per layer of the casting with 10 measurements of hardness taken on every bar.

A comparison of toughness between layer 1 and layer 2 of the castings in mold 1 and mold 2 showed that, the castings obtained from layer 2 had higher toughness than layer 1 for the TR and SR systems. In the pressurized system of mold 1, layer 1 had a toughness of 171±9.31J and layer 2 had a toughness of 150±3.5J. In mold 2, the first and second layers of the P and NP systems had comparable values. Overall, for both the molds, the P and NP systems had an impact toughness either comparable or greater than that of the naturally pressurized systems. The fractography performed on the surfaces of the Charpy bars that were broken showed the presence of dense network of bifilms. Figure 10(a, b, c, and d) show SEM images of a fractured surface of a broken Charpy bar, taken from the SR system, mold 2. Figure 10(a and c) shows the matrix chemistry of the fractured surface obtained using EDS, shown by the red dot, which is similar to the measured chemistry of the specimen. Figures 10(b and d) show the chemistry of the bifilms which were rich in aluminum oxide on the fractured surface.
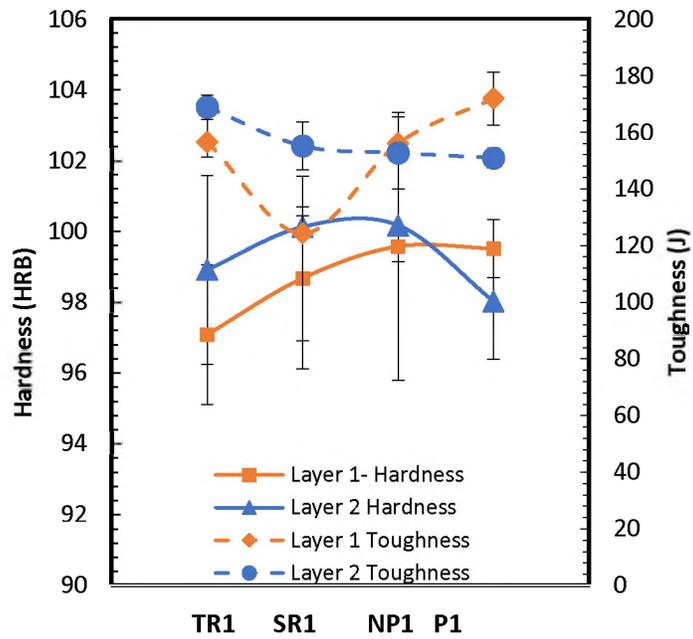
(a)
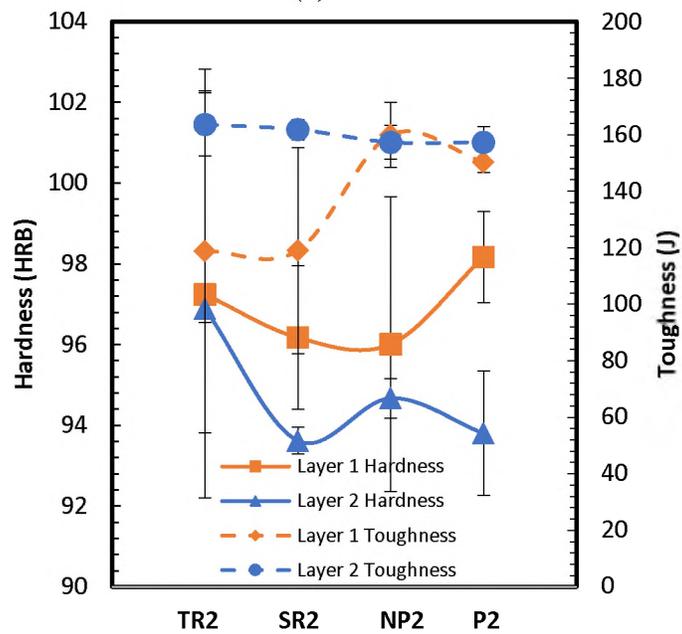
(b)

Figure 9. The hardness of and notch toughness from layer 1 and layer 2 of the castings of various gating systems shown for (a) mold 1 and (b) mold 2, respectively. Toughness was generally higher for samples sectioned from layer 2 and was not related to hardness.

(a)

(b)

(c)

(d)
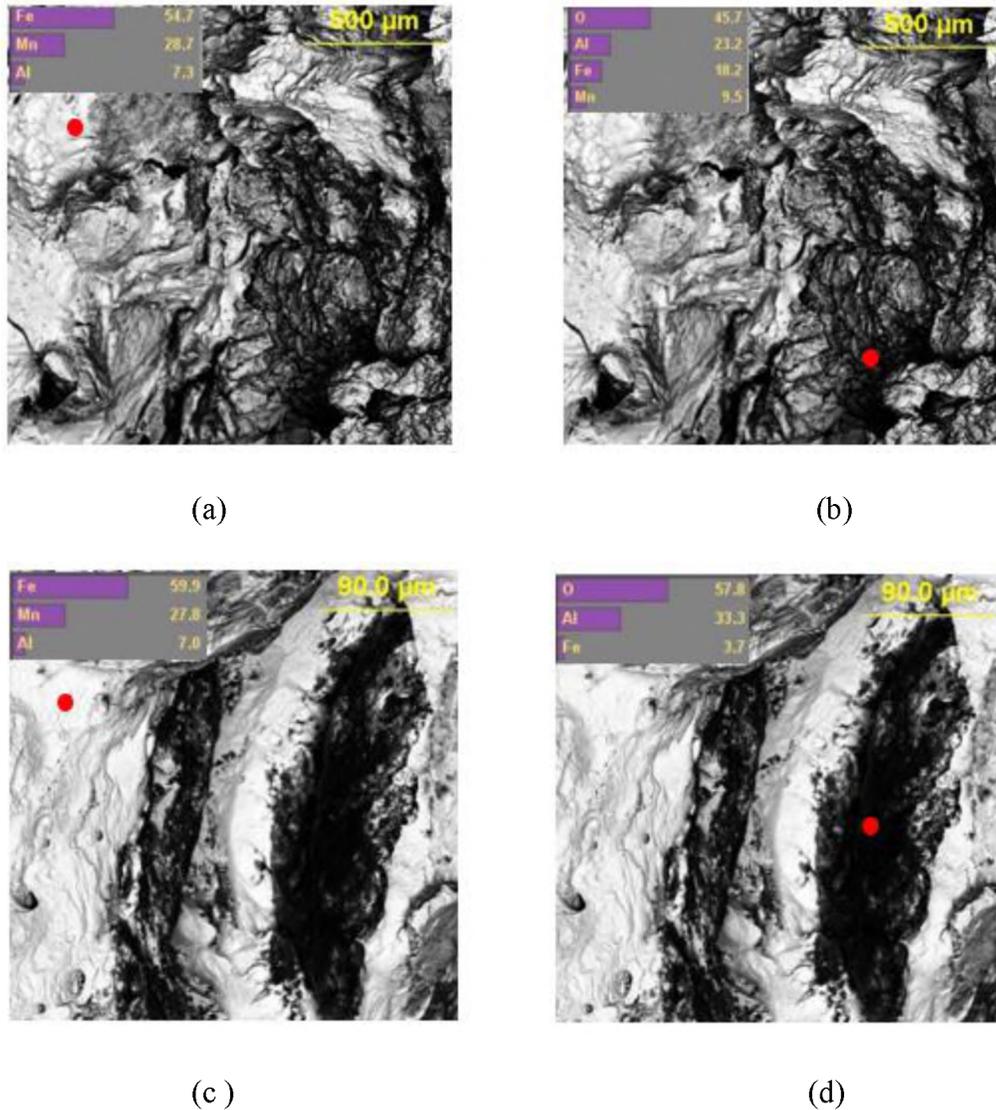
Figure 10. Backscattered electron images of fractured Charpy bars obtained from the SR system of mold 2 showing a dense layer of bifilms rich in aluminum oxide. The red dots indicate the location for chemistry analysis presented in the inset images. (a and c) The matrix chemistry was similar to the nominal steel composition. (b and d) The composition of the bifilms was determined to be mainly alumina

5. DISCUSSION

The chemistry analysis shown in Figure 5(a), showed that the maximum oxygen concentration was found in the SR system, while the remaining three gating systems

showed oxygen concentration less than 5ppm for mold 1. In Figure 5(b), for mold 2, it was observed that that concentration of oxygen was between 35-45ppm, while high standard deviations were observed across all samples. Figure 7 (a), showed the area percentage covered by bifilm according to position and SR system consistently showed high peaks because of the presence of large areas of bifilms. This is validated by the high oxygen content found in the LECO samples in mold 1, where the SR systems exhibited concentrations over 25ppm. Figure 8 showed the trends of combined area cover of bifilms across all positions for all the gating systems. The amount of total oxygen showed a direct correlation with the area of bifilm coverage in the samples as show in Figure 11. Figure 9 (a and b), show the average hardness for mold 1 to be 98 ± 1.3HRB and mold 2 to be 97 ± 1.25HRB, which is 228BHN and 222BHN when converted according to ASTM standard E140[16]. From Figure 9(a), the CVN toughness of the bars from mold 1, was the lowest for layer 1 of SR system at 125 ± 47J and highest for the pressurized system at 171 ± 9J. Similar trends were observed for mold 2, as the naturally pressurized systems showed lower toughness with larger variance.

The mechanical properties of the current steel composition can be compared to the work done by Rairu et al., for a steel of composition Fe-29.8Mn-0.96C-1.24Si-0.55Mo-8.4Al. A hardness of 218 BHN, a CVN energy of 152 J was reported for samples in solution treated condition. It must also be noted, that the sulfur, oxygen and nitrogen concentrations were comparable in this steel to the data reported in Figure 5.[17]Bartlett et al. has similarly reported a hardness of 192BHN and CVN energy of 190J for solution treated and water quenched steel of composition Fe-30Mn-9Al-1.07Si-0.9C. [2] From the data reported in previous works and comparing with the data obtained in Figure 9, it is observed that a well-

designed gating system offers improved hardness and toughness values for similar compositions of FeMnAl steel.
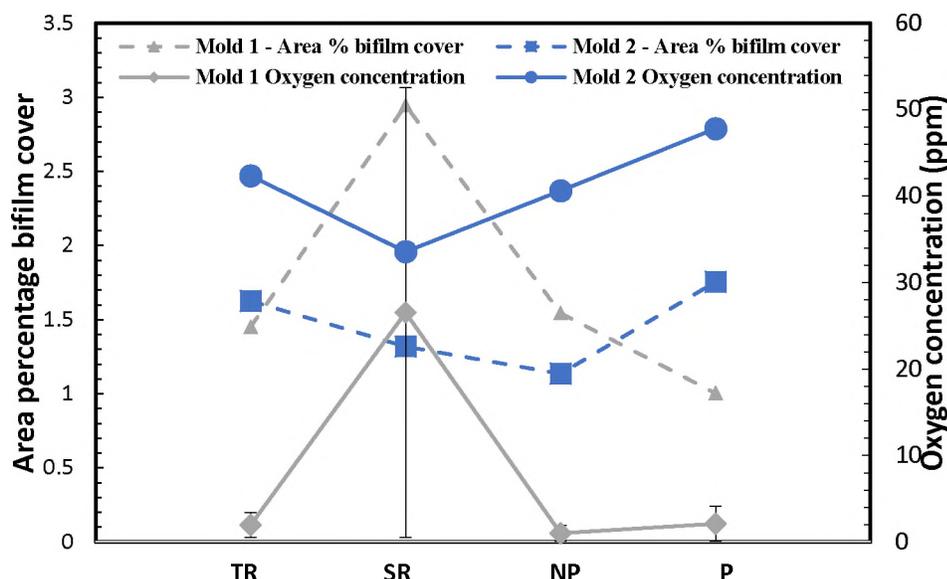
Figure 11. A comparison shown between the total oxygen concentration (ppm) and area % of bifilm cover in the castings obtained from different gating systems for mold 1 and mold 2. The amount of total oxygen was found to correlate to the total amount of bifilm coverage

To understand the contributing factor for failure and loss of toughness, a comparison between bifilm area % and toughness was studied. Figure 12(a) showed the average of the toughness of the eight Charpy bars taken from each gating system and the average of the bifilms obtained from the top section of the castings for mold 1 and Figure 12(b) for mold 2 respectively.

From Figure 12, it is seen that the toughness and area of bifilm cover share an inverse relationship with each other. For all the gating systems, a reduction in toughness is caused by an increase in area of bifilms present in the castings. The work by Dispinar et al., on A356 castings establishes a similar relationship. They found that the bifilm index,

which is a sum of the lengths of bifilms present in the casting, is inversely proportional to the toughness of the alloy. [19]From earlier works by Dispinar and Campbell on effects of entrained films on mechanical properties of castings, it is observed that the presence of folded double oxide bifilms in the steel matrix lead to porosity formation, hydrogen precipitation, and the unbonded sides of the bifilms that act as cracks in the matrix.
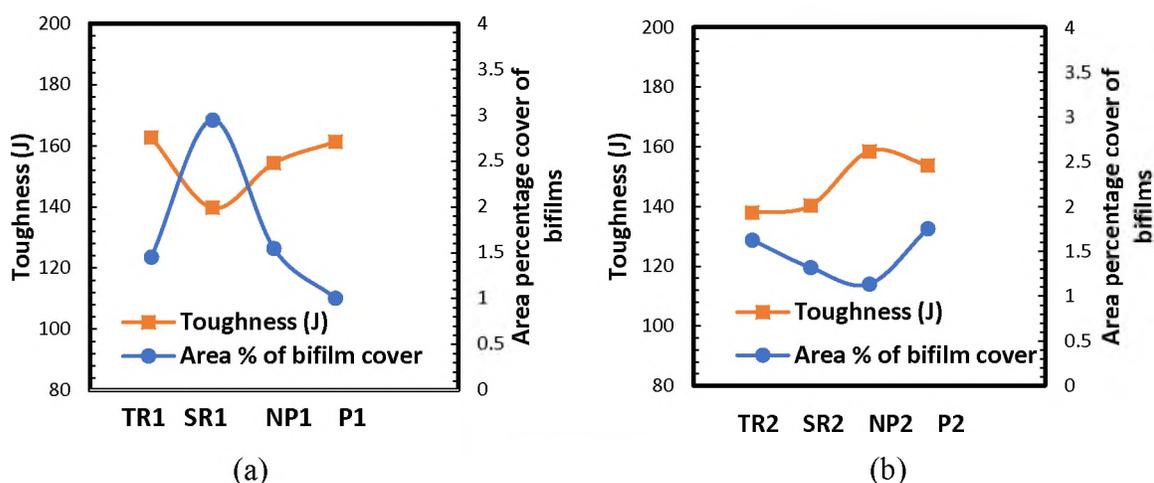
Figure 12. The comparison between the 8-notch toughness obtained from layer 1 and layer 2 of every gating system and the area % of bifilm cover from the top section of the casting for (a) mold 1 and (b) mold 2

The section beneath the fractured surface was analyzed for bifilms and inclusions. The bifilms analysis showed a direct comparison between the breaking energy and the area cover of bifilm area. Figure 13 shows a plot between the breaking energy of the fractured bars that were sectioned and the area of bifilm cover underneath the fractured surface. The values shown are an average of the bifilm area for the bars considered in every layer and their average corresponding breaking energy. It can be observed that as the bifilm cover increases, as seen in the SR system, there is a direct drop in the breaking energy. Moreover, in the other gating systems, there was a close correlation between the breaking energy and

the bifilm cover percentage like the NP system and the P system, where the values for mold 1 and mold 2 were similar to each other. The bifilms acts as a stress-raisers, which leads to premature and brittle fracture subsequently leading to a loss in toughness, ductility and mechanical strength. [4-7]
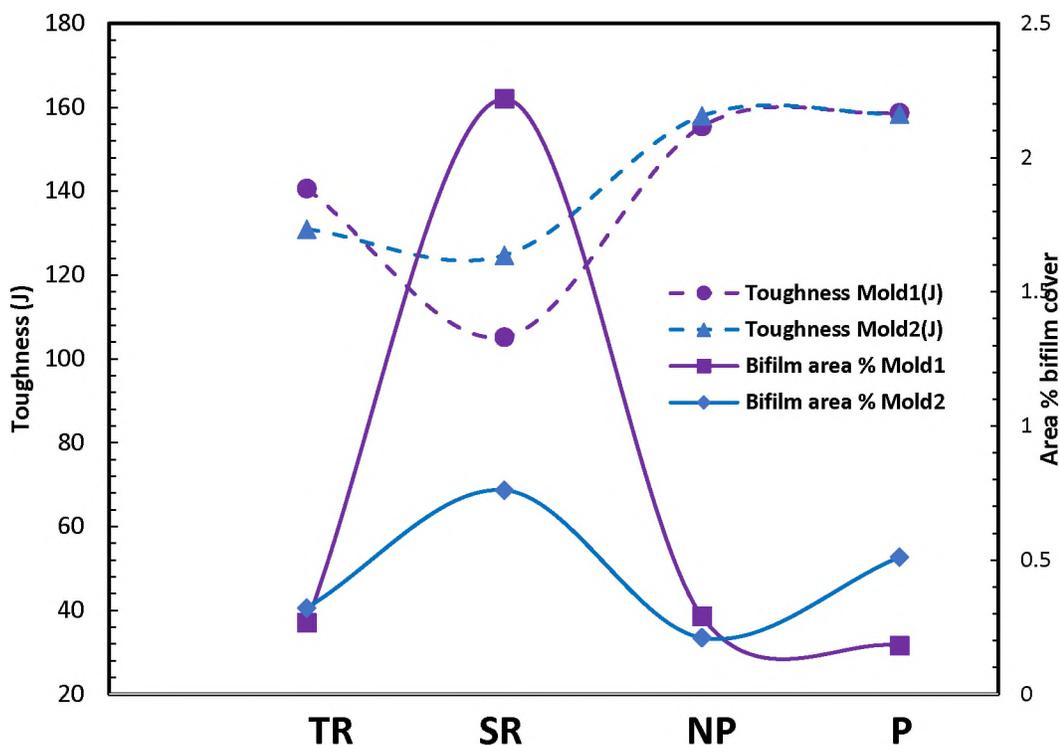
Figure 13. A comparison between the breaking energy and the area cover of bifilms obtained from right underneath the Charpy bar. It can be observed that the bifilms were the reason for failure and had a direct impact on the toughness of the steel

A bar from the SR system that was sectioned right underneath the fractured surface was polished and observed under the SEM. The Figure 14(a) captured at 75X and (b) captured at 250X, show a wide bifilm cover present on the surface of the sample and the composition of the bifilm is seen indicated by the red dot as measured using the EDS. Figure 13 and 14 clearly show that the bifilms were the main mode of failure and loss in

toughness in these castings. Inclusion analysis was also performed on the surfaces of the castings below the fracture and it was seen that AlN, AlN-MnO and AlN-MnS were the dominant inclusions in the castings with the presence of some complex nitrides as shown in Figure 15. No definite trends were established between the breaking energies and the area fraction or inclusion density of the inclusions.

(a)   (b)
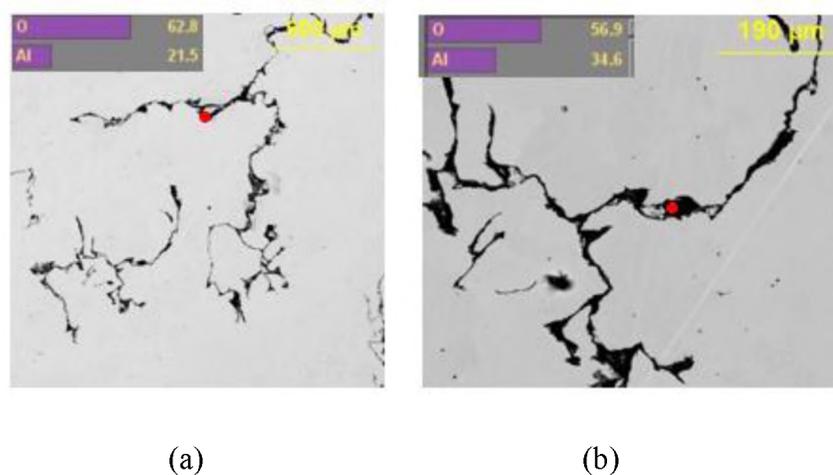
Figure 14. Backscattered electron images of the area sectioned underneath the fractured surface of a Charpy bar from the SR system shows alumina bifilms on the surface confirming that the bifilms were the main reason for failure

(a)   (b)
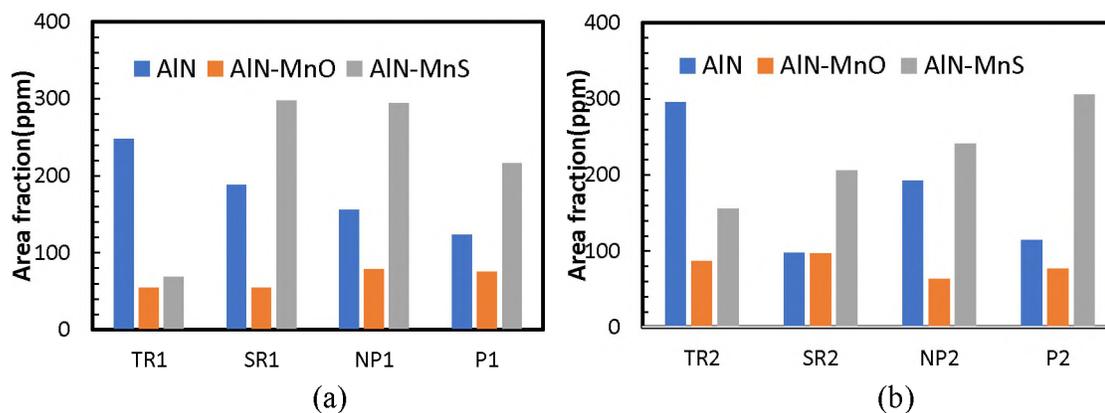
Figure 15. The area fraction of the AlN, AlN-MnO and AlN-MnS inclusions shown for the different gating systems obtained from the surface underneath the fractured Charpy bars. No trends were observed in the inclusion analysis correlating them to fracture toughness

6. CONCLUSION

The effectiveness of four different gating systems in reducing filling related defects in Fe-29Mn-8.2Al-0.91C-0.88Si-0.49Mo steel castings was quantitatively studied. The different systems included a non-pressurized system with a side riser, a pressurized system with a side riser, a naturally pressurized system with a top riser, and a naturally pressurized side riser system and were designed using commercially available filling and solidification modeling software. Solidification parameters were controlled by using identical castings and defects such as microporosity were minimized so that they did not affect the mechanical property results. All gating systems were also designed to minimize ingate velocity to less than 0.8m/s and air entrapment less than 15%. A common pouring basin was designed to unite the system so that it eliminated pouring variance between molds. An extensive network of bifilms was found across all the samples with the nonpressurized side riser system having a maximum 3.5% area coverage of bifilms in mold 1. The total oxygen concentration showed a correlation with the area percentage of bifilms. Hardness and CVN breaking energy results showed that the pressurized and non-pressurized system showed a maximum CVN energy of 160-175J consistently, while the nonpressurized systems had the lowest breaking energy and the greatest variance. For FeMnAl steel castings, the traditional pressurized and non-pressurized gating systems help in achieving cleaner castings with good mechanical properties, while the naturally pressurized gating systems had a higher bifilm content and hence lower mechanical properties.

ACKNOWLEDGEMENTS

REFERENCES

1. Hadfield, R., Burnham, T. H., "Special Steels", 2nd ed., p.100, The Pitman Press, New York (1933).

2. Laura Bartlett, David Van Aken "High Manganese and Aluminum Steels for the Military and Transportation Industry", Journal of Materials, Vol 66, No 1, (2014)

3. A.M.Schulte, S.N.Lekakh, D.C.Van Aken, V.L.Richards " Phosphorus mitigation in cast lightweight Fe-Mn-Al-C steel'" 114th MetalCasting Congress, Orlando, Florida, March (2013)

4. R.Gopalan and Narayan. K. Prabhu "Oxide Bifilms in aluminum alloy castings: A review", Materials Science and Technology,Vol 27, Issue 12, Pages 1757-1769, (2011)

5. M.A. El-Sayed; M. Ghazy, "Entrained defects in light metal cast alloys", Journal of South African Institute of mining and metallurgy", Volume 117, issue 7, (2017)

6. John Campbell, " Melting, Remelting, and Casting for Clean Steel", steel research int. 88 (2017) No. 1, (1-13)

7. L. Liu and F. H. Samuel: J. Mater. Sci., 1998, 33, 2269–2281.

8. J. Campbell, Complete Casting Handbook, 2nd Edition, Elsevier, Oxford, UK 2015.

9. Xue X, Hansen S.F, Hansen P.N, Water Analog Study of Effects Gating Designs on Inclusion Separation and mold filling control, AFS Transactions, vol. 101, pp.199-209, (1993)

10. . Lin H.J, Hwang W. S., Three-Dimensional Fluid Flow Simulation for Mold Filling, AFS Transactions, vol. 97, pp 855-862, (1989)

11. M. Masoumi, H. Hu, J. Hedjazi, M. A. Boutorabi "Effect of Gating Design on Mold Filling", AFS Transactions, pp 05-152, (2005)

12. Seyyed Hojjat Majidi "Effect of Pouring Conditions and Gating System Design on Air Entrainment during Mold Filling" International Journal of Metalcasting. AFS Transactions (2018)

13. John Campbell "Mini Castings Handbook", 2nd edition (2018)

14. Jan Jezierski, Rafal Dojka, Krzystof Janerka "Optimizing the Gating System for Steel Castings", Metals, 8(4), pp 266 (2018)

15. Koushik.K.B, L.Bartlett, M.Xu, D.Imrie, "Design of novel gating systems for steel castings", International Journal of Metalcasting, 2020 (To be published)

16. ASTM International, ASTM E140-12be1 Standard Hardness Conversion Tables for Metals Relationship Among Brinell Hardness, Vickers Hardness, Rockwell Hardness, Superficial Hardness, Knoop Hardness, Scleroscope Hardness, and Leeb Hardness, 2012.

17. R. Vaz Penna, L. N. Bartlett , and T. Constance, " Understanding the role of inclusions on the dynamic fracture toughness of high strength lightweight FeMnAl steels", International Journal of Metalcasting/Volume 13, Issue 2, 2019

SECTION

2. CONCLUSION

Two methods for increasing steel casting cleanliness were quantitatively studied, filtration and use of novel gating designs. Filtration utilizing ceramic foam filters was studied for removal of inclusions in high manganese and aluminum, or FeMnAl, steels. The bifilms in the FeMnAl steel were also effectively filtered by the foam filters. The Fe-30Mn-9Al-0.9C-1Si-0.5Mo steel studied had primarily AlN inclusions and the filters showed a maximum of 61% effectivity in reducing the AlN population in the last mold poured and an increase of 39% in effectivity from the first mold in the sequence to be poured. The last mold, which was poured from the top portion of a teapot ladle had the highest proportion of large sized inclusions ($>5\mu m$) and the highest filtration rate. This showed that the efficiency of ceramic foam filters is greater for larger inclusions in FeMnAl steel.

The second part of this study quantitatively evaluated the ability of different gating systems to reduce the filling related defects and increase the mechanical properties of two different steel alloys, a SAE 8630 steel and a Fe-29Mn-8.2Al-0.91C-0.88Si-0.49Mo steel. The following gating systems were studied, a naturally pressurized system with a side riser, a naturally pressurized system with a top riser, a pressurized and a non-pressurized system. For 8630 steel castings, the naturally pressurized top riser system showed the lowest inclusion area fraction among the four gating systems and the highest breaking energy of 55J. Alumina and alumina-manganese sulfide complex were the primary inclusions. Fractography showed that the presence of eutectic type II MnS inclusions were the reason

for failure in these castings. The overflows showed a higher inclusion area fraction than the castings. The location of the inclusions obtained in the castings were similar to the predictions made by the flow simulation software used to design the gating systems. For FeMnAl castings of composition Fe-29Mn-8.2Al-0.91C-0.88Si-0.49Mo, extensive layers of bifilms were found in the castings. The naturally pressurized side riser system had the highest area cover of bifilms and the lowest breaking energy of 140J. The pressurized and non-pressurized systems showed consistently 165J of breaking energy. The bifilms had a direct impact on the mechanical strength of the castings and were found to be the reason for lower energy ductile failure in some specimens. The breaking energy shared an inverse relationship with the area coverage of bifilms. It was observed that the naturally pressurized top riser and side riser system performed well for the 8630 steel, while the traditional pressurized and nonpressurized gating systems performed better for FeMnAl steel castings. From the filtration project, it was observed that the Charpy samples obtained from filtered castings showed better toughness properties than unfiltered castings. The overflows collected the incoming new metal with the slag, dross and inclusion defects and aided in controlling the velocity of the liquid metal. Therefore, a well-designed nonpressurized gating system with the presence of a filter is ideal to reduce reoxidation inclusion defects and improve the quality and notch toughness of FeMnAl castings. Further work should be done to ascertain the effects of these gating systems on the notch toughness of low alloy steels like 8630 using Mn-Si as a deoxidant to prevent the occurrence of type II eutectic MnS that may obscure the influence of reoxidation inclusions.

BIBLIOGRAPHY

1. Andre Costa E Silva," Non-metallic inclusions in steel- origin and control", Journal for Material Research Technology, 7(3) – 283-299 (2018).

2. Lifeng Zhang, Brian.G.Thomas " Inclusions in continuous casting of steel", XXIV National Steelmaking Symposium, Morelia, Mich, Mexico, 26-28, Nov.2003, pp. 138-183.

3. T.H.Courtney," Mechanical Behaviour of Materials,second edition", Waveland Press, pp-459-461(2005).

4. L.Bartlett, Van Aken, " Dynamic fracture toughness of high strength cast steels", International Journal ofMetalcasting, Volume 7, Issue 4, 2013.

5. Griffin, J. A., and Bates, C. E., "Ladle Treatment, Pouring and Gating for the Production of Clean Steel Castings," SFSA Research Report, No. 104, 1991.

6. R.Raiszadeh, W.D.Griffiths, " A method to study the history of a double oxide film defect in liquid aluminum alloys", Metallurgical and Materials Transactions B, volume 37, pages 865–871(2006).

7. Fu-Yuan Hsu, Kuo-Nien Wang & Cheng-Lung Li, "Bifilm defects in ductile-iron support bracket castings", International Journal of Cast Metals Research, 2017,VOL . 30, NO . 3, 148–158.

8. R.Gopalan, Narayan.K.Prabhu, "Oxide bifilms in aluminium alloy castings – a review", Materials science and Technology, 27:12, 1757-1769 , (2013).

9. John Campbell, "Mini Casting Handbook", Revised and Enlarged Second Edition book, 2018.

10. John Campbell," Castings", Butterworth Heinemann Limited, 1991.

11. S. Chakraborty, L. Bartlett, R. O'Malley, M. Xu, "Efficiency of solid inclusion removal from the steel melt by foam ceramic filter: Design and Experimental Validation",122nd AFS MetalCasting Congress, American Foundry Society, (2018)

12. MAJ Ryan Andrew Howell " Microstructural Influence on Dynamic Properties of Age Hardenable FeMnAl Alloys", Theses, Missouri University of Science and Technology.

13. Frommeyer, G., Brux, U., "Microstructures and Mechanical Properties of High-Strength Fe-Mn-Al-C Light-Weight TRIPLEX Steels," Steel Research Int., Vol. 77, pp. 627-633 (2006).

14. A.M.Schulte, S.N.Lekakh, D.C.Van Aken, V.L.Richards " Phosphorus mitigation in cast lightweight Fe-Mn-Al-C steel'" 114th MetalCasting Congress, Orlando, Florida, March (2013)

15. Ramesh Singh, "Applied Welding Engineering (Second Edition), *2016.*

16. Van Ende, Marie-Aline, "Formation and morphology of non-metallic inclusions in aluminium killed steels", Doctoral Theses,Belgium, January 2010.

17. T.B.Braun, J.F.Elliott,, M.C.Flemings, "The Clustering of Alumina Inclusions".

18. R. Dekkers, B. Blanpain and P. Wollants, Crystal growth in liquid steel during secondary metallurgy. Metallurgical and Materials Transactions B 34 (2) (2003) 161-171.

19. E. Steinmetz and H. U. Lindenberg: Oxide morphology at manganese and manganese-silicon deoxidation. Archiv Fur Das Eisenhuttenwesen 47 (2) (1976) 71-76.

20. Meng-long Li, Fu-ming Wang, "Effect of cooling rate and Al on MnS formation in medium carbon non quenched and tempered steel, International Journal of Minerals, Metallurgy and Materials Volume 22, Number 6, June 2015, Page 589

21. Yoichi ITO, Noriyuki MASUMITSU, Kaichi MA TSUBARA, "Formation of Manganese Sulfide in Steel" , Tetsu-to-Hagane, 66 (1980), 647

22. Sims,C.Dahle," Effect of aluminum on properties of medium carbon cast steel", Trans American Foundry society,46, 65-132, 1938.

23. Feng Wang and Zhongyun Fan," Characterization of AlN Inclusion Particles Formed in Commercial Purity Aluminum", Metallurgical and Materials transactions A VOLUME 50A, MAY 2019

24. Philips Charles Belding, "Control of non-metallic inclusions in steel", Master of Science Theses, Oregon state University, June (1971).

25. G. Gigacher, W. Krieger, P. R. Scheller and C. Thomser: Mater. Technol., 76 (2005), 644.

26. Min-Kyu PAEK, Jung-Mock JANG, Min JIANG and Jong-Jin PAK," Thermodynamics of AlN Formation in High Manganese-Aluminum Alloyed Liquid Steels", ISIJ International, Vol. 53 (2013), No. 6, pp. 973–978

27. Lauri Holappa, Olle Wijk, " Treatise in Process metallurgy", Industrial Processes, 2014

28. Roney Eduardo" Influence of the chemical composition on steel casting performance", Journal for Material Research Technology 2017;6(1):50–56

29. Chris.P," Magnesium: Origin and role in calcium treated incllusions',Sohn International Symposium; Advanced Processing of Metals and Amterials , volume2, Iron and Steel Making, 2.pp 373-378,2006

30. Wang and C. Beckermann: Prediction of reoxidation inclusion composition in casting of steel. Metallurgical and Materials Transactions B 37 (4) (2006) 571-588.

31. Seyyed Hojjat Majidi "Effect of Pouring Conditions and Gating System Design on Air Entrainment During Mold Filling" International Journal of Metalcasting. AFS Transactions (2018)

32. Seyyed Hojjat Majidi and Christoph Beckermann "Modelling of air entrainment during pouring of metal castings" International Journal of Cast Metals Research, vol 30, pp 301-315, (2017)

33. A.J. Melendez, K.D. Carlson and C. Beckermann, "Modelling of Reoxidation Inclusion Formation in Steel Casting", International Journal of Cast Metal Research, Vol. 32, pp. 624-638, 2009.

34. R. Kiessling: Metal Science, (1980), 15(5), 161.

35. D. C. HILL AND D. E. PASSOJA," Understanding the Role of Inclusions and Microstructure in Ductile Fracture

36. G.Y.Hahn, M. F. Kanninen, A.R.Rosenfield, " Fracture toughness of materials",

37. Chao Gu , Junhe Lian , Yanping bao , Wei Xiao, " Numerical Study of the Effect of Inclusions on the Residual Stress Distribution in High-Strength Martensitic Steels During Cooling" , Applied. Sciences, 9(3), 455, 2019

38. C. Ruggieri , " Numerical investigation of constraint effects on ductile fracture in tensile specimens, March 2004, Journal of the Brazilian Society of Mechanical Sciences and Engineering 26(2)

39. Tweed JH, Knott JF. Met Sci 1983;17:44–7.

40. G.R. Speich, W.A. Spitzig, Metall. Trans. A 13A (1982) 2239.

41. J. R. Rice and M. A. Johnson: Inelastic Behavior of Solids, M. F. Kanninen, et al., eds., p. 641, MNpraw-Hill, New York, 1970.

42. G. T. Hahn and A. R. Rosenfield: Paper PL-III-21 l, Third Int. Conf. Fracture,Munich, 1973.

43. M.A. El-Sayed; M. Ghazy, " Entrained defects in light metal cast alloys", Journal of South African Institute of mining and metallurgy", Volume 117, issue 7, (2017)

44. J.Campbell," The consolidation of metals: the origin of bifilms", J Mater Sci (2016) 51:96–106

45. John Campbell, " Melting, Remelting, and Casting for Clean Steel", steel research int. 88 (2017) No. 1, (1-13)

46. L. Pavlak: Metalurgija, 2008, 14, 31–39.

47. D. Dispinar, J. Campbell," Porosity, hydrogen and bifilm content in Al alloy castings", Materials Science and Engineering A 528 (2011) 3860–3865

48. M. A. El-Sayed & W. D. Griffiths (2014) Hydrogen, bifilms and mechanical properties of Al castings, International Journal of Cast Metals Research, 27:5, 282-287

49. L. Liu and F. H. Samuel: J. Mater. Sci., 1998, 33, 2269–2281.

50. J. Xu, F. Huang, X. Wang, Metall. Mater. Trans. B2016, 47B, 1217.

51. J. M. Svoboda, R. W. Monroe, C. E. Bates, J. Griffin,Trans. Am. Found. Soc. 1, 95, 187.

52.J. Campbell, Complete Casting Handbook, 2ndEdition, Elsevier, Oxford, UK 2015.

53. Hadfield, R. (1935). Special Steels. Nature, 135(3418), 741-745.

54. Kalashnikov, I., Acselrad, O., Shalkevich, A., Pereira, L.C., "Chemical Composition Optimization for Austenitic Steels of the Fe-Mn-Al-C System," Journal of Materials Engineering and Performance, Vol. 9, No. 6, pp. 597-602 (2000).

55. Schmatz, D. J., "Formation of Beta Manganese-Type Structure in Iron-Aluminum-Manganese Alloys," Trans. of Met. Soc. of AIME, Vol. 215, pp. 112-114 (1959).

56. Kayak, G. L., "Fe-Mn-Al Precipitation-Hardening Austenitic Alloys," Met. Sc. And Heat Tr., Vol. 11, pp. 95-97 (1969).

57. Tjong, S. C., Zhu, S. M., "Tensile Deformation Behavior and Work Hardening Mechanism of Fe-28Mn-9Al-0.4C and Fe-28Mn-9Al-1C Alloys," Mat. Trans., Vol. 38, pp. 112-118 (1997).

58. Prodhan, A., Charkrabarti, A. K., "A Study on Age Hardening in Cast Fe-Mn-Al-Si-C Alloys," J. Mat. Sci., Vol. 25, No. 3, pp. 1856-1862 (1990).

59. Howell, R. A., Weerasooriya, T., Van Aken, D. C., "Tensile, High Strain Rate Compression and Microstructural Evaluation of Lightweight Age Hardenable Cast Fe-30Mn-9Al-XSi-0.9C-0.5Mo Steel," AFS Transactions – awaiting publication.

60. James, P. J., "Precipitation of the carbide (Fe,Mn)3AlC in an Fe-Al Alloy," J. Iron and Steel Inst., Jan, pp. 54-57 (1969).

61. Kayak, G. L., "Fe-Mn-Al Precipitation-Hardening Austenitic Alloys," Met. Sc. And Heat Tr., Vol. 11, pp. 95-97 (1969).

62. Goretskii, G. P., Gorev, K. V., "Phase Equilibria in Fe-Mn-Al-C Alloys," Russian Met., Vol. 2, pp. 217-221 (1990).

63. Krivonogov, G.S., Alekseyenko, M. F., Solov'yeva, G. G., "Phase Transformation Kinetics in Steel 9G28Yu9MVB," Fiz. Metal. Metalloved, Vol. 39, No. 4, pp. 775-781 (1975).

64. Storchak, N. A., Drachinskaya, A. G., "Strengthening of Fe-Mn-Al-C Alloys During Aging," Fiz. Metal. Metalloved., Vol. 44., No. 2, pp. 373-380 (1977).

65. Rairu Vaz Penna, "Inclusion Engineering in FeMnAl steels", Masters Theses, Missouri University of Science and Technology,2019

66. Han, K. H., Choo, W. K., Choi, D. Y., Hong, S. P., "Age Hardening in Fe-Mn-Al-C Austenitic Alloys," TMS-AIME, pp. 91-106 (1987).

67. Acselrad, O., Pereira, L. C., Amaral, M. R., "Processing Condition, Microstructure and Strength of an Austenitic Fe-Mn-Al-C Alloy," Proceedings of Proc. and Prop. of Mats., pp. 829-834 (1992).

68. Van Aken, D.C, Howell, R.A., Bartlett, L.N., Schulte, A.M., Lekakh, S.N., Medvedeva, J., Richards, V.L., Peaslee, K.D., "Casting P900 Armor with Lightweight Steel," 63'" Technical & Operating Conference of the Steel Eounders' Society of America, paper 3-2 (2009).

69. Bartlett, L., & Van Aken, D. (2014). High Manganese and Aluminum Steels for the Military and Transportation Industry. JOM, 66(9), 1770-1784. doi:10.1007/s11837-014-1068

70. Park, J. H., Kim, D., & Min, D. J. (2012). Characterization of Non-metallic Inclusions in High-Manganese and Aluminum-Alloyed Austenitic Steels. Metallurgical and Materials Transactions A, 43(7), 2316-2324.

71. D. Apelian, R. Mutharasan*, S. Ali, " Removal of inclusions from steel melts by filtration", Journal of Materials Science, volume 20, pp 3501-3514, (1985)

72. L. J. Gauckler, M. M. Waeber, C. Conti, M. Jacob-Duliere " Ceramic Foam for molten metal Filtration", Journal of Materials, volume 37, Issue 9, pp 47-50 (1985)

73. Kexu Zhang, " Liquid permeability of ceramic foam filters", Norwegian University of Science and Technology, Department of materials Science and Technology, (2012)

74. P. Sandford and S.R. Sibley: Optimization of Al Casting Productivity Using Foam Filter Technology and Application, AFS Transact, 1996, 1063-1068.

75. G.S. Armatas: "Determination of the Effects of the Pore Size Distribution and Pore Connectivity Distribution on the Pore Tortuosity and Diffusive Transport in Mode Porous Networks", Chemical Engineering Science, vol. 61, 4662-4675.

76. P. Habisreuther, N. Djordjevic and N. Zaralis "Statistical Distribution of Residence Time and Tortuosity of Flow through Open-cell Foams", Chemical Engineering Science, vol. 64, 2009, 4943-4954.

77. Sarina, BAO, Martin Syvertsen, Anne Kvithyld, Thorvald ENGH," Wetting behavior of aluminium and filtration with Al2O3 and SiC ceramic foam filters", Transactions of Nonferrous Metals Society of China, Volume 24, pp 3922-3928, (2014)

78. Bajrang, "Types of Gating system in castings", Bajrang Engineering

79. Xue X, Hansen S.F, Hansen P.N, Water Analog Study of Effects Gating Designs on Inclusion Separation and mold filling control, AFS Transactions, vol. 101, pp.199-209, (1993)

80. Lin H.J, Hwang W. S., Three-Dimensional Fluid Flow Simulation for Mold Filling, AFS Transactions, vol. 97, pp 855-862, (1989)

81. Seyyed Hojjat Majidi "Effect of Pouring Conditions and Gating System Design on Air Entrainment During Mold Filling" International Journal of Metalcasting. AFS Transactions (2018).

82. R. Dojka, J. Jezierski, and J. Campbell "Optimized Gating System for Steel ", Journal of Materials Engineering and Performance, Volume 27, pp 5152-5163, (2018)

VITA

Koushik Karthikeyan Balasubramanian was born in Nagercoil, Tamil Nadu, India. As an undergraduate student, he had an internship at Tractor and Farm Equipment Limited and was a project intern at Indian Institute of Science, Bangalore. He worked on a research project involving tribology of stainless steel and polymer for medical applications. He graduated with a Bachelor of Science in Mechanical Engineering from Sir M Visvesvaraya Institute of Technology (Visvesvaraya Technological University) in 2017.

After graduating, Koushik joined the master's program in Materials Science and Engineering at Missouri University of Science and Technology in August 2017. He started as a graduate research assistant under the guidance of Dr. Laura Bartlett, Dr. Ronal O'Malley, and Dr. Simon Lekakh starting in January 2018. His research topic was on the control of inclusion population in steels. During his program, he worked on understanding the effect of filtration in steels and developed novel gating systems for obtaining steels with better cleanliness and mechanical strength. He also authored a publication in conference proceedings and three journal articles. Koushik received his Master of Science in Materials Science and Engineering from Missouri University of Science and Technology in December 2020.